UNIVERSITY of PENNSYLVANIA

The Moore School of Electrical Engineering

PHILADELPHIA, PENNSYLVANIA 19104

Interim Technical Report

AN ANALYSIS OF THE USE OF OPTICAL TECHNIQUES IN SYNCHRONOUS NAVIGATION SATELLITES

by Robert E. Lefferts

May 1970

Prepared for

NATIONAL AERONAUTICS AND SPACE ADMINISTRATION
Space Applications Programs Office
Washington, D. C. 20546

by

University of Pennsylvania
THE MOORE SCHOOL OF ELECTRICAL ENGINEERING
Philadelphia, Pennsylvania 19104

Under Grant NGL-39-010-087

Moore School Report No.: 70-10

ACKNOWLEDGEMENTS

The author wishes to express his appreciation to Drs. P. I. Klein, J. Bordogna, P. L. Bargellini, and F. Haber for their technical advice and supervision of this study. The work reported here was supported by the National Aeronautics and Space Administration, Washington, D. C., under Grant NGL-39-010-087 which was supervised by Mr. Eugene Ehrlich.

ABSTRACT

The feasibility of using optical and infrared technology for use in synchronous navigation satellites is examined. The analysis is based primarily on a determination of the quality of the image available to the detector under various conditions and not on the properties of the detector itself except for the resolving power of the detector.

Initially a passive-user system is considered where the navigation satellite detects the infrared energy emitted by the user's engines. Jet aircraft were considered first because of the relatively large amount of infrared energy emitted by their engines. By considering the energy incident on a single resolvable image element it was found that the signal energy available could not be reliably distinguished from changes in the effective background temperature of the earth. It was concluded that a navigation system using passive infrared detection from synchronous altitude is not feasible.

An active-user system is also considered where the navigating users are equipped with high-power, optical-energy sources. A comparison of the various optical sources showed that lasers would yield the highest signal-to-noise ratio because the narrow spectral regions in which their energy is concentrated would allow most of the background noise to be removed by filtering. It was found that the signal energy required for a satisfactory image could only be obtained under very restrictive conditions. Under such conditions, it was also necessary to consider the internal noise of the detector to determine if the signal could be detected. It was found that for a reasonable average source power the signal could not be detected due to the large amount of detector noise present. By using a very high peak power laser it should be possible to detect the user's signal but the present cost of such a laser makes such a system economically impractical considering the limited circumstances under which it could be used.

Although a number of optical systems other than the ones described could be considered it is concluded that optical techniques do not represent a feasible alternative to the use of radio frequency techniques for synchronous navigation satellites.

TABLE OF CONTENTS

LIST OF APPENDICES

LIST OF FIGURES

LIST OF TABLES

1.0 INTRODUCTION

1.1 Technology

The rapid progress made in optical and electro-optical technology has opened up new areas of useful application for this technology. The success of TV and photographic cameras has been well demonstrated in several space missions. The application of this technology to navigation problems has become more likely with the development of high resolution TV cameras [1, 17, 25, 58].

The application of these techniques will be considered in two categories. Initially, consideration will be given to passive users which emit no signal specifically for navigational purposes. In this case the navigation satellite will determine the position of the user by detecting, if possible, the thermal energy ($\sim$ 2-8μ) emitted by the user. The second portion of the study will deal with active users which transmit an optical signal for reception by the navigation satellite. Many of the calculations done for the passive case will result in graphs that express basic system interrelationships which apply to the active user case as well.

It should be noted that this study is limited by the fact that no classified information was used. Although the results of classified research in some areas would be useful, they would not change the primary conclusions of this report. However, conclusions based on state-of-the-art predictions may be modified. The results of research on the development of high-resolution image intensifiers would be particularly relevant. Research into this area is being done for development of night vision devices.

1.2 Basic System Configuration

One approach to the design of an optical navigation satellite system would be to have a synchronous satellite observe a portion of the earth. Light energy from the desired area would be focused on an image recording device. If the image contained reference objects of known location then the linear distance on the image would be directly proportional to the angular separation of the objects. The optical system which will be considered is therefore an angle-measurement navigation system.

The use of a synchronous satellite provides several advantages over low altitude satellites. At synchronous altitude the field-of-view would not have to be very large to provide sufficient coverage of the portion of the earth which is visible at this altitude. Narrow field-of-view systems have thinner lenses with less attendant distortion problems and in addition thin lenses cause less attenuation of the signal which is also desirable.

Another advantage provided by use of a synchronous satellite is that it is always located at approximately the same position in the sky. This is important if active sources, such as lasers, are to be used to provide the reference points. Low altitude satellites would require the

reference stations to track the satellite and in addition more satellites would be required to provide equal coverage. Another possible solution to the reference location problem would be to have star trackers provide an indication of the direction of the camera. The last approach has been rejected because it provides no indication of the atmospheric refraction that would be encountered. For ground-based reference points the refraction would be approximately the same for a signal from the reference station and users at the same elevation angle. The refraction could then be estimated for users at other elevation angles.

1.2.1 Synchronous Satellite Coverage

Since the most stable synchronous satellites are those which operate over the equator, an analysis has been made of the coverage area provided by these satellites with various antenna beamwidths [2]. The area covered is circular only if the antenna or camera is pointed at the subsatellite point. The area covered for different orientations is not easily described mathematically other than it turns out to be the intersection of a cone and a sphere, i.e., in the case of a circular field-of-view. For the purposes of this study a circular area of coverage has been assumed to simplify the calculations.

For application in the North Atlantic a camera with an 8° - 10° field-of-view will be assumed. For this field-of-view, reference stations could be located in Greenland, Iceland, or Great Britain.

1.3 Optical Position Information

Once an image is received there are several ways in which it could be processed to obtain position information. The image could be stored on film and either the film or a TV image of the film sent back for processing. This is undesirable since it is impractical to send the film back from a synchronous satellite and the transmission of a picture would require a large transmitter power and bandwidth. It might be possible to use pattern recognition techniques in the satellite to determine the position of desired objects. This, also, is impractical because of the great resolution required and the amount of computational capacity which would have to be built into the satellite.

From these practical considerations it seems undesirable for the satellite to transmit or even process a true picture. Even if a true picture could be transmitted the question remains as to how it would be processed once received. If a large amount of computation was involved a considerable delay would be introduced between the reception of the image and the computation of a user location.

A possible solution to this problem is to use a TV camera but to make a binary decision on each resolvable image element as to the presence of a user. Only the image coordinates of the elements where a user was detected would be transmitted and such a procedure would reduce the amount of data to reasonable size. The difference in the amount of data required to transmit an entire image and the amount required to transmit the locations of several points in that image could easily be many orders of magnitude. In addition, the equipment needed to

determine the user position from the image coordinates would be greatly reduced. Of course, the optical energy from the user must be sufficiently above that of the background to allow such a system to work.

1.4 Implied Restrictions on Optical Navigation Systems

It should be noted that the performance of optical systems involving the transmission of energy through the atmosphere will be considerably degraded by the presence of fog, clouds or rain in the transmission path. Even in the case of an active user it will not be possible to produce sufficient optical power to ensure reliable operation in all types of weather. For aircraft which operate above weather formations, the signal attenuation will be negligible but for low altitude users the weather will severely restrict the use of an optical navigation system. The extent to which the performance of optical navigation systems will be limited by atmospheric attenuation is analyzed in Sections 2.6 and 3.3 but in general it can be said that optical navigation systems could only operate in fair weather.

In order to simplify the initial analysis, problems such as identifying a particular user and resolving aircraft separated only in altitude will be neglected and only the problem of detection will be considered. The problem of detection, as will be shown in both the active and passive cases, is the crucial point in the analysis of the optical navigation system.

It has been argued in the previous section that it would be desirable to use a binary detection system to limit the amount of data which would have to be processed. In the passive case the use of a binary detection scheme will determine the type of users for which the system can operate and the spectral region which must be used. Both of these implications arise from the fact that for a binary detection system to operate in the manner proposed, the object to be detected must be significantly different from the background present in some manner. There are two possible sources of optical energy which can be considered in this case. The first is the reflected sunlight in the visible region (i.e., wavelengths on the order of 0.3-0.7μ) and the second is the thermal or infrared energy ($\sim$ 2-8μ) produced by the heat of the user's engines. In the visible light region a binary detection system would not work because the large amount of sunlight reflected from the atmosphere would obscure the small amount of sunlight reflected by the user. In addition such a system would not be operative at night. In the infrared region, however, the major source of background energy will be the thermal radiation produced by the earth but, as will be shown quantitatively in Section 2.5, the major portion of this energy is produced at wavelengths longer than those at which the thermal radiation of the user is produced. Hence, the thermal radiation produced by the user is in between the two major sources of background energy (i.e., the shorter wavelength reflected sunlight and the longer wavelength thermal energy produced by the earth) and this is the spectral region which will be considered.

The infrared energy radiated by a body is directly proportional to the fourth power of its absolute temperature. For a binary detection scheme using infrared energy the object to be detected should be at a

temperature much greater than that of its background. Among the three types of possible users--jet aircraft, propeller driven aircraft, and ships--jet airplanes provide the greatest temperature difference. If an optical infrared system will not work using jet planes as targets, then it certainly will not function for objects at a lower temperature. For this reason only jet aircraft will be considered in the passive case analysis. Although a reciprocating engine aircraft may produce an amount of infrared energy equal to that produced by a jet aircraft, the major portion of this energy will be at longer wavelengths and thus subject to a greater degree of interference from background radiation from the earth.

2.0 AN ANALYSIS OF OPTICAL TECHNIQUES FOR SYNCHRONOUS NAVIGATION SATELLITES WITH PASSIVE USERS

As stated previously, the passive user considered will be a jet aircraft and the signal to be detected will be the infrared energy emitted by the plane.

2.1 Infrared Radiation

All objects above $0^{o}K$ emit thermal radiation. The spectral distribution of this radiation for black bodies is given by Planck's Law

$$W_{\lambda} = \frac{C_1}{\lambda^5 \left(e^{C_2/\lambda T} - 1 \right)} \qquad (2.1\text{-}1)$$

where W_{λ} = radiation emitted per unit surface area per unit wavelength in watts/cm^2

λ = wavelength of emitted radiation (in cm)

T = absolute temperature in ^{o}K

$C_1 = 3.7413 \times 10^{-12}$ watt cm^2

$C_2 = 1.438$ cm deg.

The region of the electromagnetic spectrum in which (2.1-1) is found to be most useful is divided, somewhat arbitrarily, into five different regions:

ultraviolet	0.001	to 0.3 μ
visible	0.3	to 0.7 μ
near infrared	0.7	to 1.5 μ
middle infrared	1.5	to 20 μ
far infrared	20	to 1000 μ

The higher the temperature of the object being considered the shorter will be the wavelength of most of the energy emitted. According to (2.1-1) radiation is emitted at all wavelengths for all temperatures above $0^{o}K$ but when considering the actual range of temperatures likely to be encountered and the shape of (2.1-1) for these temperatures, it is found that for practical purposes almost all the energy will be between 0.3 and 20 μ. In Section 2.5 it will be shown that for temperatures on the order of those likely to be encountered for jet aircraft over half of the energy emitted will be in the range 2 to 8μ.

To find the total energy emitted, (2.1-1) can be integrated over all wavelengths to give the Stefan-Boltzman Law.

$$W = \sigma T^4 \qquad (2.1\text{-}2)$$

where W = total black body radiant emittance watts/cm^2

T = absolute temperature in ^oK

$\sigma = 5.673 \times 10^{-12}$ watt/cm^2 deg^4

The above laws are applicable to ideal situations and represent the maximum possible amount of emitted radiation. In practical situations the shape of the spectral distribution is the same but the radiant emittance is less. Such bodies are called "gray bodies" and for such bodies an emissivity factor is defined

$$\epsilon = \frac{\text{total radiant emittance}}{\text{total radiant emittance of a black body at the same temperature}}$$

Hence, the spectral distribution of the radiation from many real objects will be given by:

$$W_\lambda = \frac{\epsilon\, C_1}{\lambda^5 \left(e^{C_2/\lambda T} - 1\right)} \qquad (2.1\text{-}3)$$

and

$$W = \epsilon\, \sigma T^4 \qquad (2.1\text{-}4)$$

The above equations are only approximations since the emissivity is in reality a function of the wavelength. For many materials the variation of emissivity is so small that ϵ can be assumed constant and in general this assumption holds for all solid objects or objects with significant density. Significant sources of infrared energy where the emissivity is not constant are hot gases and flames such as the exhaust products from a jet engine. Analysis of situations where the emissivity is not constant is much more difficult.

Using these simple formulas, an analysis can be made of the infrared energy being emitted by a jet plane. It should be noted that the hotter parts of the plane do not necessarily emit the most infrared energy because of the varying emissivity of the materials involved. Note that surfaces which are good reflectors, such as aluminum, normally have emissivities much less than 1, the maximum value, and are therefore poor emitters.

2.1.1 Sources of Infrared Radiation from Jet Aircraft

The infrared energy emitted from a jet aircraft in the 2-8μ region can be separated into the following four categories:

1) the interior of the combustion chamber where the actual flame is located

2) the exterior combustion chamber walls and tail pipe

3) the skin of the aircraft which is heated by atmospheric friction at high speeds

4) hot, luminous gases which form the exhaust from the engine.

Each of these sources contribute to the total amount of infrared radiation generated but 2) is the predominant source which will be considered.

The energy from the interior of the combustion chamber, source 1), provides the largest amount of infrared radiation from any part of the plane. However, the energy from this source is highly directive and in normal horizontal flight the satellite's field-of-view would be normal to the direction of maximum radiation and hence very little of the radiation produced by this source would reach the satellite.

Source 2), the exterior combustion chamber walls, provide the most significant amount of infrared energy for the purpose of passive detection by navigation satellites. The walls of the combustion chamber are normally made of material with a much greater emissivity than aluminum (see Section 2.1.3).

The skin of the aircraft, source 3), can be heated to high temperatures by atmospheric friction. The usefulness of this source is limited, however, by the low emissivity of aluminum and the high speeds at which the plane must fly to produce these temperatures. The emissivity of smooth commercially available aluminum alloys varies from 0.02 to 0.07 which makes the skin a very poor infrared source [3, p. 804]. In order to provide significant radiation above the background radiation a plane would have to fly at Mach 2.5 at 40,000 ft. to produce sufficient atmospheric friction [4, p. 190]. The contribution of this source will be approximated (see Section 2.1.3).

The exhaust gases or plume, source 4), may extend several hundred feet behind the plane and reach temperatures over 1500°K depending on the size of the jet engine [3, p. 61]. The spectrum appears to be a weak black body radiation with strong emission lines whose wavelength is determined by the molecular composition of the gas. The black body radiation depends on the emissivity which depends on the density and size of the particles making up the gas. The emissivity factor is only a few per cent at sea level and decreases as much as two orders of magnitude at high altitudes in the desired spectral region due to the reduced atmospheric pressure [5].

The strong emission lines are due to the excitation of various energy levels of the molecules making up the exhaust gases. The exhaust products of the normal organic hydrocarbon jet fuels consist mainly of water and carbon dioxide. H_2O and CO_2 molecules "radiate strongly in the 2 to 3μ band, and CO_2 radiates in the 4 to 5.5μ band" [6, p. 121]. Much of this infrared energy is absorbed by the unexcited H_2O and CO_2 molecules in the atmosphere; however, a small portion is transmitted for the following reason. The radiation emitted from the hot gases does not occur at the same wavelengths as the atmospheric absorption, "since higher transitions are excited as the temperature is raised"

[6, p. 121]. A small contribution from this source will be considered (see Section 2.1.3).

2.1.2 Aircraft Modifications to Increase Infrared Energy Emission

In order to increase the effective output of infrared energy, there are several simple modifications that could be made. The user cannot be classed as an active user through these modifications since they only make use of the thermal energy already in the plane.

The emissivity of the smooth aluminum skin of the plane is very low. Increasing the roughness of the surface can improve the emissivity by an order of magnitude, e.g., 6061 aluminum alloy has an emissivity of 0.04 and sanding can increase the emissivity to 0.41 [3, p. 804]. It would also be possible to get an even greater emissivity by painting the surface of the plane and this would not have the disadvantage of increasing the aerodynamic drag as would increasing the roughness of the surface. Since this modification would be most effective at supersonic speeds, where the infrared energy from the plane body becomes most significant, the paint would have to be able to withstand considerable heat and friction.

Since the combustion chamber radiation is so highly directive, there is little that can be done to increase the infrared output in the direction desired.

The jet engines constitute the main source of useable infrared energy and any increase in their infrared output would aid detection greatly. External thrust chamber walls are usually made of highly emissive material for cooling purposes but some improvement might be made by substituting high emissivity material for the aluminum skin surrounding the other parts of the engine. The added weight and/or drag would probably be the least of any of the other possible modifications.

On many of the larger jet aircraft the engines are placed below and slightly ahead of the wing structure. This may constitute a severe problem since this will result in a shadow when the wing is between the satellite and the engine. A change in placement of the engines would go a long way towards increasing the feasibility of an infrared surveillance navigation satellite system.

The exhaust plume does not present any good possibilities of improving its infrared emission. The emissivity can only be changed significantly by increasing the pressure of the gas, which is not possible. Fuel additives which change the spectral composition of the exhaust gas would also have to change the molecular composition. Anything except the normal hydrocarbon combustion products, H_2O and CO_2, would probably be considered as pollution, and in addition, the amount of additive needed to make any significant change would be prohibitive since it would change the characteristics of the fuel.

The most promising modification seems to be the replacing of the outer engine covering with material of a higher emissivity. Most of the other methods considered are quite impractical.

2.1.3 Calculation of Thermal Energy from Jet Aircraft

Since the resolution of the navigation system will not be sufficient to resolve the structure of individual aircraft the energy from the aircraft can be considered as coming from a point source. The received signal can then be calculated by knowing the solid angle intercepted by the receiving system and the radiant intensity of the source.

The total radiant emittance is given by (2.1-4) for a unit area and the radiant intensity J(W/sr) can be found by adding all the areas of the plane according to (2.1-5) under the assumption of uniform isotropic point sources.

$$J = \frac{\sigma}{2\pi} \sum \epsilon_i T_i^4 A_i \qquad (2.1\text{-}5)$$

where J = radiant intensity in W/sr

$\sigma = 5.673 \times 10^{-12}$ watt/cm^2 deg^4

ϵ_i = emissivity

T_i = absolute temperature in ^oK

A_i = effective area or area seen in the direction for which J is desired in cm^2.

Since the only area that will be considered directly is the exterior combustion chamber wall and tail pipe,(2.1-5) reduces to

$$J = \frac{\sigma}{2\pi} \epsilon T^4 A \qquad (2.1\text{-}6)$$

where the values of ϵ, T and A are those associated with the exterior of the combustion chamber.

The result given by (2.1-6) is valid, provided the source can be considered as a point source. Since the system resolution, determined in Section 2.3, will be insufficient to resolve distances on the order of the size of an aircraft the point source assumption is justified [61,p27]. The diameter of the objective lens necessary to resolve the image of an aircraft is much too large to be practical. The source area which will be considered is the upper half of the exterior of the combustion chamber which explains the fact that the solid angle in the denominator of (2.1-6) corresponds to a hemisphere which is 2π steradians instead of the normally encountered 4π sr.

The high thermal and mechanical stresses which are encountered in the engine require high strength materials. One of the currently popular materials used for exhaust system construction is columbium-stalibized stainless steel [7, p. 201]. Normally stainless steel has an emissivity of approximately 0.2 [3, p. 810] but under such high temperatures a thin layer of oxide will form which raises the emissivity to 0.7 [4, p. 18]. The diameter of jet engines is on the order of 1 m

and the length is approximately 3 to 4 m. The effective area will be chosen as 1.0 m^2 and the exhaust system temperature ranges from 600°K to 1000°K [4, p. 190]. Using these data and the fact that there are four engines on many planes, equation (2.1-6) gives the following results:

$$J = 3.2 \times 10^3 \text{ W/sr} \qquad T = 600^\circ\text{K}$$

$$J = 2.5 \times 10^4 \text{ W/sr} \qquad T = 1000^\circ\text{K}$$

From available data on jet planes [8, p. 25] the infrared energy contributed by the skin and exhaust gases can be approximated as 20% of the total infrared output which will then be estimated as:

$$J = 3.8 \times 10^3 \text{ W/sr} \qquad T = 600^\circ\text{K} \qquad (2.1\text{-}7)$$

$$J = 3.0 \times 10^4 \text{ W/sr} \qquad T = 1000^\circ\text{K} \qquad (2.1\text{-}8)$$

A value of 7.9×10^3 W/sr is reported for the Boeing 707 [61, p. 93]. Since the data available for single engine fighter planes indicate a radiant intensity of 1.2×10^3 W/sr [8, p. 25], the figures above seem reasonable.

Note that the above calculations are quite optimistic in both the assumption of the effective area and the emissivity. It is not expected, however, that the infrared radiant intensity could be less than one order of magnitude lower than the value calculated but this conclusion is greatly dependent on the direction from which the plane is observed, e.g., there will be very little radiation observed viewing the front of the plane [8, p. 25].

2.2 Received Signal Power

The received signal power can be calculated by knowing the radiant intensity of the source in the direction of the receiver and the solid angle intercepted by the receiver. The solid angle Ω can be calculated using the relation:

$$\frac{\Omega}{4\pi} = \frac{\text{Area projected by objective lens}}{\text{Total surface area of sphere with radius equal to distance from source to objective}} \qquad (2.2\text{-}1)$$

In the case where the objective lens is at a large distance from the source, the projected area is equal to the area of the objective lens with the result that (2.2-1) reduces to:

$$\Omega = \frac{\pi d^2}{4 r_s^2} \qquad (2.2\text{-}2)$$

where Ω = solid angle intercepted in sr

d = objective lens diameter in m

r_s = altitude of synchronous satellite in m.

Substituting 36,000 km for the altitude of the satellite gives:

$$\Omega = 6.08 \times 10^{-16} d^2 \qquad (2.2\text{-}3)$$

Equation (2.2-3) is plotted in Fig. 1.

The total received power is (assuming no atmospheric attenuation)

$$P_r = J \Omega \qquad (2.2\text{-}4)$$

where J is given by (2.1-7) or (2.1-8) and Ω is given by (2.2-3). The total received power for the two radiant intensities calculated previously is plotted in Fig. 2 as a function of the objective lens diameter. The received power will be attenuated when it traverses the atmosphere, but if the plane flies at an altitude of 40,000 ft or more then approximately 99% of the cloud formations and atmosphere will be below the plane [3, p. 122] and for this reason atmospheric attenuation will be neglected. Since the density of the atmosphere decreases almost exponentially with altitude [32, p. 2-1] the atmospheric attenuation will be much less for higher altitudes.

2.3 Image Resolution

The resolution of an electro-optical system employing a television camera can be considered as being limited by four different factors:

1) diffraction limitations
2) the optical quality of the components
3) the number of lines in the television picture
4) random variations in the index of refraction along the transmission path.

The resolution of the system is only as good as the resolution in the worst case and can be no better than the limit given by the Rayleigh criterion (diffraction limitation caused by the wavelength of the light).

With the use of computer programs for lens design, the quality of the optical components available is such that the resolution is only limited by cost considerations. Hence, the optical quality of the components will be neglected in considering the resolving power of the system.

The diffraction limitation provides the fundamental criterion for resolution of the system and the number of lines in the television

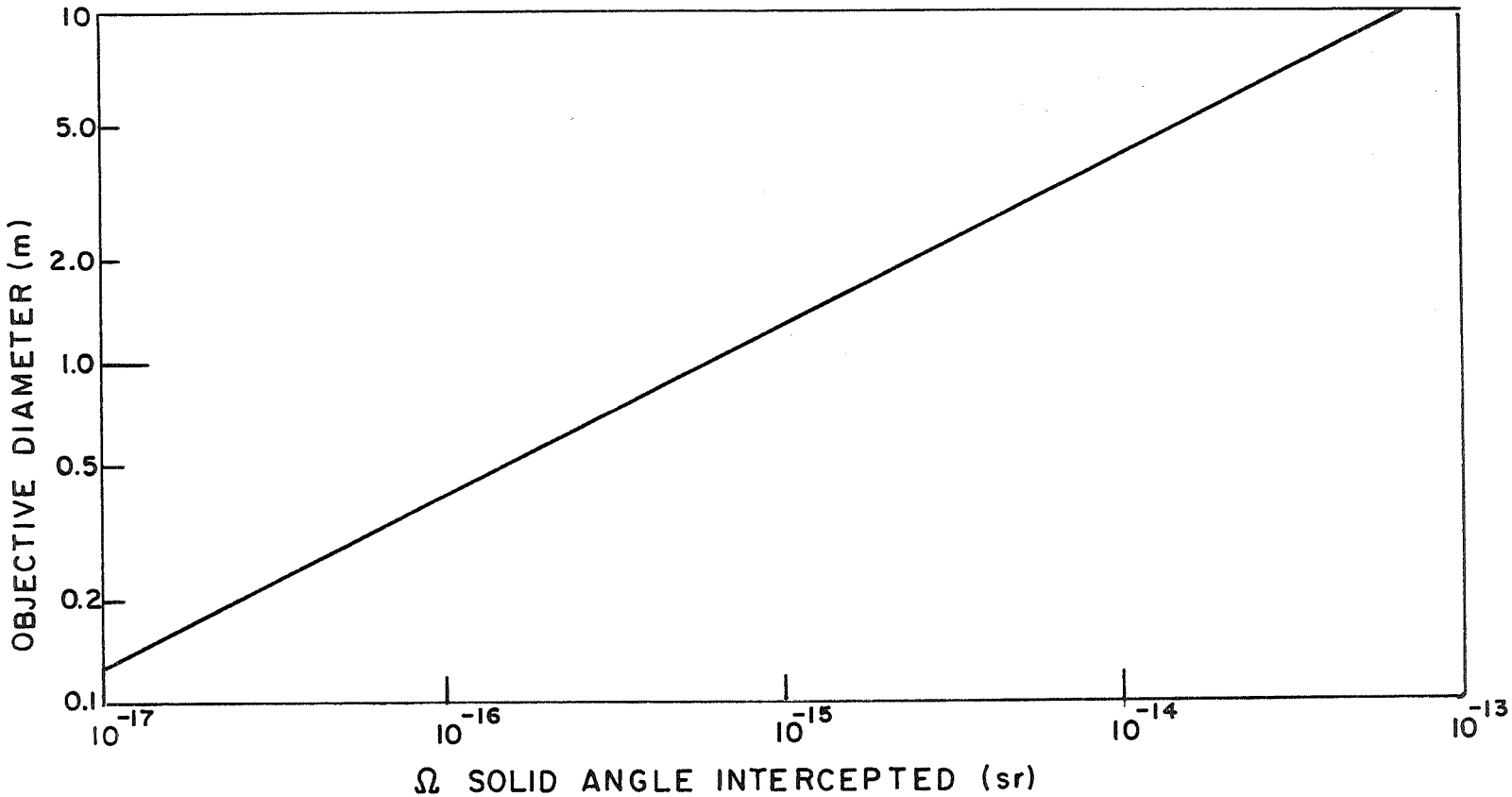

FIGURE I SOLID ANGLE INTERCEPTED BY THE OBJECTIVE

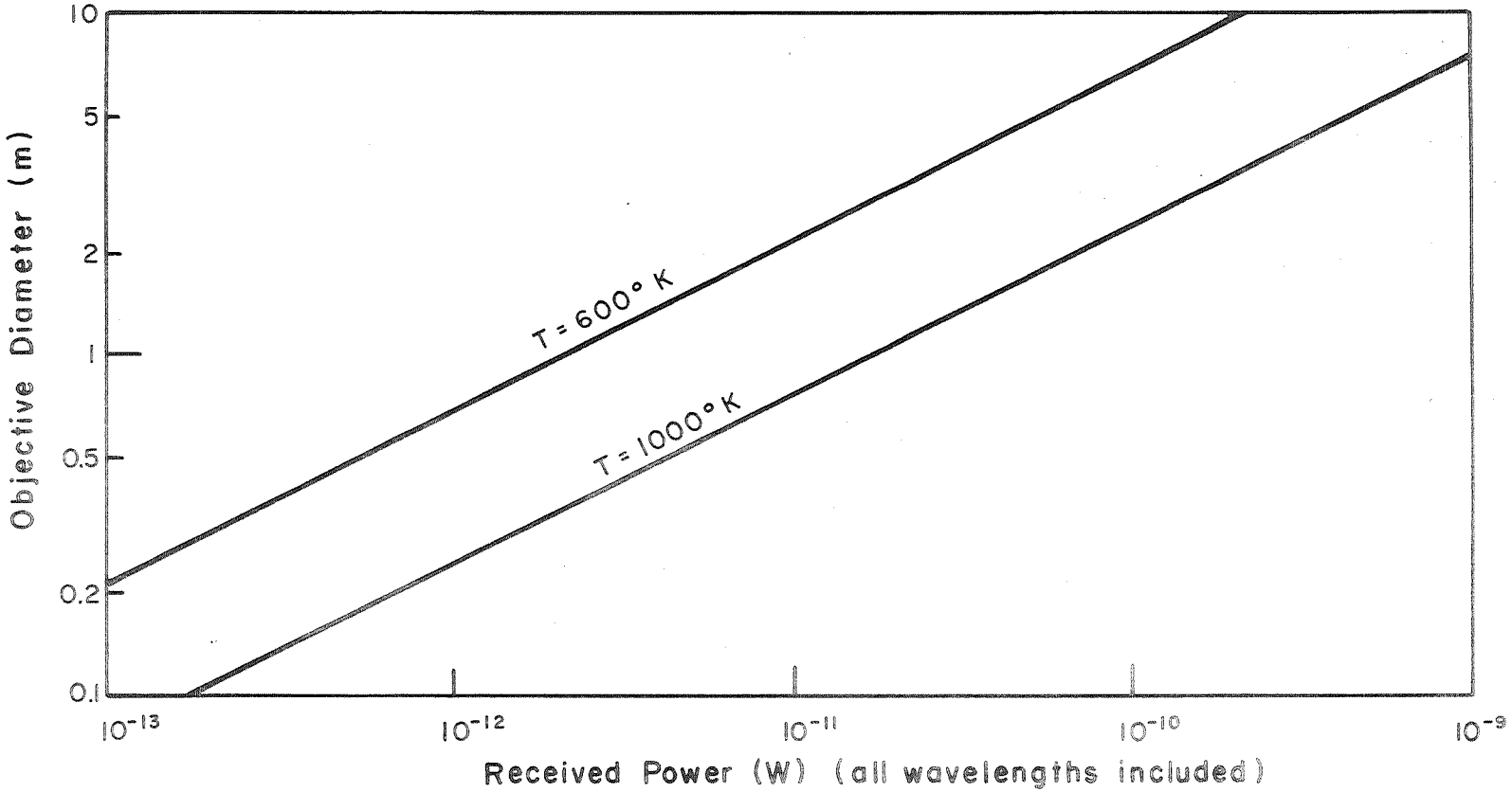

FIGURE 2 RECEIVED POWER AS A FUNCTION OF SOURCE TEMPERATURE AND OBJECTIVE DIAMETER

picture cannot exceed this limit. In other words, increasing the number of lines cannot increase the angular resolution beyond the diffraction limit.

In the following graphs and in most graphs in Section 2, the results presented will be for the user at the subsatellite point. For any other position the results must be changed to account for the geometrical dilution of precision caused by the projection of the diffraction limit on the surface of the earth (see Appendix A). The ground resolution given in Figs. 4 and 5 must be multiplied by the geometrical dilution of precision (GDOP) factor given in Fig. 3 when the user is not at the subsatellite point. In some cases, however, it would be very difficult to incorporate the GDOP factor in the results.

2.3.1 Resolution in Diffraction-Limited Systems

The angular image size of a point source in a perfect incoherent optical system with sufficient illumination is given by (2.3-1)[3, p.449]

$$\beta_r = \frac{2.44\,\lambda}{D} \qquad (2.3\text{-}1)$$

where β_r = angular image size

λ = wavelength of the radiation

D = diameter of the objective lens.

The angular resolution of a system will be defined as the angular separation between two equal intensity point sources at which the images just touch on the outer edge of the central region. The images actually look like a central region with several surrounding concentric rings but the rings will be neglected since the majority ($\sim 84\%$) of energy is in the central region. Equation (2.3-1) gives the angular size of the central region and from the definition just given it also gives the smallest resolvable angular separation between two point sources. Note that the result given by (2.3-1) is twice the size normally specified by the Rayleigh criterion [9, pp. 578-579]. The Rayleigh criterion is (2.3-1) divided by 2. In the Rayleigh criterion the centers of the images need only be separated by the radius of the images for resolution, while for (2.3-1) the centers must be separated by the diameter of the images. It was felt that (2.3-1) represents a more realistic limit in a system using a television camera than the Rayleigh criterion.

For an angular resolution limit given by (2.3-1) the ground resolution limit at the subsatellite point of a synchronous satellite at altitude r_s is:

$$r_g = \frac{2.44\,\lambda\, r_s}{D} \qquad (2.3\text{-}2)$$

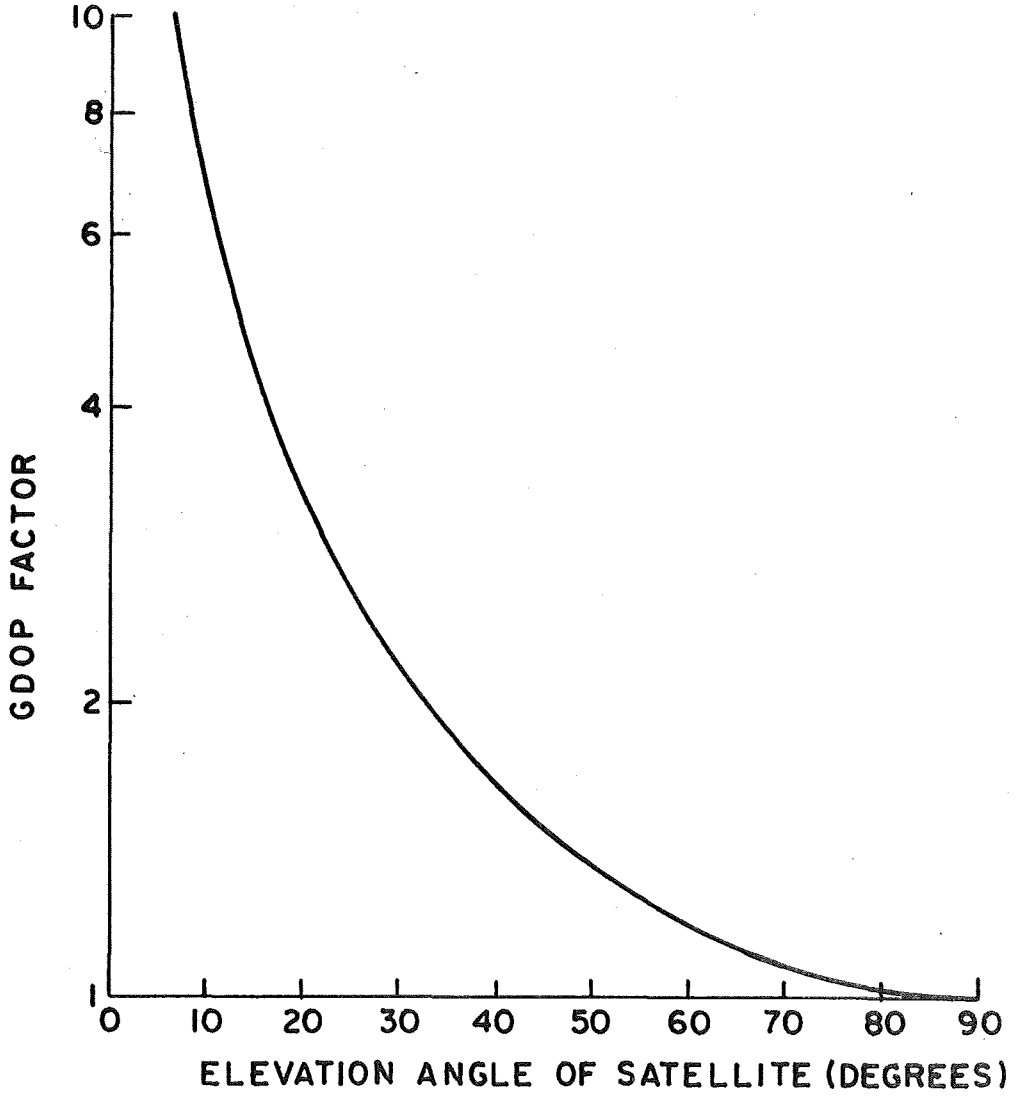

FIGURE 3. GDOP FACTOR PLOTTED AS A FUNCTION OF USER ELEVATION ANGLE.

where r_g = ground resolution.

The wavelength used will be the wavelength at which the maximum amount of radiant energy is emitted. The wavelength at which the maximum occurs is given by the Wien displacement law [3, p. 107]:

$$\lambda_m = \frac{K}{T} \qquad (2.3\text{-}3)$$

where K is a constant and for λ in microns, T in ^{o}K, K = 2897.9. Combining (2.3-2) and (2.3-3) and substituting the value of r_s gives

$$r_g = \frac{260}{DT} \qquad (2.3\text{-}4)$$

where r_g = ground resolution in km
D = objective diameter in m
T = source temperature in ^{o}K.

Equation (2.3-4) is plotted in Fig. 4 for some typical jet engine exhaust system temperatures.

The diffraction limit applies to all optical systems and it is easy to see that visible light ($\lambda \approx 0.55\ \mu$) would provide the same ground resolution with a much smaller objective lens than infrared.

In these calculations no consideration has been made for random variations in the index of refraction in the atmosphere due to wind and other phenomena which may make the calculated results overly optimistic (see Section 3.4.3).

2.3.2 Television Camera Limitations on Resolution

The fundamental limitation provided by a television camera is in the number of lines. For a camera system with an angular field-of-view FOV, the maximum angular resolution capability β_t for N TV lines is (see Appendix B)

$$\beta_t = \frac{FOV}{N} \qquad (2.3\text{-}5)$$

For a synchronous satellite at an altitude of r_s the best ground resolution possible with N TV lines is

$$r_g = \frac{r_s\ FOV}{N} \qquad (2.3\text{-}6)$$

where FOV is in radians. Hence, for given ground resolution, the number of television lines required for a ground resolution r_g is

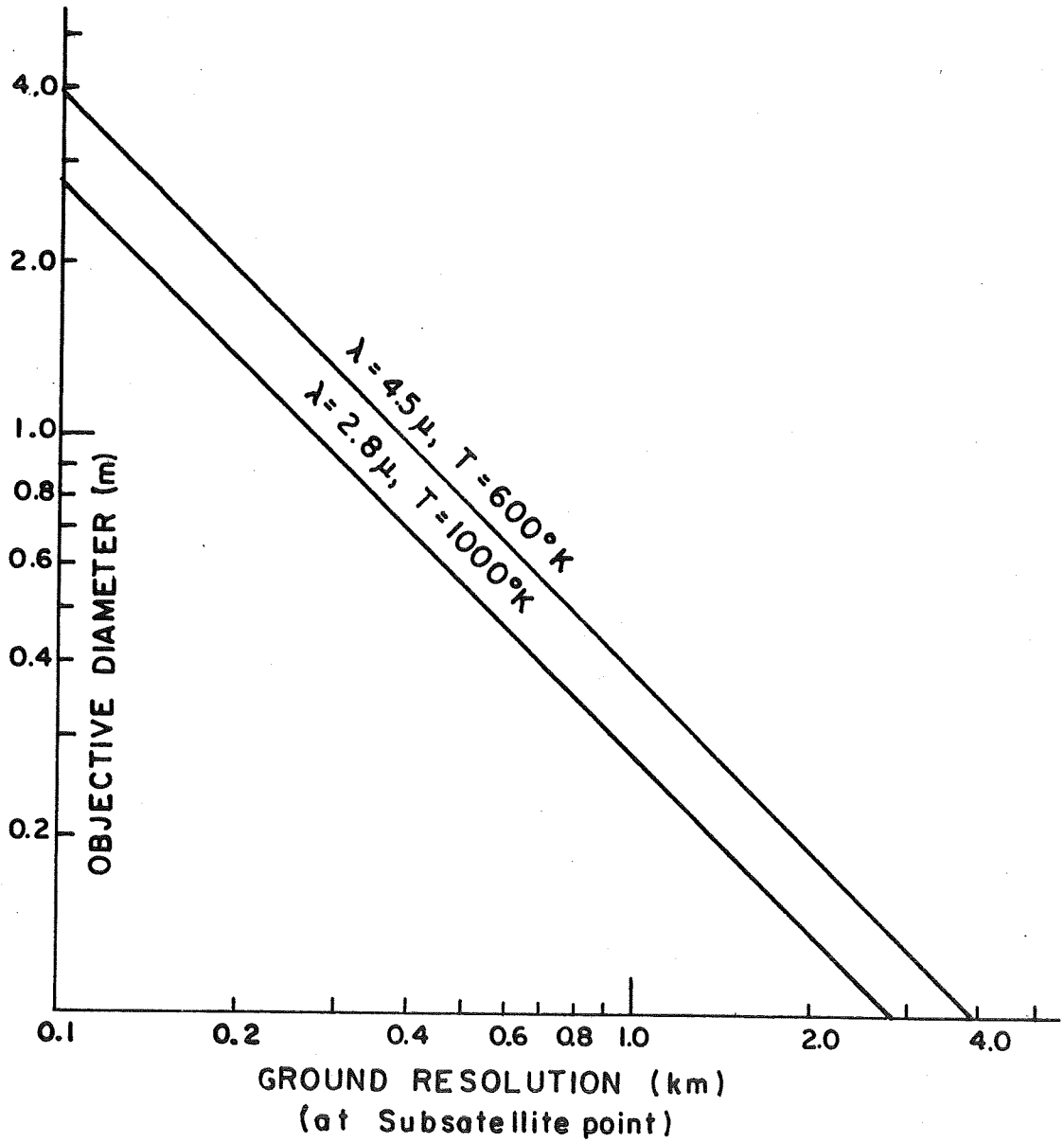

FIGURE 4 DIFFRACTION LIMITED GROUND RESOLUTION VS. OBJECTIVE DIAMETER.

$$N = \frac{r_s \, FOV}{r_g} \qquad (2.3\text{-}7)$$

where N = number of TV lines required (see Appendix B)

FOV = field-of-view in radians

r_s = synchronous altitude

r_g = ground resolution (same units as r_s).

Equation (2.3-7) is valid provided the angular resolution β_t is greater than the angular resolution available in the image β_r. In order for (2.3-7) to hold $\beta_t \geq \beta_r$ or in terms of the ground resolution using (2.3-4) and (2.3-7) the required condition is

$$\frac{260}{DT} \leq \frac{r_s \, FOV}{N} \qquad (2.3\text{-}8)$$

where D = diameter of objective in m

T = source temperature in ^{o}K

r_s = synchronous altitude in km

FOV = angular field-of-view in radians

N = number of TV lines.

The equality holds when the television camera resolution is equal to the diffraction limit.

Equation (2.3-7) is plotted in Fig. 5 for an 8^{o} field-of-view which is sufficient to cover most of the North Atlantic Ocean. The condition specified by (2.3-8) is also noted on the figure. For comparison a 2^{o} and a 16^{o} field-of-view have been used in eq. (2.3-7) and the results are also plotted in Fig. 5. The 16^{o} field-of-view is sufficient to cover most of the portion of the earth visible from the satellite while the 2^{o} field-of-view would be sufficient to cover the Northeastern United States. The majority of calculations will be done using the 8^{o} field-of-view.

Considering the present state of the art [1, 17, 25, 58] it is reasonable to expect that television cameras with over 10,000 line resolution will be available by 1970. Using this figure the results plotted in Fig. 5 show that an objective diameter of at least 1 m would be necessary. The objective diameter (1 m) was chosen as being realistic with respect to size and weight limitations (a lens of 1 m diameter could weigh several hundred pounds). In addition, a lens (or reflector) of this diameter can be made essentially optically perfect, i.e., flat to within 0.10 λ where λ is the wavelength of the light and in the case of 2-5μ light this would be on the order of 0.2μ. With a 1 m objective lens and a 10,000 line television camera, the ground resolution at the sub-satellite point would be approximately 0.5 km.

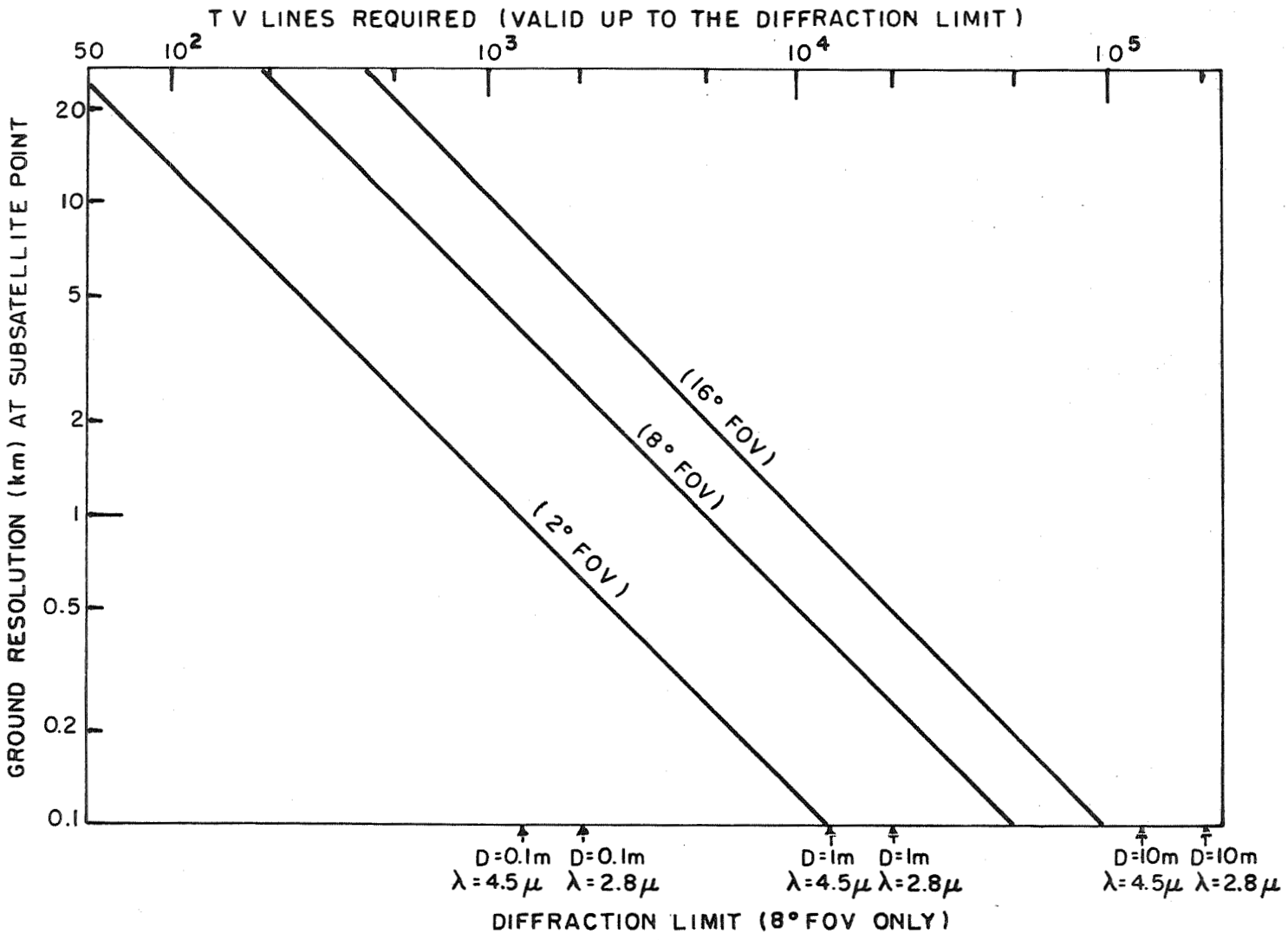

FIGURE 5 TELEVISION LINES REQUIRED FOR GIVEN GROUND RESOLUTION

2.4 Image Exposure Time

The maximum image exposure time which can be used is limited by the motion of the user and the motion of the satellite. Although the image exposure time is not used in the calculation of the signal-to-noise ratio in the passive case the exposure time must be sufficiently long to allow the detector to respond to the signal available.

In order to know the image exposure time necessary to stop the observed motion, the length of time in which the image motion is negligible must be known. The effect of the motion of the object observed will be greatest at the subsatellite point. The image exposure time must be less than the time it takes for the image of one user to travel from one resolvable picture element to the next. The element-to-element transition time can be calculated by dividing the ground resolution distance, which corresponds to a center-to-center transition from one resolvable picture element to the next, by the ground speed. Dividing (2.3-6) by the ground speed gives

$$T = \frac{r_s \, FOV}{NS} \qquad (2.4\text{-}1)$$

where N = number of TV lines

T = element-to-element transition time in seconds

r_s = synchronous satellite altitude in m

FOV = angular field-of-view in radians

S = ground speed in m/seconds

Considering an 8^o field-of-view and using suitable conversion factors, (2.4-1) reduces to

$$T = \frac{1.12 \times 10^7}{NS} \qquad (2.4\text{-}2)$$

where T = element-to-element transition time in seconds

N = number of TV lines

S = ground speed in mi/hr

Equation (2.4-1) is plotted in Fig. 6 for some speeds that might be expected for aircraft like the SST. The transition time must be multiplied by the GDOP factor for user positions other than at the subsatellite point. Note that these calculations assume that the optical system is capable of the resolution required so these results are valid up to the diffraction limit on the number of lines.

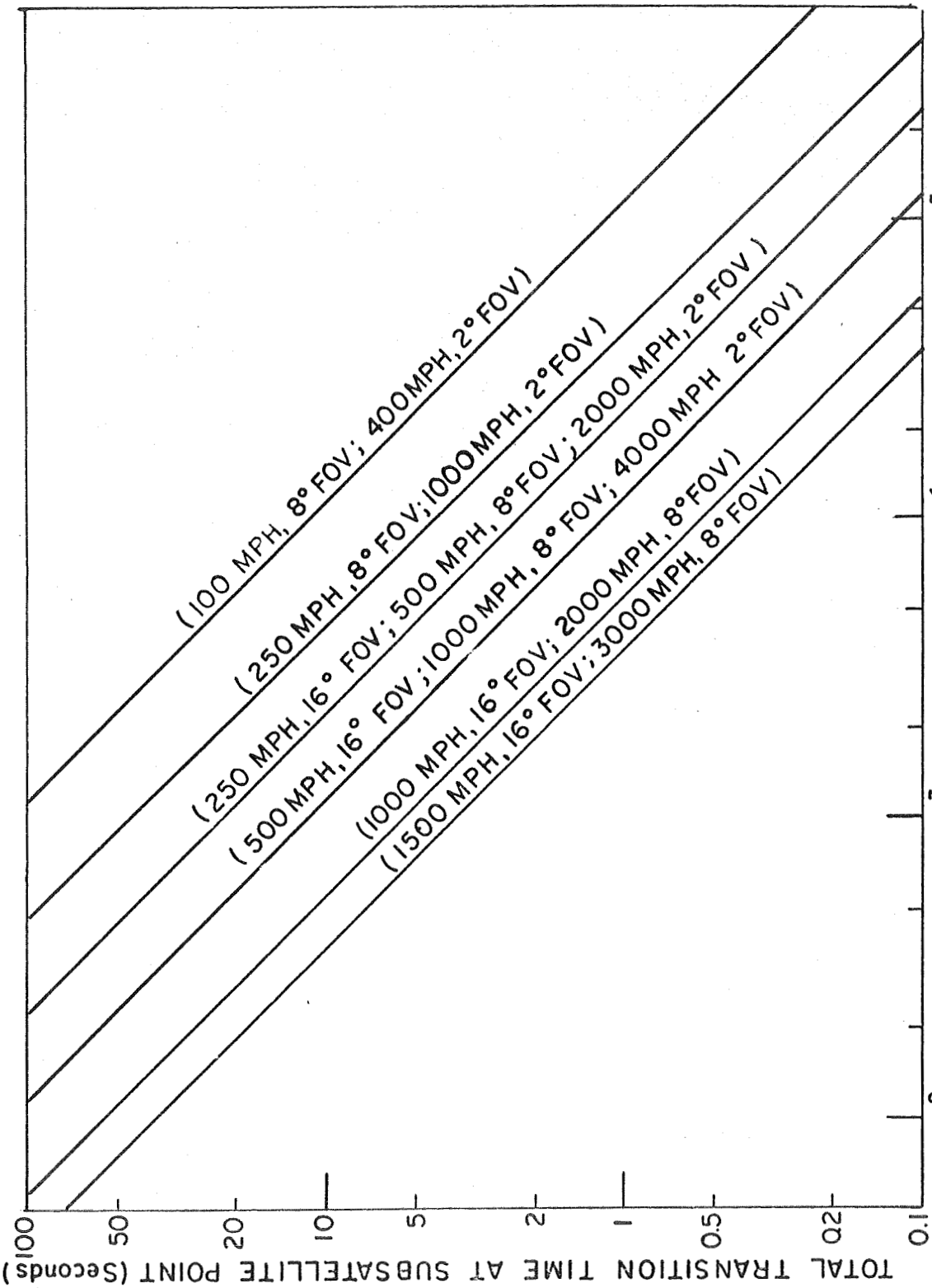

FIGURE 6 ELEMENT-TO-ELEMENT TRANSITION TIME

The transition time calculated using (2.4-2) is the total transition time. If it is assumed that the energy density of the user image decreases linearly as the user image moves to the next picture element then the user signal will decrease to 50% of its original value in half the transition time. Using the assumption of a state-of-the-art of 10,000 television lines and an image exposure time equal to half the total transition time, the maximum image exposure time in which the image motion will be negligible is 0.2 s.

While an exposure time of 0.2 s may not be possible due to motion of the satellite there are several useful conclusions that can be drawn from it. Slow-scan techniques could be used to lengthen the observation time in order to allow greater resolution of weak signals. If statistical processing of the received information is performed then a longer observation time will yield better results. It is easy to see that there is little to be gained by using a frame rate greater than 5 per second since very little will have changed from the previous frame. Since the GDOP factor will lengthen the transition time the average image motion over the whole image may be so slight as to allow a frame rate of only one in several seconds to convey all the desired information.

In addition to stopping the image motion due to a moving target the exposure time must be short enough to stop any image motion due to the movement of the satellite. If it is assumed, as before, that the user image intensity at a resolvable image element reduces linearly as the target moves away then the point at which image degradation takes place can be taken as the point where the image intensity is reduced to 50% of its maximum value. The image degradation is then equivalent to a target movement of $r_g/2$ if the satellite is perfectly stable. If a satellite at distance r_s is revolving with an angular rotation rate θ' then the equivalent ground movement is $\Delta T \theta' r_s$ where ΔT is the length of time being considered. If the degradation point is an equivalent ground movement of $r_g/2$ then ΔT, the maximum image exposure time, will occur when ΔT = image exposure time

$$\frac{r_g}{2} = \Delta T \theta' r_s \qquad (2.4\text{-}3)$$

where r_g = ground resolution in km
r_s = satellite distance in km
θ' = rate of angular rotation in rad/s
ΔT = image exposure time in sec

Hence

$$\Delta T = \frac{r_g}{2 r_s \theta'} \qquad (2.4\text{-}4)$$

Equation (2.4-4) is plotted in Fig. 7 for a typical range of rotation rates.

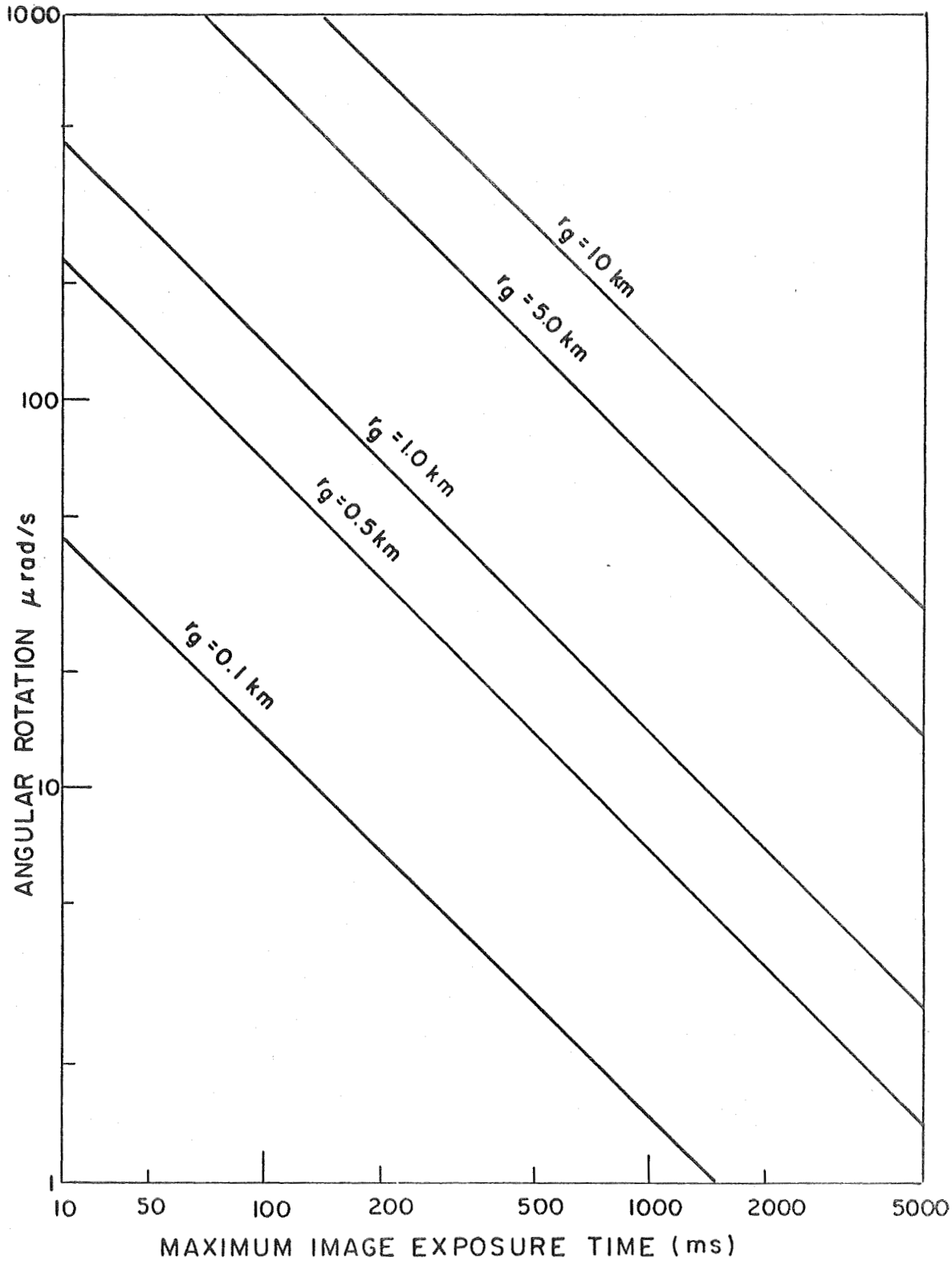

FIGURE 7 EXPOSURE TIME VERSUS ANGULAR ROTATION RATE

For an objective diameter of 1 m, 10^4 television lines, and an 8^o field-of-view, the ground resolution would be about 0.5 km. A typical rate of movement in a well-stabilized satellite might be 30 μrad/s giving a maximum image exposure time of 0.2s as before.

2.5 Determination of the Optimum Spectral Region for Passive User Detection

In choosing the optimum spectral region to use for a passive user navigation system there are two basic factors that must be considered. In order to detect a target at a given temperature a spectral region must be chosen which contains as much of the energy for that particular temperature as possible. The radiation from higher temperature black bodies will be at the shorter wavelengths and that of a lower temperature black body at longer wavelengths. The temperature range of the target (600^oK - 1000^oK) is above that of the earth ~ 250^oK and below that of the sun 5800^oK; hence, the shorter wavelength cutoff must be chosen to eliminate sunlight and the longer wavelength cutoff must be chosen to eliminate background radiation from the earth. The low average earth temperature is due to the fact that some of the infrared energy seen outside the atmosphere comes from the cold upper layers of clouds containing ice crystals. Further discussion of these topics is given in Sections 2.7 and 3.5.

In order to find the optimum spectral region the amount of energy in a given spectral region must be known. The percentage of energy below a given wavelength is found by integrating (2.1-1) from 0 to the desired wavelength λ_c and dividing by the total energy given by (2.1-2) which gives

$$E_\lambda = 100 \int_0^{\lambda_c} \frac{c_1 \, d\lambda}{\sigma T^4 \lambda^5 \left(e^{c_2/\lambda T} - 1 \right)} \qquad (2.5\text{-}1)$$

Since no explicit form yet exists for finite limits on this integral a numerical integration is necessary. A computer evaluation of (2.5-1) has been performed for some typical passive user temperatures and earth background temperatures which might be encountered. Tables for the evaluation of the black body radiation functions (2.1-1) and (2.5-1) are also available [10]. Computer programs are necessary to evaluate the radiation functions for temperatures and wavelengths which are not covered in the available tables. The results of these calculations are given in Figs. 8 and 9. Figure 8 shows that a considerable amount of signal energy lies between 2 and 8μ. Figure 9 shows that a considerable amount of the background radiation from the earth lies above 6μ.

Using Fig. 8 the amount of energy in some possible spectral regions has been determined for the temperature range of interest and the results are given in Fig. 10. The range which has been chosen for consideration is the 2 to 6μ range. Extending the range down to 1μ will at most increase the signal power by 6% but a considerable amount of the sun's energy lies in the 1 to 2μ region. Increasing the range to 7μ will increase the background noise from the earth by an average of 2.5 times

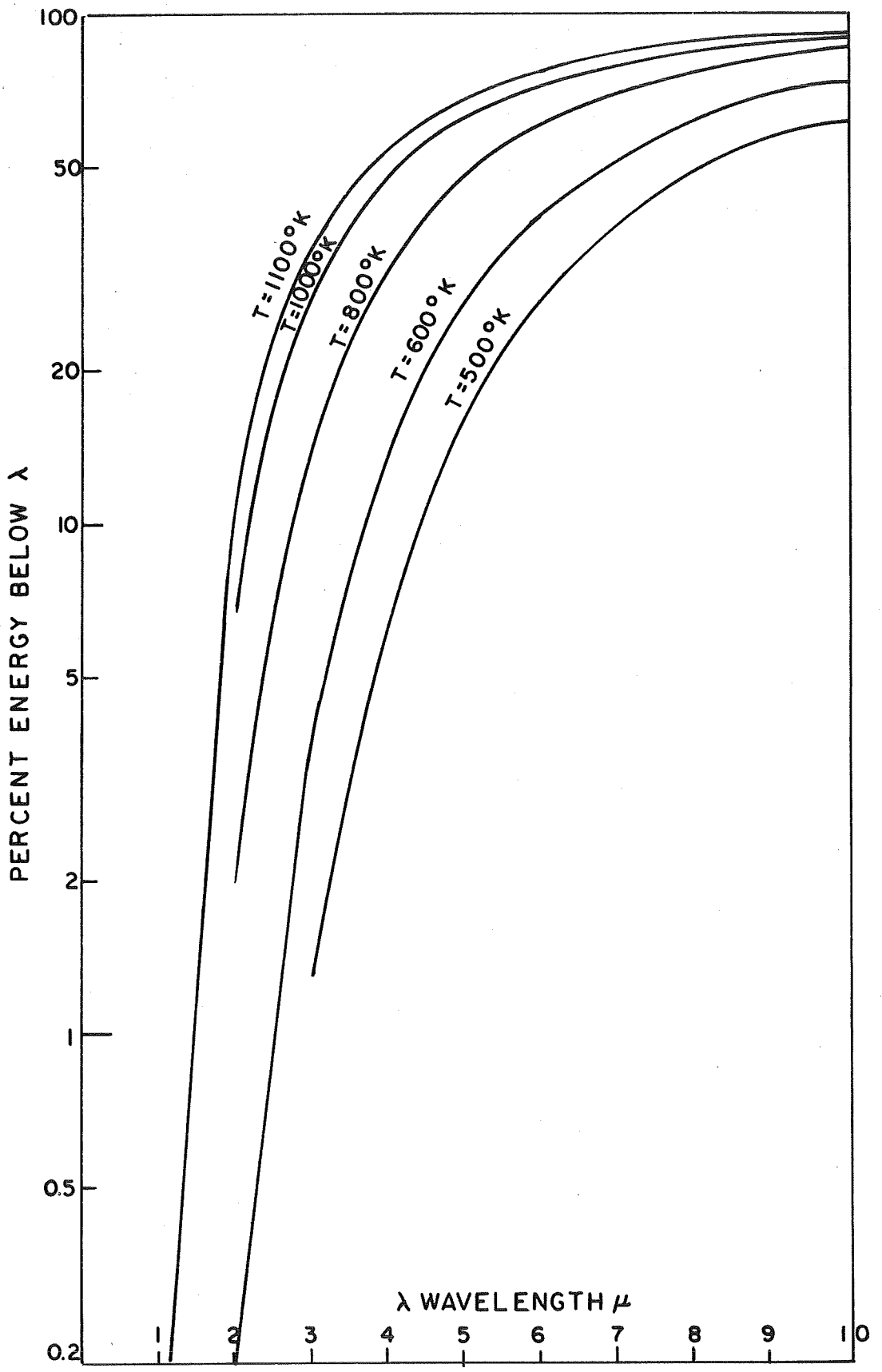

FIGURE 8 SPECTRAL DISTRIBUTIONS FOR VARIOUS SOURCE TEMPERATURES.

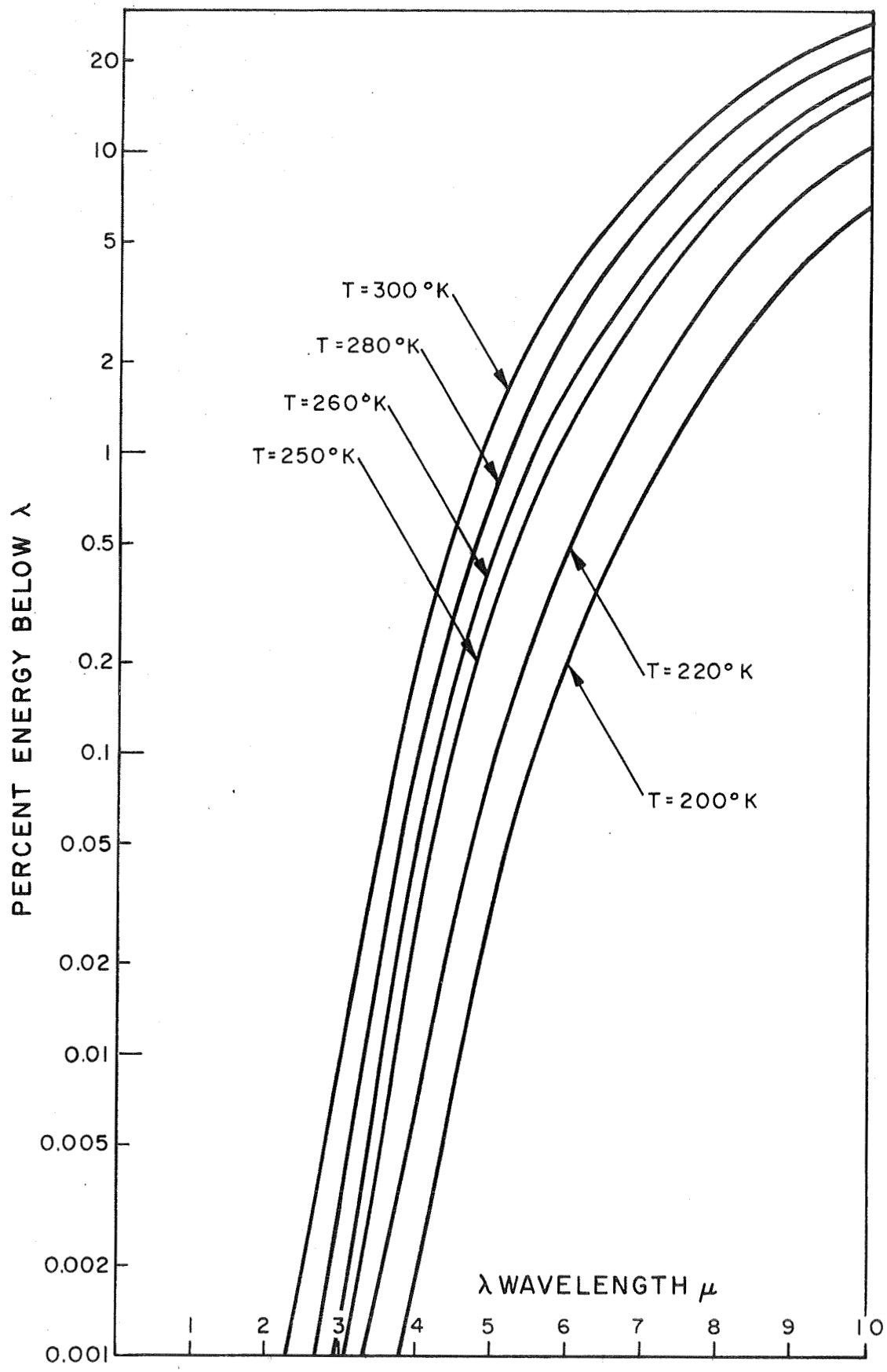

FIGURE 9 SPECTRAL DISTRIBUTIONS FOR VARIOUS BACKGROUND TEMPERATURES

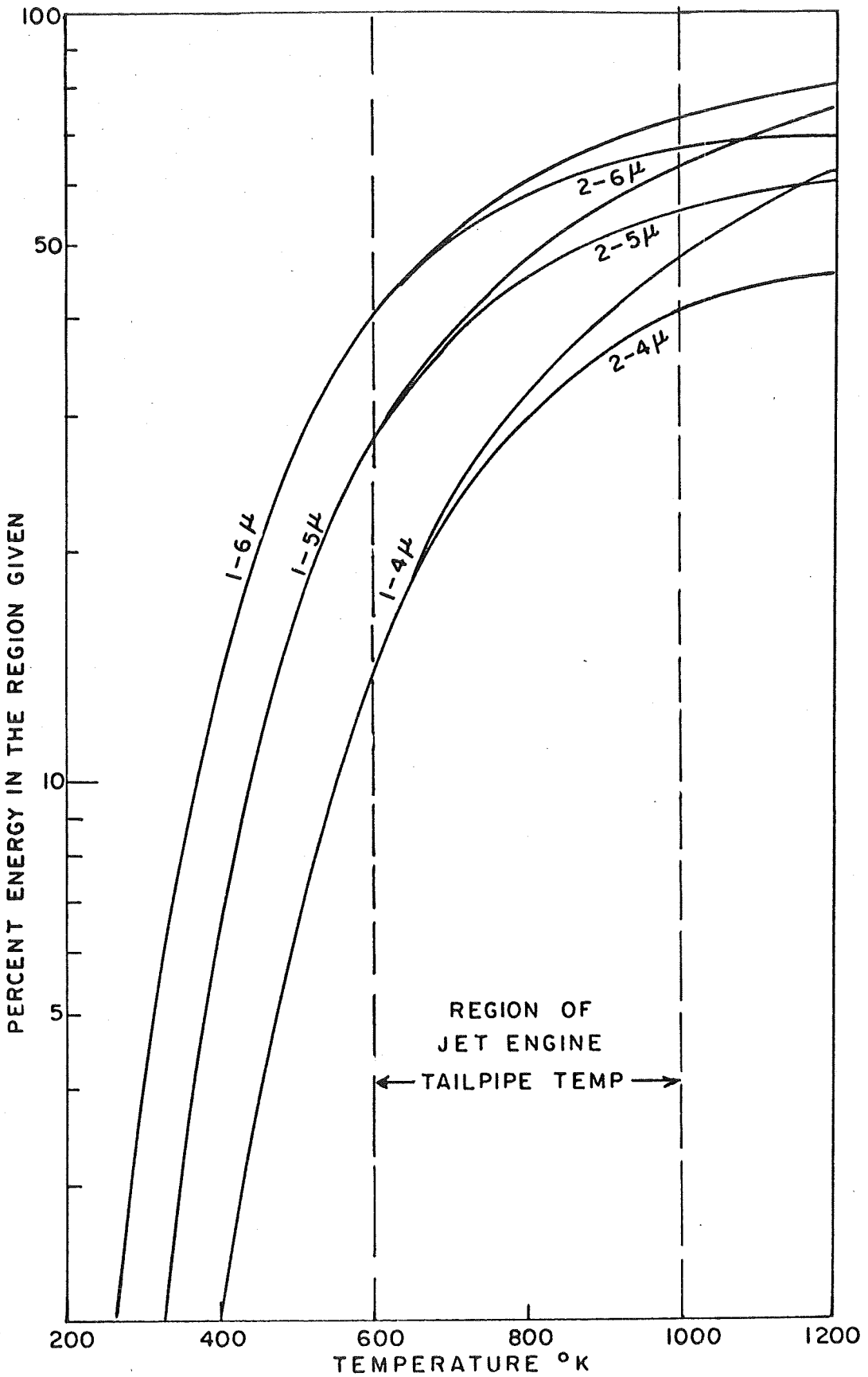

FIGURE 10 ENERGY DISTRIBUTIONS FOR VARIOUS SPECTRAL REGIONS

and hence the SNR will decrease by a factor of 2.5. The only real test of the optimality of the spectral region chosen is to determine the signal-to-noise ratio and find if any other region can significantly improve the SNR without greatly reducing the received power.

2.6 Atmospheric Attenuation Due to Scattering (Infrared Region)

Previously, the effects of atmospheric attenuation were neglected since the aircraft was flying at a high altitude. In order to further justify the conclusion that the system being considered would not work for users flying under a cloud cover one of the factors involved in atmospheric attenuation will be examined. Atmospheric attenuation may be caused by selective absorption by the molecules of the medium or scattering by the molecules and particles in the path. In this section the effect of scattering will be investigated.

For the infrared wavelengths being considered the type of scattering that will be considered is Mie scattering (i.e. larger particle scattering). The transmission factor, or ratio of received intensity to transmitted intensity for a narrow beam expressed as a fraction or a percentage, is given by (2.6-1) for a vertical atmospheric path from altitude R_1 to R_2 [11, p. 17].

$$T = \exp\left[H_m \sigma(0) \left(e^{-\frac{R_2}{H_m}} - e^{-\frac{R_1}{H_m}} \right) \right] \qquad (2.6\text{-}1)$$

where T = ratio of received intensity to source intensity (transmission factor)

H_m = 1.2 km = Mie scale factor from empirical data

$\sigma(0)$ = Mie scattering coefficient for the wavelength being considered at sea level

R_2 = upper altitude in km

R_1 = lower altitude in km.

The two exponentials result from the fact that the intensity ratio decreases exponentially with distance and the scattering coefficients decrease as the atmospheric pressure which also decreases exponentially. Although most data available on the scattering coefficient are for the visible region [12] it can be estimated that the scattering coefficient for 2 to 6μ is equal to approximately one-fifth of the visible region scattering coefficient [13, pp. 32-33]. Equation (2.6-1) has been evaluated for several different path lengths of interest and the results have been plotted in Fig. 11 with the various meteorological conditions specified in terms of the scattering coefficient (see Table 3).

The result given by (2.6-1) is valid provided the attenuation due to scattering is much greater than the attenuation due to absorption. If, at a particular wavelength, both attenuation due to scattering and attenuation due to absorption occur, then the total overall transmission

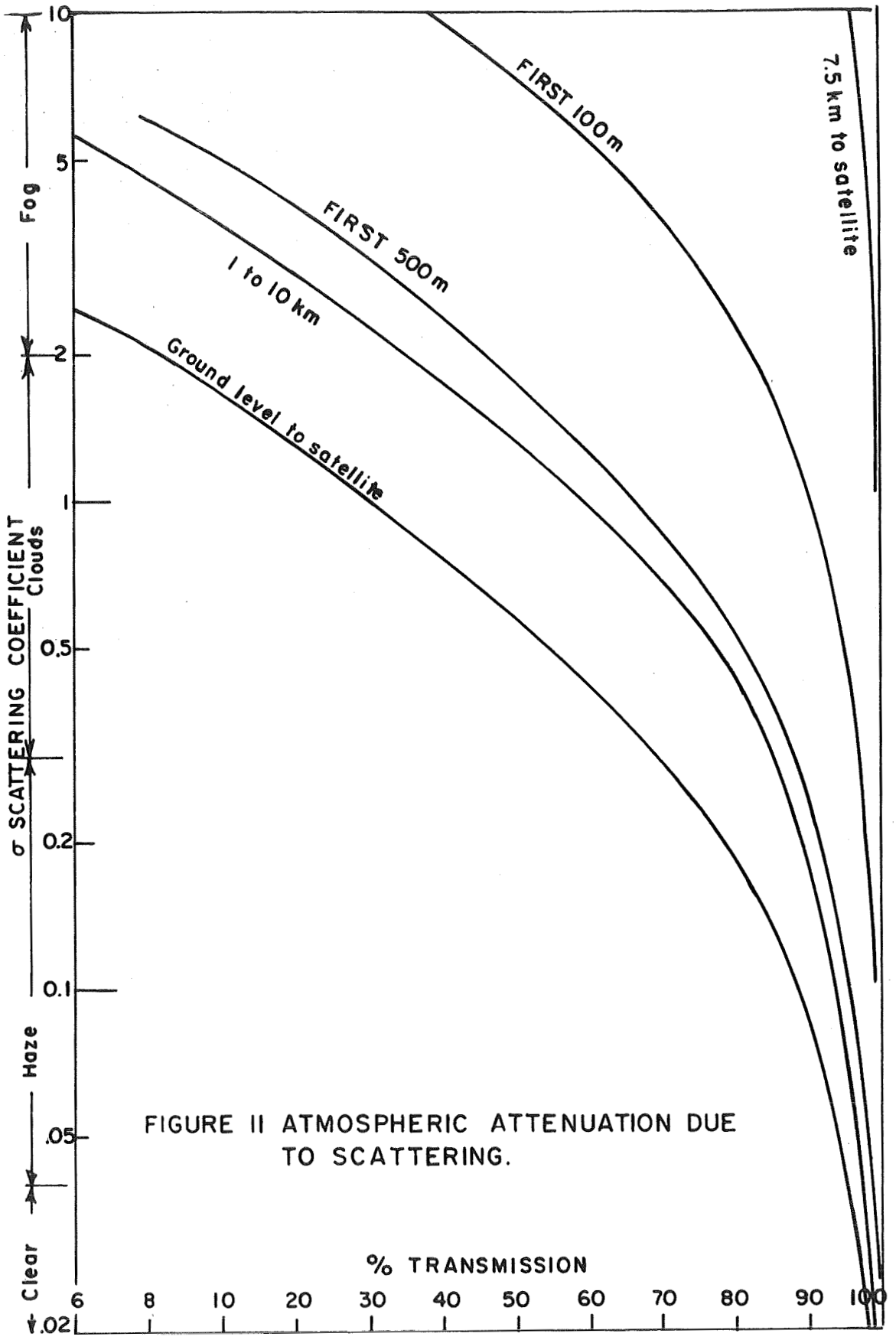

FIGURE II ATMOSPHERIC ATTENUATION DUE TO SCATTERING.

factor will be much less than that indicated by (2.6-1). The results given in Fig. 11 thus represent an optimistic calculation of the attenuation under the assumption the atmospheric absorption is negligible. In the region 2 to 6μ the assumption of negligible absorption is valid in the so-called "atmospheric windows" which are 2.0-2.4μ, 3.4-4.1μ and 4.6-5.1μ. In these regions the absorption normally results in an average transmission factor greater than 0.60 while outside these regions the transmission factor is often below 0.01 [13]. The assumption of negligible atmospheric absorption is valid even outside the atmospheric windows in the case of relatively low scattering coefficients, i.e., in fair weather. The reason for this is that water vapor and droplets, carbon dioxide, and ozone are responsible for the major part of atmospheric absorption while the most common atmospheric gases, oxygen and nitrogen, have very weak absorption bands in the infrared [6, p. 43].

Note that the scattering coefficient is assumed to be "constant" along a path length except for its variation with altitude, i.e., the meteorological conditions are the same along the path. Actually this cannot be true since clouds will only occupy a very small fraction of the path length. The conclusion drawn from Fig. 11 is that atmospheric attenuation due to scattering occurs primarily in the lowest altitude portion of the path travelled. For users on the ground most attenuation would occur in the first 500 m and for planes above 7.5 km, the attenuation due to scattering is entirely negligible. The average user altitude must therefore be as high as possible to insure the feasibility of an optical navigation system. Additional information on scattering and attenuation is given in Section 3.3.

2.7 Analysis of the Signal-to-Noise Ratio in the Passive Case

In order to draw a final conclusion on the feasibility of an optical navigation system with passive users it is necessary to evaluate the signal-to-noise ratio at the satellite to determine the probability of detection. For the purposes of this calculation only the background radiation from the earth will be considered.

To evaluate the irradiance at the satellite due to the earth's infrared emission, the following equation will be used [8, p. 12; 61, pp. 27-30;]:

$$H = \frac{WA}{\pi r^2} \cos \theta \qquad (2.7\text{-}1)$$

where H = irradiance in W/m^2

W = power emitted by a black body

A = area of the black body

θ = complement of the elevation angle

r = distance from A to the detector

If the source area A is not plane then an integral form of (2.7-1) must be used:

$$H = \int_A \int \frac{W}{\pi r^2} \cos\theta \, dA \qquad (2.7\text{-}2)$$

where A is the surface area of the earth which is seen in the image focused on the TV camera. In order to evaluate (2.7-2) a numerical integration was performed (see Appendix C) for an area A specified by the great circle distance covered in the image. The numerical integration was performed over a circular area and since the area, and hence the radiant emittance, is approximately equal to the square of the great circle distance covered the results should appear as a straight line when plotted on log-log graph paper.

The numerical integration required determining the distance to the user and the elevation angle in terms of the synchronous altitude, earth radius and great circle distance shown in Fig. 12. Using the geometrical relationships, the following results are obtained:

$$r = \left[r_s^2 + 2r_e r_s \left(1 - \cos \frac{d\Delta}{r_e} \right) + 2r_e^2 \left(1 - \cos \frac{d\Delta}{r_e} \right) \right]^{1/2} \qquad (2.7\text{-}3)$$

$$\theta = \tan^{-1} \left[\frac{r_e \sin \frac{d\Delta}{r_e}}{r_s + r_e \left(1 - \cos \frac{d\Delta}{r_e} \right)} \right] + \frac{d\Delta}{r_e} \qquad (2.7\text{-}4)$$

where θ = complement of the elevation angle

r = distance from the satellite to the elemental area dA

$d\Delta$ = GCD = great circle distance

r_e = radius of the earth

r_s = synchronous satellite altitude.

Using these relationships, eq. (2.7-2) was evaluated numerically for incremental areas of 100 sq. km for circular regions having a given diameter (great circle distance). The results are plotted in Fig. 13. Note that the background noise power density is directly proportional to the square of the great circle distance up to a distance of about 7000 km where the cosine factor and distance increase have more of an effect. In order to check the validity of the numerical integration (2.7-1) will be evaluated for a plane area having a diameter of 10^4 km. Since the cosine factor and distance increase will be neglected the resulting background noise power density should be somewhat larger than that predicted by Fig. 13.

$$H = \frac{WA}{\pi r^2} = \frac{\sigma T^4 A}{\pi r^2} = \frac{5.673 \times 10^{-8} (250)^4 \pi (10^4)^2}{\pi (3.6 \times 10^4)^2 \, 4} = 4.09 \text{ W/m}^2 \qquad (2.7\text{-}5)$$

The result of (2.7-5) is about 28% higher than the value found in Fig. 13. For a great circle distance of 10^4 km which justifies the results of the

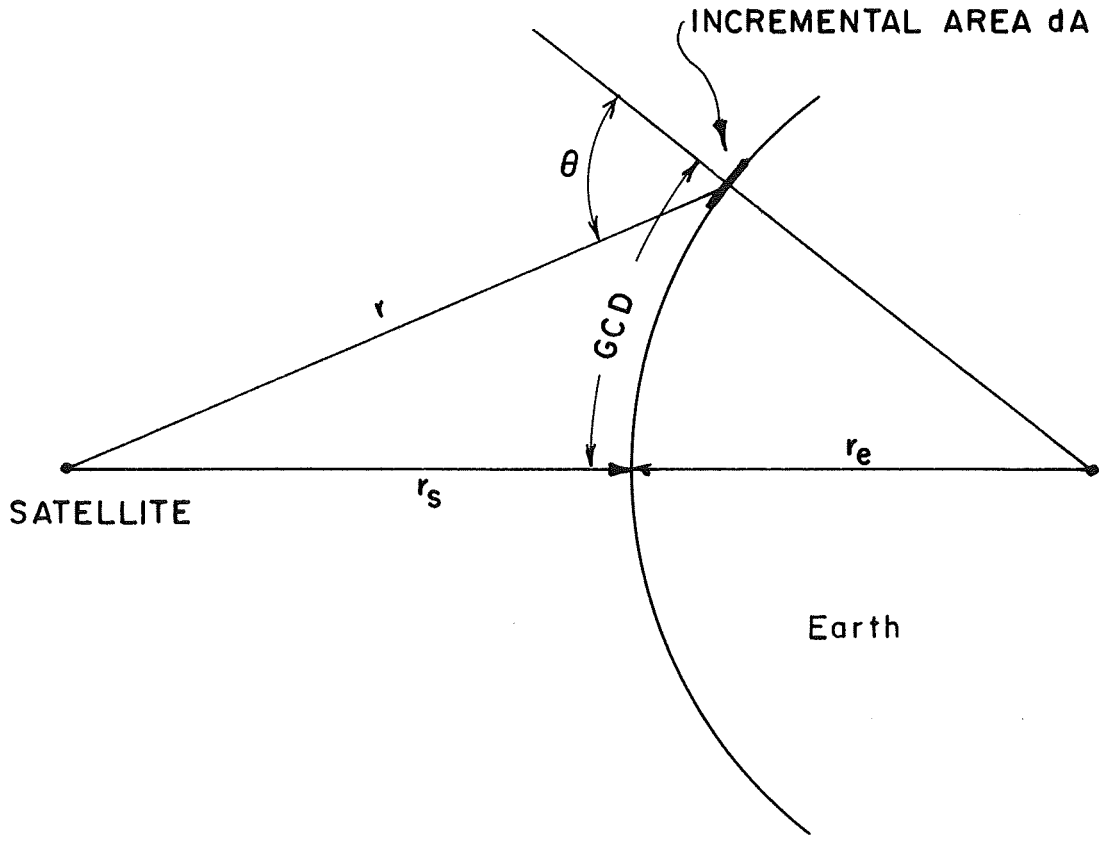

FIGURE 12. GEOMETRICAL RELATIONSHIPS BETWEEN r, θ and GCD.

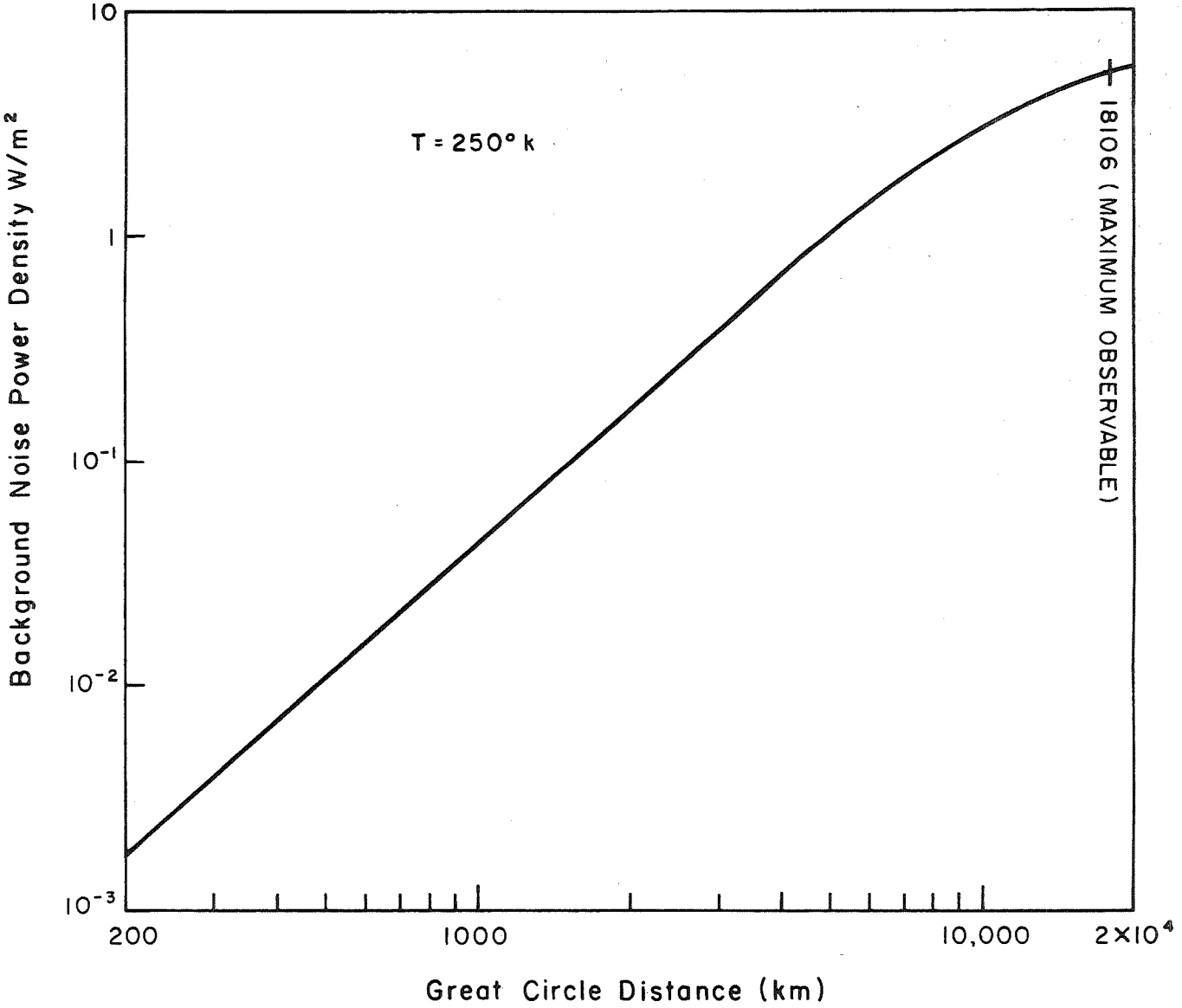

FIGURE 13 NOISE POWER DENSITY

numerical evaluation.

The earth was assumed to be a black body at 250°K for these calculations [3, p. 794]. This temperature may seem somewhat low but it represents the average temperature of the entire surface of the earth. While 95% of the outgoing infrared radiation comes from the ground [14, p. 32] the presence of large cloud banks will lower the average observed temperature because the upper layers of clouds often consist of ice crystals which can have an equivalent black body temperature as low as 190°K [14, p. 17]. For a given area a significant variation between the average earth temperature and the observed temperature can occur due to the temperature variation on the earth. For example, the highest and lowest temperatures likely to be encountered on earth are about -140°F and 140°F corresponding to the temperatures reported in Antarctica and the Sahara Desert. These temperatures correspond to 193°K and 333°K, respectively, which means that a satellite that observed the whole earth and had sufficient resolution could reasonably be expected to observe variations in the equivalent earth temperature of 140°.

The straight line relationship between the background power and the diameter of the observed region is important in determining the distribution of the background power over the area of the received image. Consider the situation described in Fig. 14 where two different images are formed on the image plane. Since the received power is proportional to the area of the observed region, the power density incident on the image area for the first observed area is the same as that for the second provided the observed regions are not over 7000 km in diameter. The fact that the background noise power incident on the image plane is uniformly distributed over the image is useful in determining the signal-to-noise ratio. Figure 14 also illustrates why the background power is dependent on the size of the observed region. While the total power incident on the objective lens is constant the construction of the lens determines what fraction of the total power received is actually focused on the active image area.

Using (2.2-3) and (2.2-4) the total received signal power is given by (neglecting atmospheric attenuation)

$$P_r = 6.08 \times 10^{-16} \, d^2 \, J(T) \qquad (2.7\text{-}6)$$

where P_r = received signal power in W on an image element

d = diameter of the objective in m

$J(T)$ = radiant intensity in W/sr (see (2.1-7) or (2.1-8)).

Since the received signal will be filtered to improve the signal-to-noise ratio, eq. (2.7-6) must be modified by the fractional amount of the received energy in the spectral region chosen, $\rho_s(T)$, which can be found from Fig. 10 for the desired temperature and spectral region. Equation (2.7-6) becomes

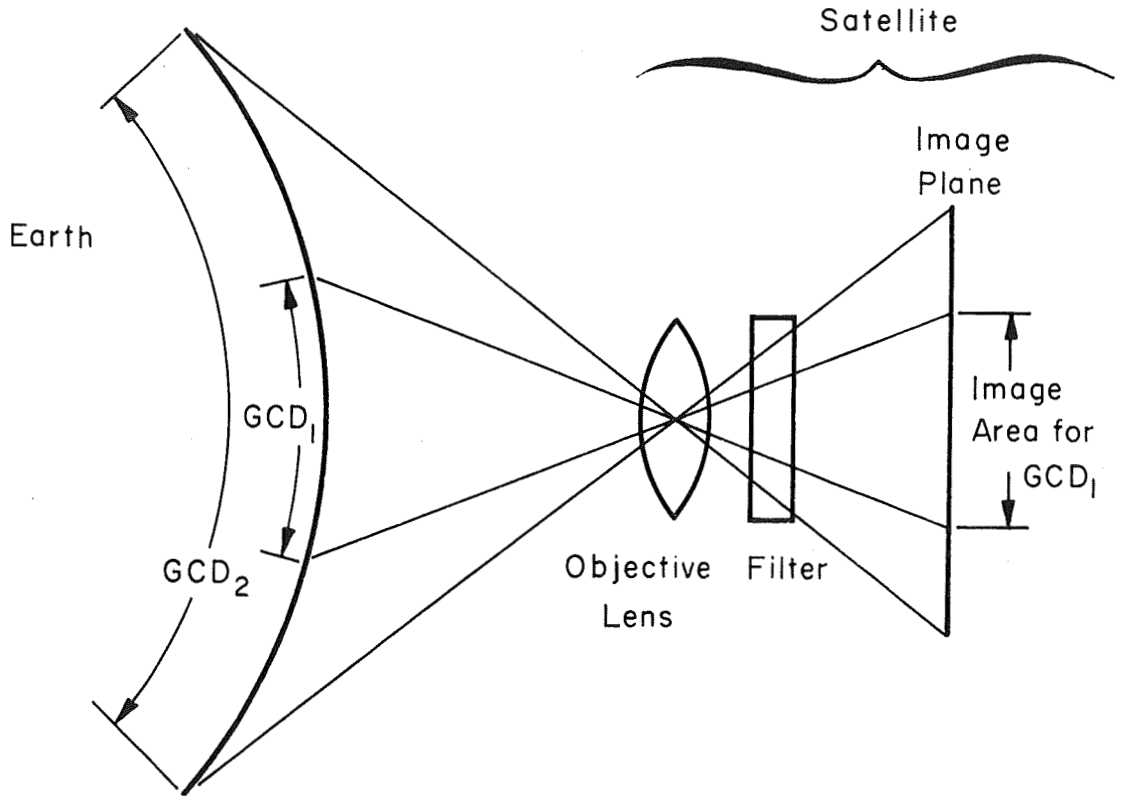

FIGURE 14 IMAGE FORMATION FOR TWO DIFFERENT OBSERVED AREAS

$$P_r = 6.08 \times 10^{-16} \rho_s(T)\, d^2\, J(T) \qquad (2.7\text{-}7)$$

or

$$P_r = \rho_s(T)\, P_r' \qquad (2.7\text{-}8)$$

where P_r' is the received signal power given in Fig. 2.

The total background power in the entire image can be found by multiplying the area of the objective lens by the background noise power density, N_{GCD}, given in Fig. 13.

$$P_N' = \frac{\pi d^2}{4} N_{GCD} \qquad (2.7\text{-}9)$$

If the system is designed so that the television line limit resolution is less than the optical resolution limit, then the energy of the user image in the diffraction limited system will be focused on an individually resolvable element. Assuming that the vertical and horizontal resolution is the same, then the average total noise power on each resolvable image element is

$$P_N = \frac{P_N'}{N^2} = \frac{\pi}{4} \left(\frac{d}{N}\right)^2 N_{GCD} \qquad (2.7\text{-}10)$$

where P_N = average total background power on each individually resolvable image element

N = number of TV lines

d = objective diameter in m

N_{GCD} = background noise power density for the image of the earth consisting of a circle with diameter GCD.

The justification for dividing the background power equally among all the image elements is that the background power is found to be directly proportional to the observed area and thus is constant over the entire image since the effective area seen by each element is the same. While the actual area represented by each individual image element increases because of the GDOP factor the effective infrared producing area remains the same as shown by Fig. 13.

The total background noise power will consist of a continuous average background level plus variations due to parts of the image having different equivalent temperatures which may be due to changing cloud formations, ocean currents or weather conditions on the ground. In calculating the signal-to-noise ratio only the changing portion of the total background power will be used which is similar to filtering out the dc component from a time-varying waveform. As the image is scanned there will be time variations, due to changing weather

conditions, and spacial variations due to different types of backgrounds, but both changes manifest themselves as changes in the effective temperature of the background. In order for a binary detection system to work effectively it will be necessary for the received signal to produce a response in the camera tube which is significantly greater in magnitude than the peak variation which can be expected in the background temperature.

In order to accurately calculate the magnitude of the received background power it is necessary to know the average emissivity of the region being observed. The problem of calculating the infrared energy emitted by the earth is essentially a small portion of the heat balance problem which is concerned with the heat exchange between the earth and its atmosphere, the sun and the surrounding space. A reliable computation of the heat balance problem has not yet been made [15] and part of this problem is due to a lack of accurate knowledge of the average emissivity of large areas. The large area occupied by the seas make the emissivity of water one of the prime factors to be considered in estimating the average emissivity of the earth. Since the emissivity of water is on the order of 0.97 [3, p. 167], the assumption will be made that the earth can be considered as an ideal black body with an emissivity of 1.0. The average emissivity of sand and vegetation is between 0.75 and 0.95 in the 3 to 5μ region [3, p. 75].

In order to calculate the signal-to-noise ratio it will be necessary to determine the range of effective background temperatures which may be encountered. The maximum range was calculated previously as on the order of 140° but this is not likely to be encountered in actual operation since it is unlikely the two extremes would occur simultaneously. Two effective background temperature ranges will be considered in this report. The first temperature range is 250°K to 280°K which corresponds to the temperature range that could be expected over an area with relatively mild weather and few very high cloud formations. The second temperature range is 200°K to 280°K which corresponds to the temperature range that could be expected over a region with a severe storm. Note that these temperature ranges are much less than the maximum temperature range that could be expected. In order to illustrate the type of data that could be expected from an infrared camera an example of the infrared data obtained from the Nimbus I weather satellite is given in Fig. 15.

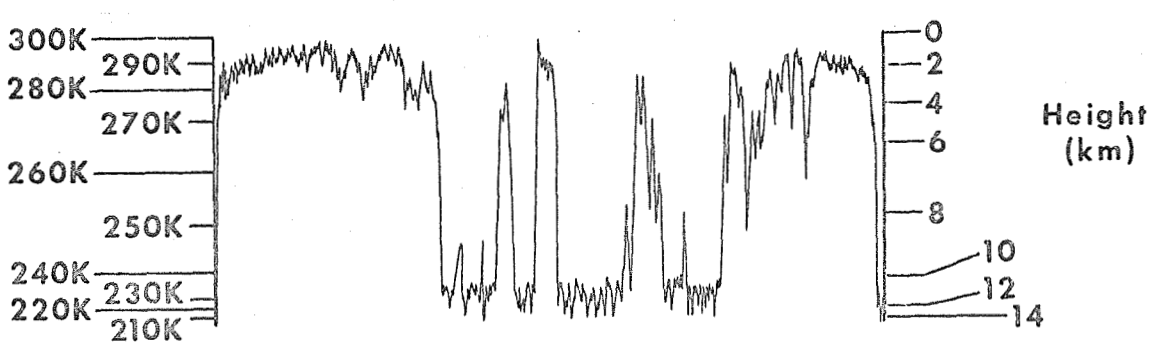

Figure 15 BACKGROUND TEMPERATURES OBTAINED BY THE INFRARED RADIOMETER IN NIMBUS I [14, p. 62]

The data presented in Fig. 15 was obtained by Nimbus I while passing over Hurricane Gladys on September 18, 1964. It represents the effective background temperature estimated from the infrared energy in the region 3.5 to 4.1μ which was measured by a scanning radiometer with a lead selenide photoconductive cell. The trace represents a region 5 km wide and 2500 km long. The height scale represents the height of the cloud formation which has the corresponding temperature and was obtained from radiosonde measurements. The region on the left of the trace, with a temperature variation of about 15°, represents relatively mild weather compared to the center of the storm. Note that the temperature measuring process is an averaging process which gives the average effective background temperature over the resolvable image area. The assumption of a 30° range of temperature in mild weather is not contradicted by the measured 15° change since the resolution in the navigation system would be better than 5 km. High resolution systems will have higher temperature variations because of the fact that low resolution systems tend to smooth out the large variations which would be observed by high resolution systems. The data presented in Fig. 15 may be considered as representative of one raster line of the output of an infrared sensitive camera tube with a ground resolution of 5 km.

The effective value of the background noise will be taken to be the difference between the received power at the highest and lowest temperatures. In order to determine the background noise power density at different temperatures, the results given in Fig. 13 must be modified as in (2.7-11)

$$N_{GCD}(T) = N_{GCD}(250)\left(\frac{T_D}{250}\right)^4 \qquad (2.7\text{-}11)$$

where $N_{GCD}(T)$ = background noise power density for an effective background temperature of T°K

$N_{GCD}(250)$ = value obtained from Fig. 13

T_D = desired effective background temperature.

The variational background noise power on each resolvable image element for the two temperature ranges being considered is:

$$P_N = \frac{\pi}{4}\left(\frac{d}{N}\right)^2 N_{GCD}\left[\rho_N(280)\left(\frac{280}{250}\right)^4 - \rho_N(250)\right] \qquad (2.7\text{-}12a)$$

for $\Delta T = 30^\circ$

$$P_N = \frac{\pi}{4}\left(\frac{d}{N}\right)^2 N_{GCD}\left[\rho_N(280)\left(\frac{280}{250}\right)^4 - \rho_N(200)\left(\frac{200}{250}\right)^4\right] \qquad (2.7\text{-}12b)$$

for $\Delta T = 80^\circ$

where P_N = variational noise power per resolvable image element in W

d = objective diameter in m

N = number of TV lines

N_{GCD} = noise background power density for a black body at 250°K obtained from Fig. 13

$\rho_N(T)$ = fractional amount of power in the chosen spectral region at temperature T (determined from Fig. 9).

The signal-to-noise ratio can then be determined by dividing the received power P_r (2.7-7) by the variational noise power P_N (2.7-12) which yields:

$$SNR = \frac{7.75 \times 10^{-16} \rho_s(T) N^2 J(T)}{N_{GCD}[1.75 \rho_N(280) - \rho_N(250)]} \quad \text{for } \Delta T = 30^\circ \qquad (2.7\text{-}13a)$$

$$SNR = \frac{7.75 \times 10^{-16} \rho_s(T) N^2 J(T)}{N_{GCD}[1.75 \rho_N(280) - 0.41 \rho_N(200)]} \quad \text{for } \Delta T = 80^\circ \qquad (2.7\text{-}13b)$$

where the coefficients ρ must be evaluated for the spectral region and source temperature, T, under consideration. Originally the region of 2-6μ was chosen as being the region with the highest probable signal-to-noise ratio but evaluation of (2.7-13) will yield an equation of the form:

$$SNR = k \frac{N^2}{N_{GCD}} \qquad (2.7\text{-}14)$$

and the spectral region which yields the largest value of k will give the best results. The constant k is defined by:

$$k = \frac{7.75 \times 10^{-16} \rho_s(T) J(T)}{1.75 \rho_N(280) - \rho_N(250)} \quad \text{for } \Delta T = 30^\circ \qquad (2.7\text{-}15a)$$

$$k = \frac{7.75 \times 10^{-16} \rho_s(T) J(T)}{1.75 \rho_N(280) - 0.41 \rho_N(200)} \quad \text{for } \Delta T = 80^\circ \qquad (2.7\text{-}15b)$$

and has been evaluated for the desired spectral regions with the results given in Table 1.

Table 1

Values of k for Evaluation of SNR

$k(\Delta T = 30^{o})$	$k(\Delta T = 80^{o})$	Source Temperature ^{o}K	Spectral Region
3.5×10^{-11}	2.4×10^{-11}	600	2-6μ
4.6×10^{-10}	3.4×10^{-10}	1000	
7.2×10^{-11}	5.6×10^{-11}	600	2-5μ
1.2×10^{-9}	8.6×10^{-10}	1000	
2.6×10^{-10}	2.2×10^{-10}	600	2-4μ
5.9×10^{-9}	5.0×10^{-9}	1000	

Table 2

Conversion Factors to find SNR From Normalized SNR in 2-4μ Region

C or $C'(\Delta T = 30^{o})$	C or $C'(\Delta T = 80^{o})$	Source Temperature ^{o}K	Spectral Region
C = 0.135	C = 0.092	600	2-6μ
C' = 0.08	C' = 0.058	1000	
C = 0.26	C = 0.216	600	2-5μ
C' = 0.20	C' = 0.145	1000	
C = 1	C = 0.85	600	2-4μ
C' = 1	C' = 0.85	1000	

Multiply SNR in Fig. 16 by C or C' to find SNR.

The 2-4μ region has the highest k value and hence will have the highest signal-to-noise ratio, which indicates that the decrease in signal strength obtained by using a narrow spectral region is much less than the noise power decrease. It should not be assumed that these results definitely indicate the use of a narrow spectral region. Further investigation of the effects of solar energy must be considered at the shorter wavelengths. It is known, for example, that in the 2-2.5μ region the energy present under certain circumstances is much greater than that indicated by a 270°K black body [6, p. 118]. It has also been assumed that filters are available which provide perfect bandpass action for the desired spectral region, but all practical filters will transmit some energy in the stopband. While the transmission factor for energy in the stopband may be lower than 0.01%, it still must be considered (see Section 3.6.2).

Since the effect of a more exact analysis including solar energy can only decrease the signal-to-noise ratio the results obtained must be considered as optimistic. One source reports an effective atmospheric temperature variation of 200°K to 300°K and while this may occur only over the whole surface of the earth the assumption of a 30° or 80° range is optimistic [6, p. 103]. In addition the received signal will be modified by the spectral characteristics of the detector which may also reduce the signal-to-noise ratio. Equation (2.7-13) has been plotted in Fig. 16 for the constants given in Table 1 for the 2-4μ region and to obtain the signal-to-noise ratio for other cases the conversion constants of Table 2 can be used. The C constants are used to convert the lines associated with a source temperature of 600°K while the C' constants are used with the 1000°K source temperature.

It should be emphasized that the signal-to-noise ratio just calculated is for the power incident on the objective lens or reflector and assuming ideal filtering. It is not the signal-to-noise ratio at the input to the binary detector which would be the output signal of the infrared detector. The actual signal on which the binary detector would operate would have a lower signal-to-noise ratio because of the noise introduced by the detector itself. The prime sources of the additional noise that would deteriorate the signal are thermal noise, dark current noise, shot noise and 1/f or flicker noise, all of which could be present at the same time. In addition, the quantum efficiency of all detectors is spectrally dependent and considering the present state of the art in infrared television cameras, the quantum efficiency would probably be greater at the lower end of the spectral region, i.e., 2μ, which would increase the effect of reflected sunlight and decrease the signal-to-noise ratio.

Some explanation of the results expressed in Fig. 16 is necessary. Note that it is necessary for (2.3-8) to be satisfied in order for the results to be valid. Consider the smallest resolvable image element: what is the source of the energy on the element? The energy from a point source, the plane if any, and the background energy from the area of the earth corresponding to the smallest resolvable area will fall on top of each other because of the resolution limit. Even though the source and background temperatures are quite different the background energy may be much greater than the source energy if the resolvable area is large.

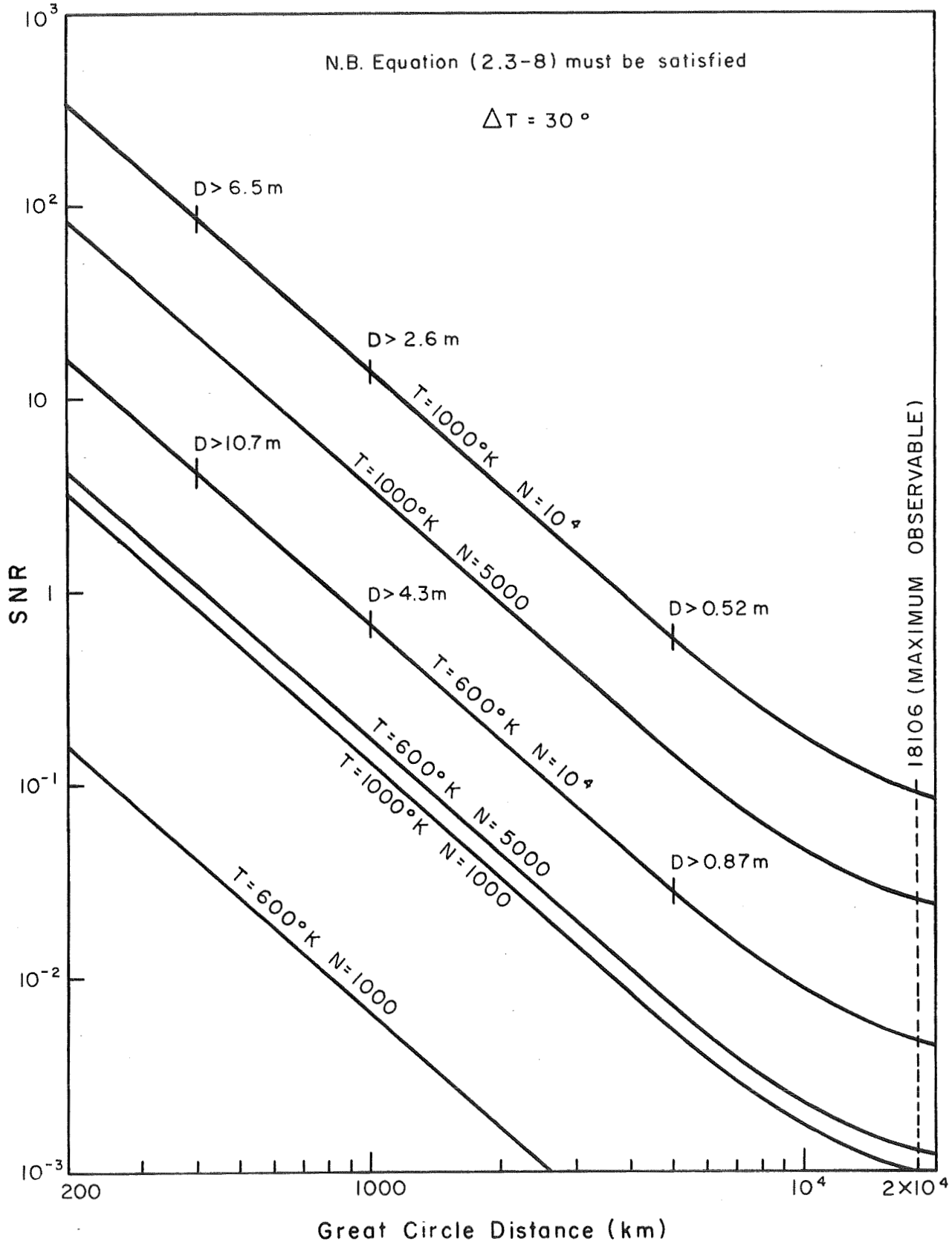

FIGURE 16 SIGNAL-TO-NOISE RATIO

The consequences of the restriction provided by (2.3-8) are now evident: in order to cover a large area a very large objective is needed to ensure that the background energy from the smallest resolvable area is small. The size of the objective is limited by practical considerations and hence either the useful area of coverage will be very small or the signal-to-noise ratio for the size of the area desired may be so low as to make the system useless.

The results expressed in Fig. 16 were derived under the assumption that the optical image resolution was better than the television camera limited resolution-- the restriction of (2.3-8). In order for the results of Fig. 16 to be valid the actual objective lens size would have to be somewhat greater than that indicated by (2.3-8) in order to compensate for a loss in resolution due to imperfect optical components and television camera performance. Aberrations or distortion in the objective lens and non-uniformity in the quantum efficiency of the photosensitivity surface used as the detector will cause certain image elements to respond differently, which in turn will decrease the signal-to-noise ratio. Since Fig. 16 represents the response of a perfect optical system a real system would have a somewhat poorer response. The size restriction on the objective lens (2.3-8) is noted in Fig. 16 for the case $N = 10^4$ lines.

For example, consider the system which has been postulated with 10^4 lines, 8^o FOV and a 1 m objective. An 8^o FOV corresponds approximately to a great circle distance of about 5000 km and since the above parameters almost satisfy the equality in (2.3-8) they represent about the best that can be done with a 1 m objective. From Fig. 16 the SNR ranges between 3.5×10^{-2} and 0.5 which is hardly sufficient to allow an accurate binary decision to be made. The values given in Fig. 16 are very optimistic and apply only to the actual image and not the signal received by the binary detector.

The results of this section can be summarized in the following manner. The size of the objective lens determines the size of the area which is represented by the minimum resolvable image element. A binary detection system operating on each resolvable image element would not work because it is not possible to reliably distinguish between an image element with a user present and one with a user absent for feasible objective lens sizes. The difference between the user present image element and the user absent image element cannot be distinguished from the difference which could be expected to occur naturally from the background temperature differences between the resolvable areas.

2.8 Conclusions on a Passive Optical Navigation System

The present and potential feasibility of an optical navigation satellite system for passive users can be evaluated from the results presented in Fig. 16. In order to reduce the bandwidth and power requirements a simple binary detection scheme was chosen; however, in order for such a system to operate the signal-to-noise ratio must be very high ($\gg 1$) in order to have a high probability of detection. From Fig. 16 it is concluded that for a practical size objective lens (1 m) and a reasonable number of television lines (10^4) the area that could be covered effectively (high SNR) is very small (a circular area with

diameter of a few hundred km). In order to increase the area covered, a larger objective lens is needed to overcome the diffraction limit and will also require a higher resolution television camera.

If it becomes possible to construct large diameter (> 10 m) reflectors in space at synchronous altitudes, the objective could be a lens or a reflector; a reevaluation of the concept would then be necessary. Of course, the structure would have to be very rigid both structurally and thermally in order to obtain a high quality optical image and camera tubes with resolution in excess of 2×10^4 lines would be needed. For the present it is concluded that passive optical techniques for navigation satellites do not allow coverage of sufficient area to warrant their use. Remember also that it was assumed that the engine structure was "visible" to the satellite and if the engines are mounted below the wings passive detection would be impossible.

So far nothing has been said about the detector that would be necessary, except for the resolution, and this may prove to be a major problem. Since no photoemissive surface has been developed which has a usable quantum efficiency beyond 1.25μ [8, p. 108; 16, p. 146], this eliminates the use of devices such as image intensifiers and image orthicons which use photoemission as the principle of operation. The high resolution television camera (vidicon) which is available has a response to only 0.8μ [17, p.14] and is totally useless in the infrared region, but since photoconduction is the basis of operation extended spectral response is possible using other materials. Some work has been done on developing infrared television cameras [18-22], using photoconduction as the basis of operation, with some response in the desired spectral region (2-4μ), but development of a sufficiently sensitive version with adequate resolution will require a substantial development program. Other devices which might prove useful in the future are mosaic detectors which consist of small infrared detectors in a square array but it is doubtful that sufficient resolution could be obtained (arrays 200 × 200 are being developed [23]). Most of the present "high resolution" infrared pictures obtained from space are obtained using mechanically scanned infrared photocells but to obtain the resolution required over a large area is out of the question because of the long length of time required to scan large areas.

It is concluded that optical techniques with passive users do not represent a feasible solution to the navigation problem for large areas. The low signal-to-noise ratio and the lack of suitable detectors represent major problems and while the signal-to-noise ratio might be improved by using non-synchronous satellites in low orbits, the lack of a suitable detector eliminates this possibility. Small area coverage ($< 10^4$ km^2) might be possible since the signal-to-noise ratio is much larger but again a suitable detector is not available.

While the capability of constructing large diameter reflectors at synchronous altitude can be considered as an expected outgrowth of increased space capability the same is not true of high resolution infrared television cameras. The predominant need for television camera tubes sensitive in the near infrared has always been the desire of the military for night vision devices. There are two practical ways to construct

night vision devices. One is to use photoemissive surfaces and phosphors cascaded in an image intensifier configuration; this method uses light in the visible region and near infrared up to 1.1μ. The other is to use photoconductors which are sensitive in the near infrared. It is more desirable to use the near infrared region 1-2μ because there is greater illumination at night in that region than in the visible region. The energy emitted by many stars has a spectral distribution which peaks between 1 and 2μ and, in addition, a small amount of the moon's reflected sunlight is in this region [16, p. 34-35]. Because of the ability of near infrared, radiation to penetrate clouds and fog better than energy in the visible region and the fact that more energy is available in the near infrared the operation of the devices using the near infrared is often much more reliable than devices operating in the visible region. In the region above 2μ a great deal of the energy present is due to self-emission by the earth and the atmosphere, which makes this region somewhat less attractive than the 1-2μ region.

There is, at present, little incentive to develop television camera tubes sensitive in the desired 2-4μ region and practically no incentive to develop high resolution camera tubes in this region. The techniques which are used to increase the resolution in television camera tubes for the visible region could probably be applied to tubes which operate in the infrared, however. A need for camera tubes with a response in the 10μ region will exist in connection with the increased mapping of earth resources by satellite. The black body radiation of the earth peaks in the 10-12μ region and thus the peak radiation of the earth's features would also be in this region. The mechanically scanned photocells currently available for the longer wavelength region use photoconductive alloys or compounds of lead or indium for the 2-6μ region and germanium for the 5-60μ region. The need for remote sensing devices operating on the longer infrared wavelengths in the fields of earth resources and geological survey is likely to stimulate interest in developing far infrared television cameras but the order of magnitude increase necessary in the maximum useable wavelength is not likely to be achieved in the near future.

The future potential of optical navigation techniques for use with passive users depends almost entirely on the development of high resolution infrared sensitive television cameras and this is not likely in the near future.

The negative conclusion reached on the feasibility of a passive infrared navigation system is supported by a recent calculation which gave 120 km as the maximum reliable detection range for a Boeing 707 [61, p. 450]. The conditions under which these calculations were made are similar to the conditions that would be encountered in a navigation system.

3.0 AN ANALYSIS OF OPTICAL TECHNIQUES FOR SYNCHRONOUS NAVIGATION SATELLITES WITH ACTIVE USERS

The detection of passive users was shown to require objective lenses of impractical size. Also, the spectral region of maximum signal energy was not compatible with presently available detectors. The problem will now be modified by providing each user with a source of optical energy. In the case of an active user the source and detector can be chosen so that the spectral characteristics of the source match those of the detector. The feasibility of an active optical navigation system will be analyzed by finding a compatible source-detector combination and determining if the state-of-the-art of the devices involved is sufficient to ensure a reliable system.

3.1 Basic System Considerations

The type of navigation system that will be analyzed for the active case will be essentially the same as that proposed for the passive case. A synchronous satellite will observe a portion of the earth with a television camera which will detect the optical signals transmitted by the users. In order to reduce the power, bandwidth and equipment complexity of the system,a binary decision will be made on each resolvable image element as to the presence or absence of a user. The image coordinates of the user detected and several ground-based reference stations will then be used to compute the position of the user. The altitude of the user must be known in order to accurately calculate the user's position so if the calculation is done by equipment on the satellite, the user will have to correct the calculated position. If the field-of-view is small and the resolution is not very fine, it may be unnecessary to correct for the altitude of the user.

As in Section 2, the objective of this analysis will be to show various interrelationships among system parameters and to assume representative values of these parameters to determine the feasibility of the system. It should be noted that the results of this analysis will be inherently more dependent on the available technology than in the previous section. The feasibility will depend directly on the maximum capabilities of high power light sources and on the sensitivity and resolution of the camera tubes available. With the large amount of classified research being carried on for night vision devices, it is reasonable to expect that the typical system chosen to determine the feasibility may well be two to three years behind the current technology in ultra-sensitive television cameras.

3.2 A Comparison of the Active and Passive Cases

The active user case has certain inherent advantages and disadvantages compared to the passive user case. A comparison of the two cases will be made to determine what portion of the calculations made in Section 2 can be used or modified for use in the active case.

An active system provides many advantages over a passive system which will increase the feasibility of such a system. One of the advantages is that if a higher signal-to-noise ratio is needed, it may

be obtained simply by increasing the power of the source whereas in the passive case there was not much that could be done to increase the signal-to-noise ratio. Since some of the high-power light sources currently available produce visible energy, there are a number of detectors available with sufficient spectral response to allow the use of commercially available camera tubes. In the active case a spectral region can be chosen which will minimize the effect of background noise provided suitable sources and detectors are available for this region.

Other advantages in the active case will arise predominantly from the use of shorter wavelengths (0.3 to 2.0μ) as compared to wavelengths used in the passive case (2.0 to 6.0μ). As shown in Section 2.3.1 the image resolution is proportional to the wavelength of the source producing the image so the use of shorter wavelengths will yield a better image resolution. In addition,for equal ground resolution the shorter wavelengths will require smaller objective lenses than the longer wavelengths. The spectral region chosen for the passive case would have required that special material be used to construct the objective lens whereas for the active case ordinary optical glasses and/or reflective coatings can be used. The use of an active source will allow an increased variety of users to make use of the system if it proves feasible.

In addition to these advantages there are also several disadvantages associated with the active case. The presence of a source will increase the cost of the user's equipment. While the use of a shorter wavelength will place less restrictions on the type of material used for the optical components the shorter wavelength will mean higher tolerances in order to obtain optically perfect components. A shorter wavelength will mean that sunlight will become the predominant source of background noise. A system which requires active users has the disadvantage that the presence of non-cooperating users will not be detected. The signal power needed for detection may require very high power sources with very narrow beamwidths, such as a laser, which may prove to be a safety hazard should a pilot be observing a user at a lower altitude. The chances of such an accident seem to be almost negligible but nevertheless it is a possibility.

While the calculated results of Section 2 may not be very useful in the active case, many of the methods of calculation will be quite similar and only the wavelength of the source will have to be changed to correct the results. The GDOP factor, Fig. 3, will play the same role in modifying the results of the calculations which will be made at the subsatellite point. The total system resolution can be calculated exactly the same way as it was in Section 2.3. It is quite probable that the diffraction limitation will be so small compared to the television camera resolution that it can be neglected except for systems with very small objective lenses. The received signal can be calculated in the same manner as that given in Section 2.2 once the radiant intensity, J, is found for the sources and spectral region being considered. The results of Section 2.4 on the required image exposure time hold for the active case as well as the passive case.

Since the spectral region used for the active case will probably be in the visible region, which has much shorter wavelengths, the predominant source of background energy will be reflected sunlight. The calculation of the background energy will be quite different since the source is different. A greater consideration will have to be given to the propagation of the signal and background energy since the shorter wavelengths are more easily scattered by particles in the transmission path. The results given in Section 2.6 will still apply, but the correlation between the scattering coefficient and weather conditions, Fig. 11, will change with the scattering coefficient increasing at the shorter wavelengths for a given weather condition.

The analysis of the active case will be done in a manner similar to that of the passive case. An analysis of the signal-to-noise ratio will be performed under idealized conditions to determine if the binary detection system will operate reliably. The problem of the acquisition of the satellite by the user will also be considered since the fact that the user can be detected is not sufficient to ensure a feasible system.

3.3 Atmospheric Attenuation (Visible Region)

The problem of atmospheric attenuation due to scattering was discussed in Section 2.6 for the spectral region in which the passive user's signal was located. For the situation where the user has an active source, the problem of atmospheric attenuation will have to be reconsidered for two reasons. The use of an active source may reduce the problem of atmospheric attenuation to simply increasing the source power. Also, the shorter wavelength radiation which will be used changes the type of scattering process that will be encountered.

Aircraft which are capable of operating above most weather formations will not encounter the problem of atmospheric attenuation to any significant extent. The signal received from low altitude aircraft and ships may be attenuated several orders of magnitude if the user moves under a large cloud formation. It is reasonable to expect that the amount of time a particular user could make use of an optical navigation system will be proportional to the percentage of cloud cover at the average altitude of the user. Detailed information is available on the amount of cloud cover that can be expected above various altitudes for each month of the year [3, pp. 118-140; 27; 28]. At ground level the mean cloudiness in percentage of sky cover above the North Atlantic averages about 50% while 90% of the clouds will be below 9.8 km (32,000 ft) and 99% will be below 11.5 km (36,000 ft) [3, pp. 118-122]. Since most atmospheric absorption of optical energy is due to water vapor the conclusion that only low altitude users will be subject to attenuation problems is strengthened by the fact that "More than 90 per cent of the water vapor lies in the atmosphere below 15,000 to 20,000 ft , ..." [13, p. 35].

In view of the restricted use low altitude users could make of optical navigation systems, it would be necessary to equip them with two navigation systems to ensure reliable operation in poor weather. Only a detailed analysis of the costs involved could determine if it is economically feasible to equip low altitude users with both an optical

and a standard radio navigation system. The expense of two navigation systems might be justified if much higher accuracy could be obtained from the optical navigation system in which case the radio navigation system would be used as a back-up system. The deterioration of performance of an optical navigation system in bad weather will be drastic and the system will either work well or not at all. The optical system will not have a gradual reduction in position accuracy which might be expected of radio navigation systems as propagation conditions become worse.

The results of Section 2.6 must be modified because a different type of scattering mechanism becomes important at wavelengths in the visible region and near infrared. The same formulas apply; however, the weather conditions associated with a given value of the scattering coefficient change. The predominant form of scattering in the 2-10μ region is Mie scattering or larger particle scattering and the scattering coefficient is constant in this region as far as practical results are concerned. In the visible and near infrared region the type of scattering changes from Mie scattering to Rayleigh scattering which is highly wavelength dependent.

Under certain restrictions on the type of scattering particle the Rayleigh scattering coefficient is given by [3, p. 205]:

$$\sigma_R(h, \lambda) = \sigma_R(0)\, e^{-\frac{h}{H_R}} \qquad (3.3\text{-}1)$$

$$\sigma_R(0) = \frac{0.827\ NA^3}{\lambda^4} \qquad (3.3\text{-}2)$$

where $\sigma_R(h, \lambda)$ = Rayleigh scattering coefficient as a function of wavelength and altitude per cm^{-1}

$\sigma_R(0)$ = scattering coefficient at sea level

h = altitude in km

H_R = 8.0 km = atmospheric scale factor for Rayleigh scattering

λ = wavelength in cm

N = average number of particles per cm^3

A = average cross-sectional area of the scattering particles in cm^2.

The Rayleigh scattering coefficient is inversely proportional to the fourth power of the wavelength and dominates over the Mie scattering coefficient at short wavelengths. Mie scattering theory is applied in cases where the particle size is comparable to or larger than the radiation wavelength and Rayleigh scattering theory applies when the radiation wavelength is much larger than the particle size.

The nature of the scattering process is dependent on the particle composition of the atmosphere through which the radiation travels. The particle composition of the earth's atmosphere is such that the Mie and Rayleigh scattering coefficients are equal somewhere in the range 1 to 2μ. Particles the size of the molecules of the atmosphere give rise to Rayleigh scattering while particles like dust and water droplets in fog give rise to Mie scattering. In the visible region in fair weather it is reasonable to assume that all the scattering is Rayleigh scattering. However, in poor weather, light in the visible region is subject to both Rayleigh and Mie scattering. The reason for this is the change in the size of the particles making up the atmosphere. In fair weather the atmosphere is composed mainly of air and water molecules which range in radius from $10^{-4}\mu$ to 0.1μ [12] thus giving rise to Rayleigh scattering. Haze, fog and clouds on the other hand are composed of water droplets which range in radius from 0.3μ to 30μ [12] and give rise to Mie scattering. Attenuation due to atmospheric absorption also increases greatly as the water content of the atmosphere increases.

In order to calculate the attenuation due to scattering in the visible region the data presented in Table 3 [11, p. 15] will be used. Table 3 gives the total sea level scattering coefficients for various meteorological conditions and for bad weather the scattering coefficients for the visible region are generally four to five times greater than the scattering coefficients for the same weather condition in the infrared given in Fig. 11. The results presented are experimentally measured values and represent the average value of the scattering coefficient for the weather condition given. Since the scattering coefficients are averages for measurements made with visible light the results probably represent the true value of the scattering coefficient only in the middle of the visible region ($\sim 0.55\mu$). For low values of the scattering coefficient which correspond to fair weather and Rayleigh scattering the true scattering coefficient will be higher than the value given for blue light and lower than the value given for red light. If it is assumed that the scattering coefficients given represent the value at 0.55μ then (3.3-2) could be used to find the Rayleigh scattering at other wavelengths from the data given in Table 3.

To evaluate the results which would be obtained by using the data of Table 3 in the equation for atmospheric transmission (2.6-1) it is necessary to know how and why these experimental results were obtained. In theory, to accurately calculate the scattering coefficient along a given path it is necessary to know the total composition of the atmosphere, the size distribution of all the atmospheric components and the index of refraction of each component all as a function of the position along the given path. A statistical approach to the problem may provide some simplification but the data required to perform such calculations is not available. In order to obtain useful results it is therefore necessary to use experimental data which is usually sufficient for a first approximation.

Since it is not possible to separate the attenuation due to Rayleigh scattering, Mie scattering and atmospheric absorption in experimental measurements the scattering coefficient is a combination of all three.

Table 3

Scattering Coefficient for Various Meteorological Conditions
[11, p. 15]

Scattering Coefficient	Meteorological Condition
80	Dense fog
20	Thick fog
8	Moderate fog
4	Light fog and clouds
2	Thin fog or clouds
1	Haze
0.4	Light haze
0.2	Clear
0.08	Very clear
0.014	Pure air

All three types of attenuation affect the transmission factor in an exponential fashion, hence the experimentally determined scattering coefficient may be represented as:

$$\sigma_T = \sigma_R + \sigma_M + \sigma_A \qquad (3.3\text{-}3)$$

where σ_T = measured value of the scattering coefficient
σ_R = Rayleigh scattering coefficient
σ_M = Mie scattering coefficient
σ_A = atmospheric absorption coefficient

The assumption of a transmission factor which decreases exponentially with distance for atmospheric absorption is valid in the atmospheric windows and regions sufficiently far away from the extreme absorption near the spectral lines of the atmospheric components.

The total scattering coefficient is determined experimentally by measuring the transmitted and received intensities of a narrow beam of light which are related to the scattering coefficient by:

$$\frac{I_R}{I_T} = e^{-\sigma_T R} \qquad (3.3\text{-}4)$$

or

$$\sigma_T = \frac{1}{R} \ln \frac{I_T}{I_R} \qquad (3.3\text{-}5)$$

where I_R = received intensity

I_T = transmitted intensity

R = path length

σ_T = total scattering coefficient.

Reliable experimental results will be obtained provided the weather conditions along the path are reasonably constant and the spectral region being used is relatively free from atmospheric absorption. Measurements are normally made in the atmospheric windows where it is assumed that $\sigma_A \ll \sigma_R$ or $\sigma_A \ll \sigma_M$ in fair weather and hence can be neglected. The data is then interpolated to find the value of the scattering coefficient in regions where absorption occurs. Depending on the wavelength and path conditions, the assumption is also made that the scattering is either entirely Rayleigh scattering or entirely Mie scattering.

Since the experimentally determined scattering coefficient σ_T often includes a significant contribution from atmospheric absorption, especially at high values of σ_T which correspond to water droplets along the path, some authors prefer to call σ_T the extinction coefficient. The significance being that for low values of σ_T the attenuation is due primarily to scattering while for high values of σ_T there is a significant contribution from atmospheric absorption.

An example of the experimental results obtained is given in Fig. 17. The flatness of the curves above 2μ indicates the transition from Rayleigh dominated scattering below 2μ to Mie dominated scattering above 2μ. The curves of wavelengths below 1μ are above the calculated values for Rayleigh scattering in pure air because of additional scattering due to the presence of water vapor and absorption which occurs to some degree even in the atmospheric windows. The data points were taken at wavelengths chosen to be as far away from the extreme absorption lines as possible.

Since the scattering coefficients given in Table 3 were obtained from measurements in the visible region, it can be assumed that the predominant form of attenuation was attenuation due to Rayleigh scattering at least for the lower values of the scattering coefficient. The transmission factor or intensity ratio is calculated for Rayleigh scattering by using the data in Table 3 and the scale factor from (3.3-1) and then using (2.6-1) with the applicable Rayleigh parameters. The atmospheric scale factor, derived from empirical data, is a measure of the decrease in particle density with altitude. A large scale factor means a slow decrease in density and comparing the Rayleigh scale factor (8.0) with the Mie scale factor (1.2) shows that significant Rayleigh scattering occurs at higher altitudes than does Mie scattering. This result is consistent with the fact that atmospheric gas molecules, which cause Rayleigh scattering, are found at higher altitudes than the water droplets

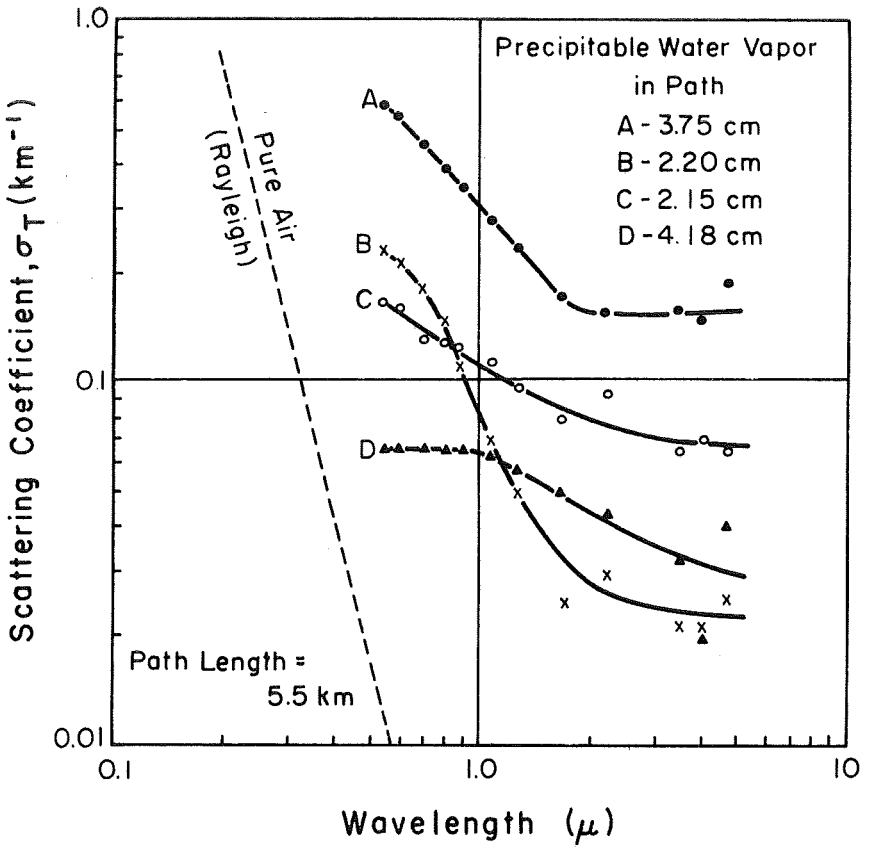

FIGURE 17 SCATTERING COEFFICIENTS DETERMINED FROM EXPERIMENTAL RESULTS AT WAVELENGTHS AWAY FROM ABSORPTION BANDS [13, p.33]

which cause Mie scattering. The results of evaluating (2.6-1) with the Rayleigh scattering parameters are given in Table 4. Note that (2.6-1) assumes a vertical transmission path and for users not at the subsatellite point the atmospheric attenuation would be greater because of the increased path length in the atmosphere.

Table 4

Atmospheric Attenuation Due to Rayleigh Scattering

Transmission Factor I_R/I_T

Range / σ_T	Ground to Satellite	7.5 km to Satellite	First 100 Meters	First 500 Meters	1 km to 10 km
0.1	0.45	0.73	0.99	0.95	0.62
0.3	0.09	0.39	0.97	0.87	0.24
0.7	3.7×10^{-2}	0.11	0.93	0.71	3.6×10^{-2}
1.0	3.4×10^{-4}	4.7×10^{-2}	0.90	0.62	8.5×10^{-3}
3.0	3.8×10^{-11}	8.3×10^{-5}	0.74	0.23	6.1×10^{-7}
7.0	4.8×10^{-25}	3.0×10^{-10}	0.50	3.4×10^{-2}	3.2×10^{-15}
10.0	1.8×10^{-35}	2.5×10^{-14}	0.37	7.9×10^{-3}	2.0×10^{-21}
30.0		1.5×10^{-40}	5.1×10^{-2}	4.8×10^{-7}	7.6×10^{-63}
70.0			9.5×10^{-4}	1.8×10^{-15}	

Since the type of scattering changes from Rayleigh to a mixture of Rayleigh and Mie scattering in cases where there is a significant concentration of water droplets (i.e. cases where $\sigma_T \geq 3.0$), the results given in Table 4 may not be correct. The increased significance of atmospheric absorption due to the presence of the water droplets may make the transmission factor even less than those given in Table 4. As in Section 2.6 these results were calculated assuming that the meteorological conditions, are constant (i.e. σ_T is constant) along the entire path. Clouds which can give high values of the scattering coefficient can only occur up to altitudes of about 50 km. The justification for the assumption of a constant scattering coefficient is found by comparing the transmission factors in the first and fifth columns of Table 4. The comparison shows that the majority of the attenuation occurs in the first ten km. of the atmosphere over which σ_T can be constant without the need for any assumptions.

The results given in Table 4 indicate that it will not be possible for ground-based ships or even low altitude planes to overcome

the problem of atmospheric attenuation. Comparing the results in column one of Table 4 shows that ground based users could expect a variation of four orders of magnitude in the atmospheric attenuation from clear days ($\sigma_T = 0.1$) to days with haze ($\sigma_T = 1.0$). For low-altitude users to overcome even Rayleigh scattering with no clouds present would require a source power four orders of magnitude greater than that needed for high altitude users. To overcome the attenuation introduced by the presence of a moderately thick cloud bank (4-7 km) would probably require a source power ten orders of magnitude or even more larger than the source power required for the high altitude user. The relative size of the power in one case compared to that in the other makes it apparent that it will not always be possible to overcome the limitations imposed on low altitude users by atmospheric attenuation by increasing the source power.

Since it does not appear to be possible to overcome atmospheric attenuation in poor weather a more accurate analysis will be made of the attenuation which could be expected on clear days in order to give reliable operation when the system could be expected to overcome the attenuation. The calculation of the optical properties of a standard atmosphere has been done [29] using one of the several standard atmospheres which have been developed [30, 31].

The standard atmosphere corresponds to a clear day with a visual range of about 20 km, a relative humidity of about 55% and an extinction coefficient on the order of 0.2 in the middle of the visual region ($\sim 0.55\mu$). The model is valid on clear days with some clouds provided the transmission path does not pass through the clouds. The total extinction coefficient in this model was taken to be the sum of the coefficients for Rayleigh scattering, aerosol (Mie) scattering and ozone absorption. The ozone absorption coefficient is very significant at certain wavelengths in the visible region. The Rayleigh scattering coefficients were computed using the atmospheric density values from reference [30] and experimental measurements were used to find a model for the aerosol density. The resultant model for atmospheric attenuation is a series of tables for 22 wavelengths from 0.27 to 4.0μ in which the individual and total attenuation coefficients are listed for 1 km increments in altitude from 0 to 50 km. In addition the sums of the total attenuation coefficients for all the 1 km regions above and below the given altitude are listed (denoted as the optical thickness for $h-\infty$ and $0-h$) which allows calculation of the transmission factor from the given altitude to infinity and ground level to the given altitude, respectively.

Although the standard atmosphere data is applicable only for fair weather, it gives reasonable results for the nominal atmospheric attenuation under normal operating conditions. The properties of a clear atmosphere are reasonably consistent so that systems which are designed to overcome the attenuation predicted by the clear standard atmosphere will normally operate in fair weather. The wide variations encountered in the optical properties of other weather formations, especially clouds, make any attempt to predict a nominal value of attenuation useless.

The transmission factor for vertical paths is related to the optical thickness by

$$T = e^{-\tau} \tag{3.3-6}$$

where T = transmission factor to the satellite

τ = optical thickness for the desired altitude

and the attenuation above 50 km is assumed to be negligible compared to that below 50 km. Since the transmission factor is not a function of the angular resolution the GDOP factor cannot be used to find the transmission factor for users not at the subsatellite point. Instead of using the GDOP factor the optical thickness will be made proportional to the length of the slant path through the atmosphere in which case

$$T = e^{-\tau/\sin\theta} \tag{3.3-7}$$

where θ is the elevation angle to the satellite.

The formula is accurate for elevation angles above 20° since the transmission factor for elevations below 20° is much too low and must be calculated in a different manner. Using the tabulated values [32] for the sum of the total attenuation coefficients, the transmission factor for a vertical path from a given height to the satellite was calculated for various wavelengths and the results are plotted in Figs. 18 and 19.

The results presented in Fig. 19 show that for wavelengths greater than 0.4μ in a clear standard atmosphere at least 55% of the transmitted energy will reach the satellite and from Fig. 18 over 91% of the transmitted energy will reach the satellite for users above 10 km. The increased effect of Rayleigh scattering at short wavelengths is readily apparent but is also interesting to note that in a clear atmosphere the use of the near infrared region as opposed to the visible region results in an average increase in the transmission factor of about 30%. The increase in the transmission factor is even less for high altitude users. Using the value $\sigma = 0.2$ in (2.6-1) and using the Rayleigh atmospheric scale factor gives a transmission factor of 0.20 for $\lambda \approx 0.55\mu$ which is somewhat pessimistic compared to the value given in Fig. 19. The discrepancy may be due to the fact that a more accurate distribution for the atmospheric density was used to obtain the results in Fig. 19.

In view of the data presented, the following conclusion seems reasonable. If the required source power is calculated neglecting atmospheric attenuation, then the use of a source power an order of magnitude larger could reasonably be expected to overcome any atmospheric attenuation present when the system should be capable of operation. A more exact analysis of the relationship between the source power and the usefulness of the system would require a statistical analysis of the amount of cloud cover, the thickness of the cloud bank, and the average attenuation coefficient in the cloud.

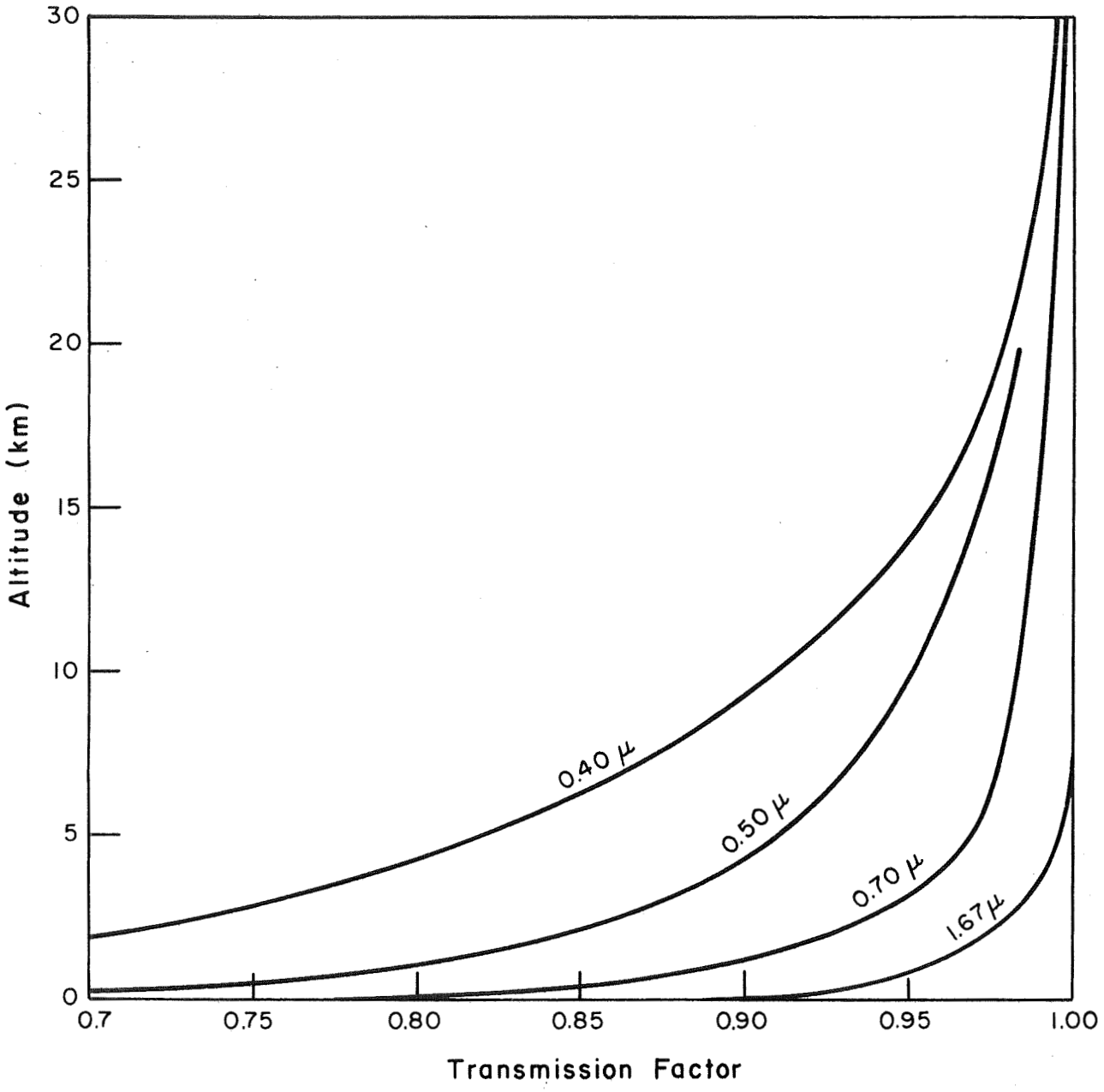

FIGURE 18 CLEAR ATMOSPHERE TRANSMISSION FACTOR AS A FUNCTION OF ALTITUDE

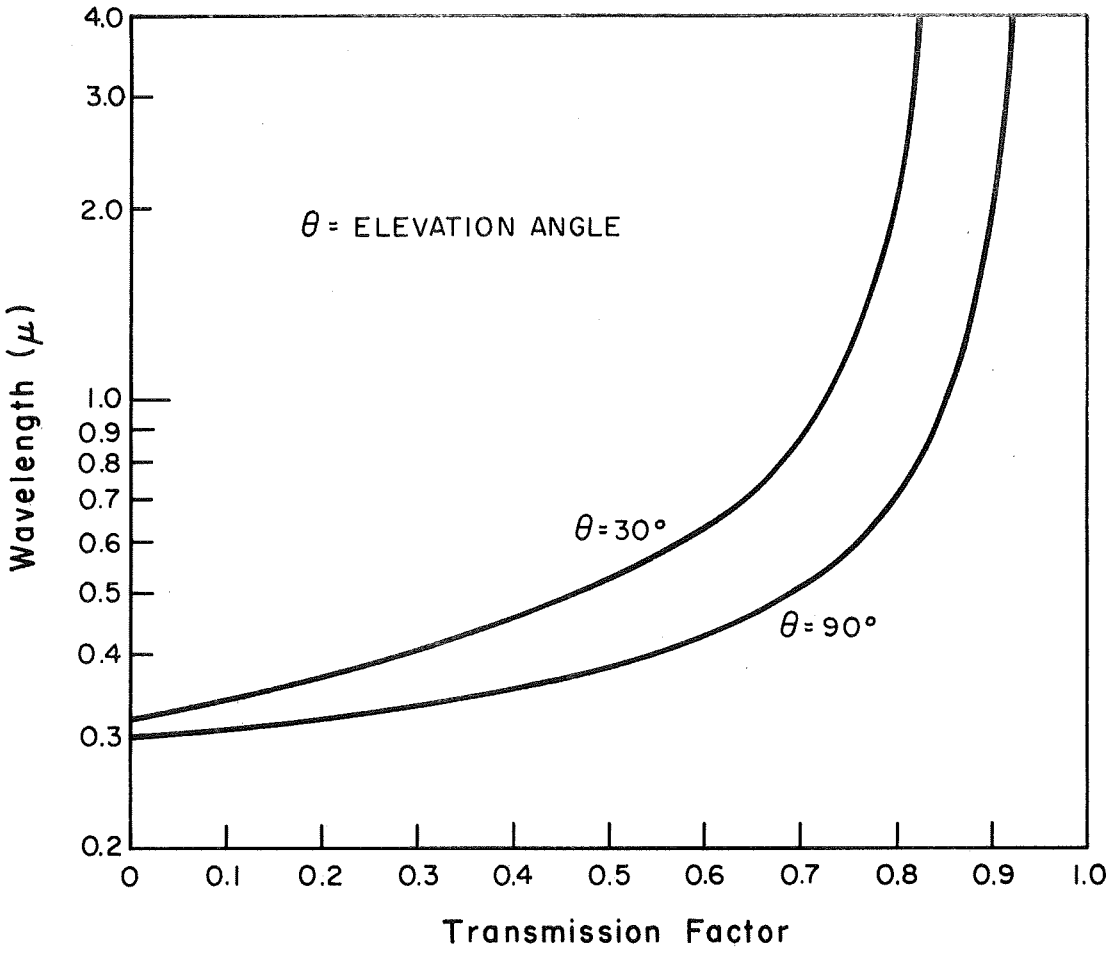

FIGURE 19 CLEAR ATMOSPHERE TRANSMISSION FACTOR FOR GROUND BASED USERS AS A FUNCTION OF WAVELENGTH

3.4 Image Resolution

As discussed previously in Section 2.3, the resolving capability of any optical system is limited by the wavelength of the energy which forms the image. Other limitations on the resolving power of an optical system are due to imperfections in the optical components which are used in the system. The methods used to analyze the image resolution in the passive case can also be used in the active case by changing the wavelengths under consideration. In the active case the wavelength of the light used will be assumed to be in the visible or near infrared region.

3.4.1 Resolution in Diffraction-Limited Systems

From Section 2.3.1 the diffraction-limited ground resolution is given by (2.3-2):

$$r_g = \frac{2.44\ \lambda\ r_s}{D} \qquad (3.4\text{-}1)$$

where r_g = ground resolution
r_s = synchronous altitude
λ = wavelength
D = objective diameter.

The ground resolution r_g represents the minimum ground separation which will result in a pair of images which will be on adjacent scan lines of the television camera output. An evaluation of (3.4-1) is given in Fig. 20. for some typical parameter values that might be encountered in the active case.

The results given in Fig. 20 indicate that in the active case the ground resolution will average about five times better than in the passive case for a given objective lens diameter. For example, in the case of a 1-m diameter objective, the ground resolution in the passive case was 400 m while in the active case (and $\lambda \approx 0.55\mu$) the resolution will be on the order of 60 m. As a result of the increased optical resolution in the active-user system, the total system resolution will be essentially that of the number of scan lines in the television camera used. The use of an objective lens which provides an image of much greater resolution than the resolving power of the television camera is justified because of the increased signal power that would be available with a larger objective lens. Since the image resolution is determined by the angular resolving power of the objective lens the ground resolution given in Fig. 20 must be multiplied by the GDOP factor, Fig. 3, for users which are not at the subsatellite point.

3.4.2 Television Camera Limitations on Resolution

The total angular resolution of the system can be no better than that of the television camera β_t (2.3-5) which in turn can be no better than the image resolution available β_r (2.3-1). Equating the two

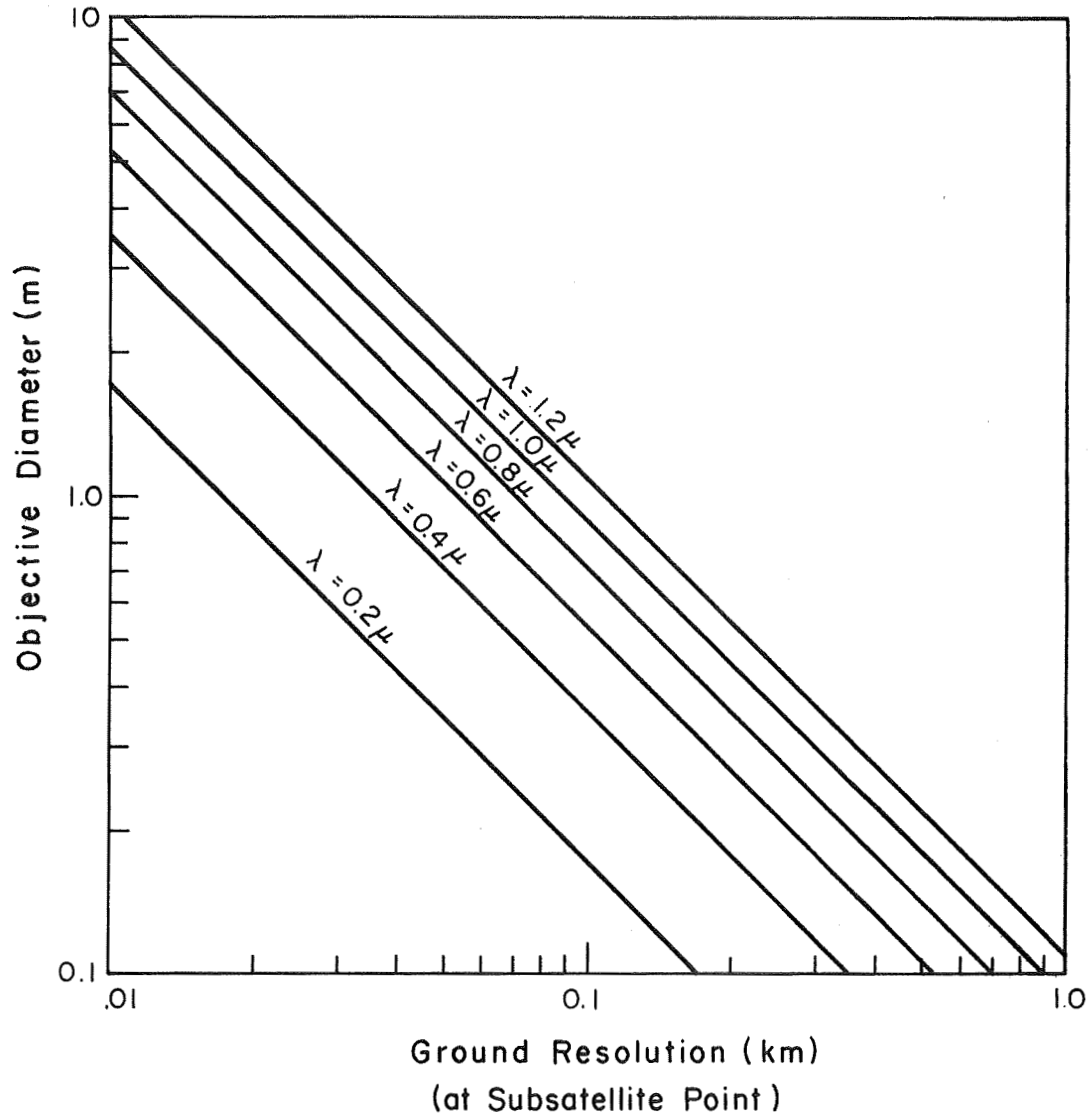

FIGURE 20 DIFFRACTION LIMITED GROUND RESOLUTION VS. OBJECTIVE DIAMETER

resolution limits gives the point at which increasing the number of television lines (or lens diameter) will not result in an increased system resolution provided the lens diameter (or number of television lines) is constant. Hence,

$$\frac{FOV}{N} \leq \frac{2.44\ \lambda}{D} \qquad (3.4\text{-}2)$$

where FOV = field-of-view in radians

λ = wavelength in m

N = number of TV lines

D = objective lens diameter in m.

Equation (3.4-2) is plotted in Fig. 21 for some typical parameter ranges which might be encountered (assuming the equality holds, i.e., $\beta_t = \beta_r$).

For a given number of TV lines Fig. 21 can be used to find the minimum objective diameter necessary to give the required resolution, or for a given objective diameter, the maximum number of television lines which can be used with the image formed can be found. Considering the present state-of-the-art in high resolution television cameras ($\sim 10^4$ lines) a 1-m objective would provide more than sufficient resolution for the camera tubes presently available. The resolution limit in the active user case will thus be determined by the number of television lines available.

The analysis used to derive the system resolution in this section has been based on geometrical consideration of the minimum angular resolution. An analysis of this type is valid provided the received image is of sufficient intensity. At low illumination levels it is also necessary to find the quantum-limited resolving power of the photoemissive or photoconductive surface being used as a detector [24, 25]. If the total received energy is very low, the resolution may not be that predicted by Figs. 20 and 21. An analysis of the resolving power of the detector surface will be made if a suitable detector and source combination is found to determine if the resolution will be reduced significantly below that predicted in Figs. 20 and 21.

3.4.3 Refractive Index Variation and Its Effect on Image Resolution

The changing index of refraction of the medium along the transmission path will cause perturbations in the received signal which will cause a degradation of the image resolution. Random changes in the index of refraction are caused by changes in the atmospheric density which in turn are caused by atmospheric turbulence, thermal gradients and changes in the atmospheric composition. Since the effects of refraction generally increase at shorter wavelengths, it was considered necessary to compare the relative magnitude of the resolution limit due to refractive index changes with the resolution limits due to other causes.

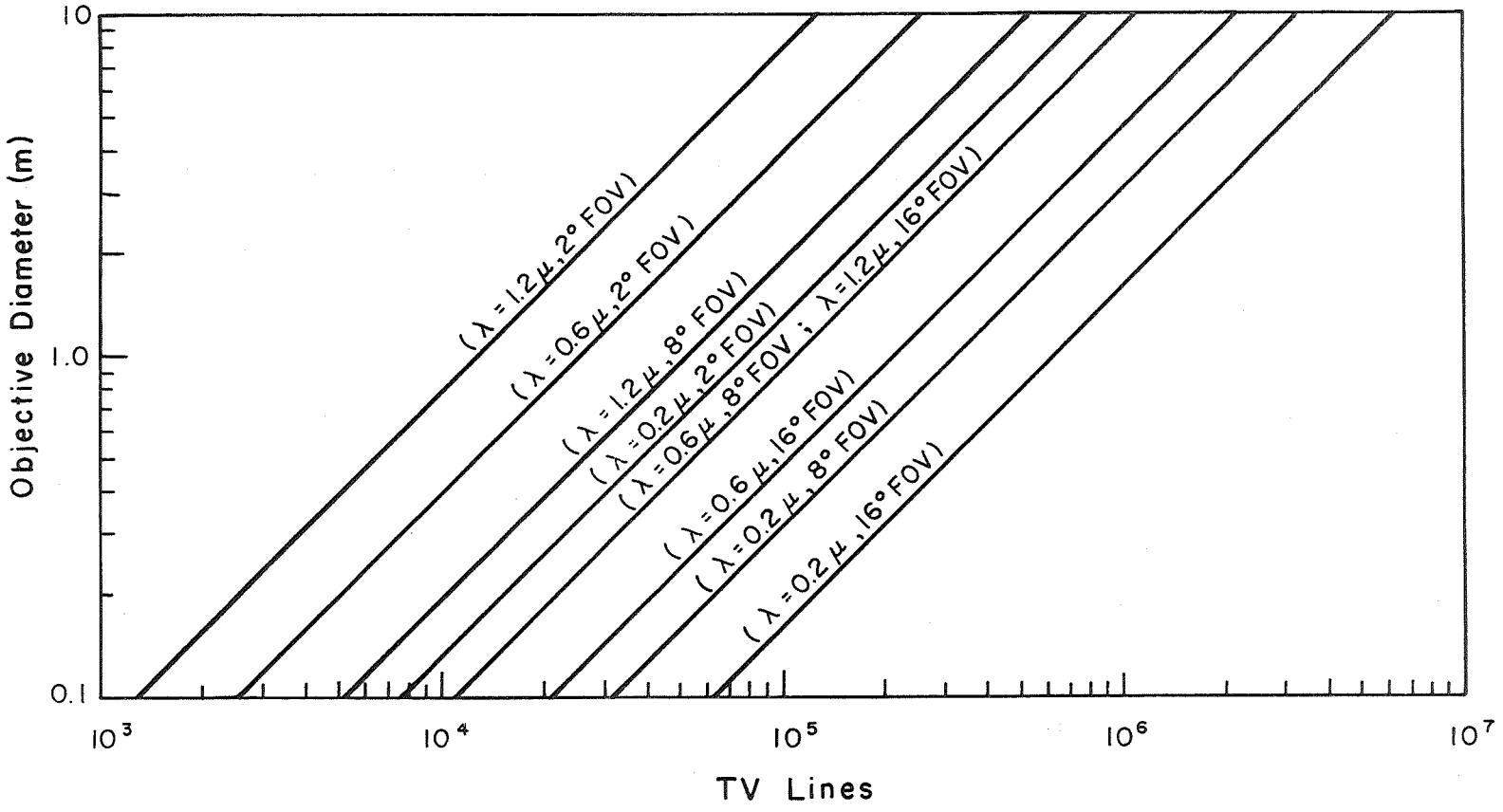

FIGURE 21 TELEVISION LINES REQUIRED FOR A DIFFRACTION LIMITED IMAGE

"The amount of wavefront distortion resulting from density and, hence, refractive index variations through the atmosphere will ultimately limit the performance of aerial reconnaissance systems," [33] and the optical navigation system is basically an aerial reconnaissance system.

Recent studies have shown that atmospheric turbulence places an absolute limit on the resolution that can be obtained with atmospheric transmission paths [34, 35]. In these studies it was assumed that perfect optical systems were available and that there was no restriction on lens diameter. In other words the system resolution was much better than the resolution limit introduced by atmospheric turbulence. It was found that the limit on ground resolution due to atmospheric turbulence is no worse than 5 to 10 cm for light in the visible region and at altitudes above 10 km [35, p. 1384]. Although the resolution stated above is for vertical paths and would become worse for slant paths the effect of atmospheric turbulence on resolution is approximately four orders of magnitude less than that of the diffraction limitation. For objective lenses of practical size and considering the resolution needed for a navigation system the effect of atmospheric turbulence is entirely negligible for practical purposes. Note that this statement does not mean that refraction can be neglected, but only the changes in refraction due to atmospheric turbulence.

3.5 Background Noise due to Reflected Sunlight

In the passive case it was found that the predominant source of background noise was the infrared energy emitted by the earth and reflected sunlight was neglected. The active user, however, will make use of an energy source having most of its energy in the visible or near infrared region, in which case reflected sunlight will be the predominant source of background noise. The infrared energy emitted by the earth and the reflected light due to other stars will be neglected.

The spectral distribution of the energy emitted by the sun is approximately that of a 5800°K to 6000°K black body which is given in Fig. 22 [10, p. 163]. The black body representation is sufficiently accurate for most purposes except in the ultraviolet region below 0.3μ. Since the surface of the sun consists of ionized gases with many elements present certain wavelengths may have a much higher energy content than that predicted by Fig. 22 because of contributions by the individual spectral lines of the elements. In the passive case it was assumed that reflected sunlight could be neglected and from Fig. 22 it can be seen that over 90% of the energy in sunlight lies below 2μ. Considering that the background energy from the earth's infrared radiation was sufficient to produce an extremely low signal-to-noise ratio introducing the reflected sunlight would just have produced somewhat worse results in the passive case.

If the predominant source of background noise is reflected sunlight it is reasonable to expect that the power requirements of the active source will change greatly from day to night. The feasibility of an optical navigation system with active users may in fact depend on when during the day or night it is used and a system which can operate during the day could also be expected to operate at night but at a much lower

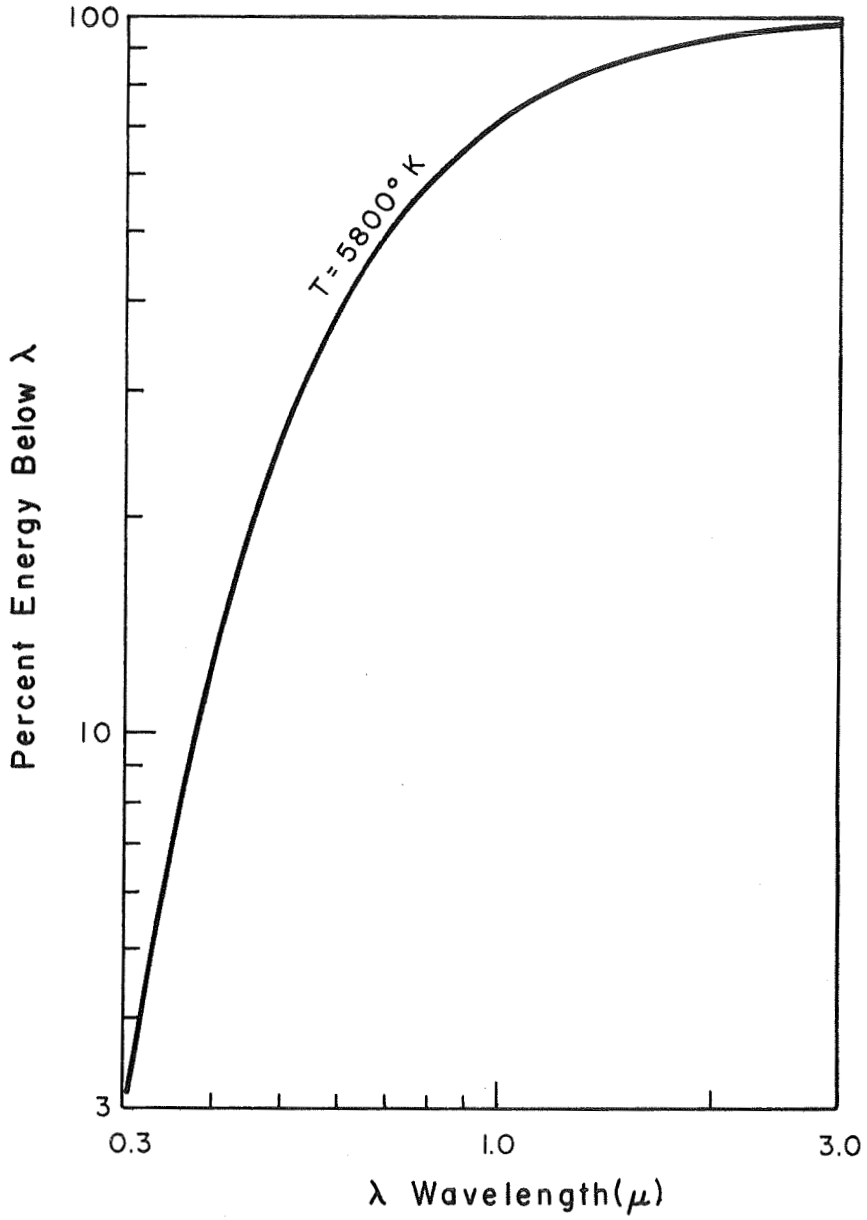

FIGURE 22 APPROXIMATE SPECTRAL DISTRIBUTION OF SUNLIGHT

power level. The usefulness of any system which will operate at night but not during the day is questionable.

The problem of determining the power received from reflected sunlight has been solved previously. Extensive results are available for the reflected sunlight received at a given distance from a given planet [36, 37]. The results of this study which are applicable to a satellite at synchronous altitude orbiting the earth are given in Fig. 23. The calculations are based on the assumptions that the sun is a 6000°K black body and that the earth has an albedo of 0.4. The albedo, or fractional reflectance, is the ratio of the total reflected energy to the total incident energy and by this definition it is independent of the wavelength of the light involved.

In determining the actual spectral distribution of the reflected sunlight and not just the total energy received it is necessary to know how the albedo changes with wavelength. The relationship between the albedo and the wavelength of the incident light is given in Fig. 24 [37, Fig. 7-15]. The data presented in Fig. 23 can be modified to give the illumination in a narrow spectral region by finding the percentage of energy in the desired spectral region for a 6000°K black body (approximately that given in Fig. 22) and then correcting the albedo from 0.4 to the average albedo in the region being considered. In other words:

$$I_\lambda = I_T \rho_s \frac{\alpha_\lambda}{\alpha} \qquad (3.5\text{-}1)$$

where I_λ = illumination for a narrow spectral region

I_T = total illumination given by Fig. 23

ρ_s = fractional amount of energy in the region being considered (obtained from Fig. 22)

α_λ = average earth albedo in the region being considered Fig. 24

α = 0.4 = average total earth albedo.

The phase angle is the plane angle between the user-satellite line and the user-sun line. The phase angle geometry is illustrated in Fig. 25. The highest phase angles are found at night and the change in background energy can be over seven orders of magnitude from day to night. Considering the wide range in the background noise the source power required could also be expected to vary greatly although not over such a wide range as the background noise. From these results a reasonable value for the total background energy received under the worst case conditions is 10^{-3} W/cm^2 which is the value that will be used to calculate the maximum source power required.

In the passive case a large portion of the background energy was constant and could be filtered out and thus neglected. Unfortunately in the active case no such reduction is possible for several reasons. The

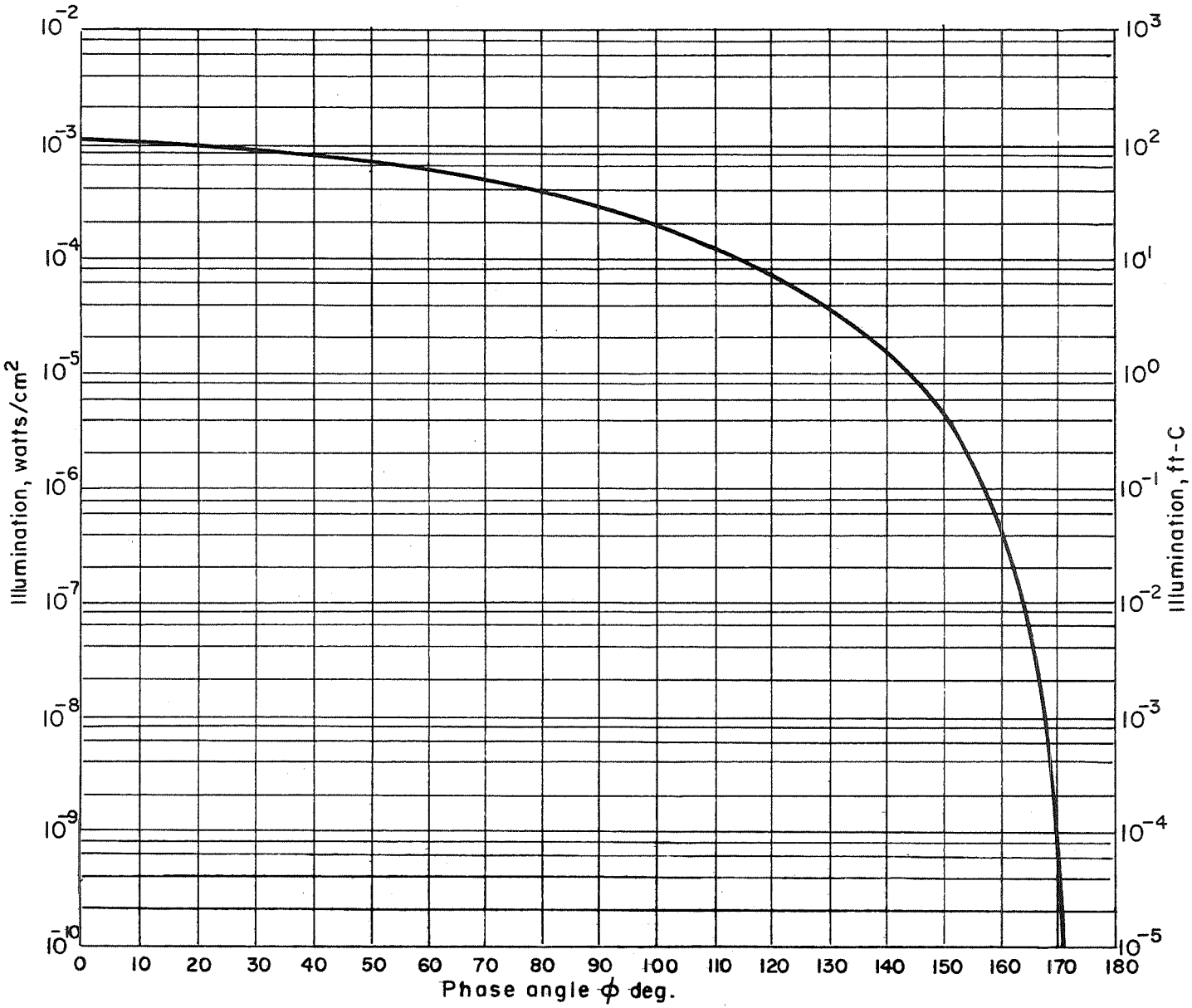

Figure 23 LIGHT INTENSITY VERSUS PHASE ANGLE FOR A SYNCHRONOUS SATELLITE ORBITING THE EARTH [77]

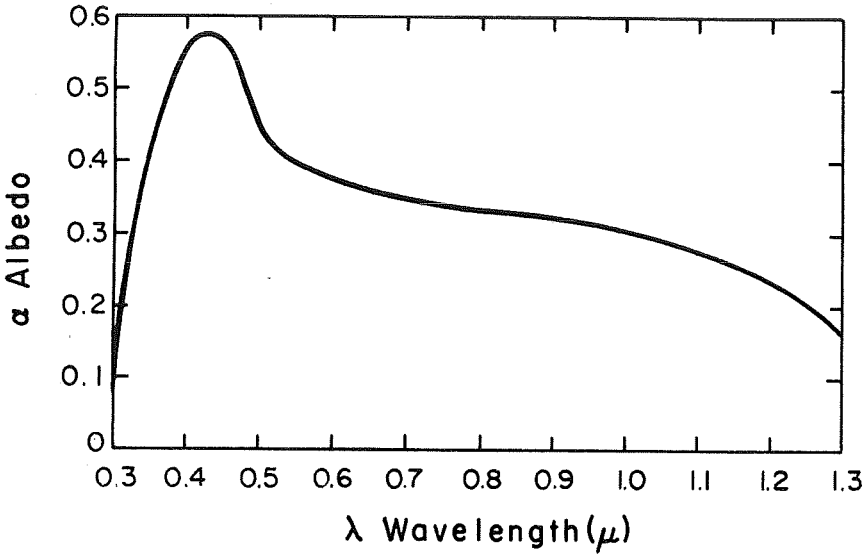

FIGURE 24 EARTH ALBEDO VERSUS WAVELENGTH [37]

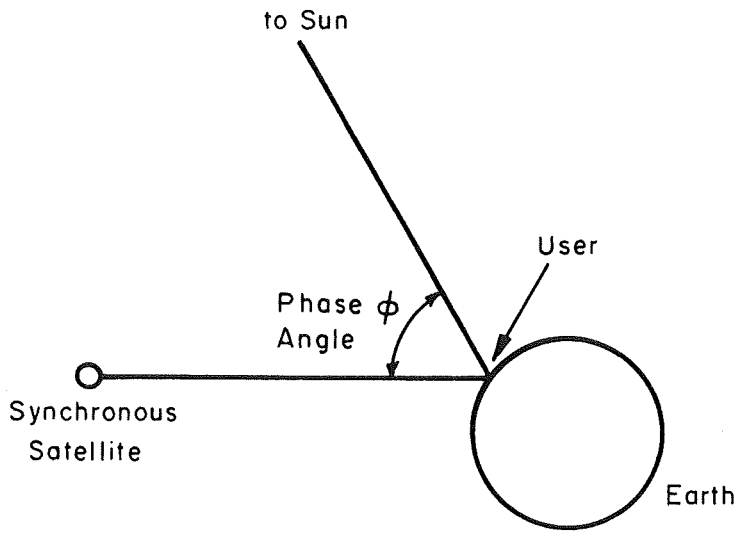

FIGURE 25 PHASE ANGLE GEOMETRY [37]

variations in the total background energy cannot be treated simply as changes in the effective temperature of the background as in the passive case. The various possible backgrounds such as clouds, land masses and the oceans have radically different reflective properties when considering small areas. The albedo, or average reflectance, of 0.4 is only a representative value when taken over large areas and will not necessarily hold when comparing small areas of the size that each resolvable image element is likely to represent. The variation in the amount of reflected light is readily apparent by observing some of the colored photographs of the earth that have been sent back from satellites (see [15] for example). Some of the cloud banks appear white while some of the land masses appear dark brown or almost black indicating not only a change in the amount of reflected energy but also a significantly different spectral composition. Hence it is not possible to conclude that there will be a given constant amount of background energy on each resolvable image element which can be filtered out and, therefore, it will be necessary to consider the total amount of reflected sunlight as the effective background noise.

As was true in the passive case the fraction of the energy incident on the objective lens which is actually focused on the detector will depend on the field-of-view. The explanation for the dependence of the background noise on the field-of-view was given in Section 2.7. While the exact distribution of the background noise in the image focused on the detector will depend on both the phase angle and the field-of-view a simplification is possible in the worst case. The worst-case situation is a field-of-view sufficient to observe the entire earth and a phase angle of 0^{o}. While the phase angle will vary with the time of day the field-of-view is constant so that if the background noise is calculated as a function of the field-of-view with a phase angle of 0^{o}, this will give the maximum background noise density.

The background noise power is proportional to the size of the projected area observed by the satellite. The fraction of the total background noise which is actually incident on the detector is thus equal to the ratio of the projected area observed to the total projected area on which the reflected sunlight calculations were based. The field-of-view or the diameter of the maximum observable region determines the size of the projected area observed. The projected area of the observable region, the plane area projected in the direction of the satellite, is

$$A = \pi r_e^2 \sin^2\left(\frac{GCD}{2r_e}\right) \qquad (3.5\text{-}2)$$

where A = projected area corresponding to the maximum observable region

r_e = radius of the earth

GCD = diameter of the maximum observable region (great circle distance).

The total reflecting area, A_T, used in the reflected sunlight calculations is approximately equal to the plane area projected by one hemisphere which is

$$A_T = \pi r_e^2 \qquad (3.5\text{-}3)$$

The fractional amount of the energy incident on the objective lens which is actually focused on the detector is thus

$$\rho_f = \frac{A}{A_T} = \sin^2\left(\frac{GCD}{2r_e}\right) \qquad (3.5\text{-}4)$$

and modifying the result previously obtained, (3.5-1), gives

$$I_\lambda = I_T \rho_s \rho_f \frac{\alpha_\lambda}{\alpha} \qquad (3.5\text{-}5)$$

or

$$I_\lambda = I_T \rho_s \frac{\alpha_\lambda}{\alpha} \sin^2\left(\frac{GCD}{2r_e}\right) \qquad (3.5\text{-}6)$$

where I_λ is the amount of the background noise actually incident on the detector.

3.6 A Comparison of Various High Power Light Sources

A large variety of light sources capable of high power output have been developed including arc discharge lamps, xenon flashtubes and lasers. Each of these possible active sources has various advantages and disadvantages in terms of cost, power, efficiency, reliability, etc. A thorough analysis of these sources has been performed [38-41] and the data presented will be used to compare the possible active sources by means of an example. The primary consideration in selecting an active source will be the signal-to-noise ratio which can be achieved in a typical system.

Since the sun represents a wideband noise source, it seems reasonable to expect that the laser with its very narrow spectral output will give the highest signal-to-noise ratio. The laser however, has the disadvantage of being relatively more expensive than some of the other possible sources.

3.6.1 Light Sources

The data which will be presented is intended to give an indication of what is currently available in the field of high power light sources. The data given in references [38-41] were obtained primarily from manufacturers' data and may not represent the latest research developments. Most of the high power light sources currently available were designed for some specific purpose and there are no apparent theoretical reasons why more powerful sources could not be developed if needed. The primary limitations to the size of optical sources are practical ones such as the

cost and size of the power supply needed and the problem of removing the thermal energy generated during operation. Both continuous duty and pulsed sources will be considered.

In order to compare the various types of light sources some uniform basis of comparison must be determined. The basis that will be used will be the signal-to-noise ratio which can be attained in an aerospace television system which has been successfully operated in space. Before this comparison can be made, the methods used to rate the light output of a source must be examined. The light output of a given light source may be expressed in either candlepower or lumens. The term candlepower refers to the luminous intensity or light radiating capacity in a given direction and is expressed in candelas (cd). The term lumen (lm) refers to the total luminous flux emitted in a unit solid angle and is related to the luminous intensity by:

$$F = \int I \, d\Omega \qquad (3.6\text{-}1)$$

where F = luminous flux in lm

I = luminous intensity in cd

$d\Omega$ = solid angle differential.

A complete description of the light output of a source would consist of specifying the light output in all directions from the source but this involves a great deal of data and normally only the candlepower in the intended direction of operation or the total lumens is given. For sources with a highly directive output the candlepower rating given is usually either that of the center of the beam or the average over the useful region of the beam. In the case of pulsed sources the light output may be expressed in lumen seconds which is the time integral of the intensity over the pulse duration. It should be noted that the rating of light sources in terms of watts usually refers only to the input power and cannot be directly related to the light output.

In the case where the direction of the desired receiver is known, then the ability of a source to produce a narrow beam of light must be analyzed. The practice of providing only the maximum or average light output ratings makes it difficult to determine the exact beam intensity which could be obtained, but the following simplification will normally suffice. The solid angle over which the light output rating is given can either be estimated or calculated from the specifications of the source. If this source is then put into an optical system which concentrates all the light output into a beam of a different size, the intensity of the new beam will be increased or decreased by the ratio of the solid angle of the new beam to that of the original light output. This procedure makes it possible to compare light sources of different shapes and power by a relatively easy method. A summary of the important characteristics of the sources which will be considered is given in the following sections.

3.6.1.1 Incandescent lamps

One of the most common sources of light is the incandescent lamp which is available in thousands of varieties. One of the largest lamps of this type has an input power rating of 10 kW and a light output of 3.3×10^5 lm [41, p. 8-77]. The highest power incandescent lamps are those designed for use with parabolic reflectors or Fresnel lenses as searchlights. A 1-kW incandescent lamp used in combination with a 36" reflector produced a beamwidth of 4^o at an intensity of 3×10^6 cd [41, p. 18-10] so it is not unreasonable to assume that with a higher power lamp and a smaller beamwidth a luminous intensity of 1×10^8 cd could be obtained. The spectral output of incandescent lamps with tungsten filaments is approximately that of a black body with an emissivity of 0.3-0.5 at a temperature of 1600°K to 3300°K. At 3300°K the peak output occurs at approximately 1μ, but over 70% of the energy produced lies below 1.7μ. The exact spectral density will vary from the predicted density because the emissivity is not constant and, also, the light output will be modified by the spectral transmission characteristics of the glass envelope.

3.6.1.2 Arc discharges (continuous operation)

The electrical arc discharge represents the highest power practical light source yet developed for continuous operation. The most common form of arc discharge used for extremely high power light sources is the unenclosed carbon arc. Other elements commonly used for enclosed arc discharge lamps are mercury, sodium and xenon. The input power to the enclosed discharge lamps is limited by the ability of the glass envelope to dissipate the heat produced by the arc. The carbon arc, however, does not require enclosed operation and can be operated at much higher power levels. In some instances the heat generated is so intense that only water-cooled operation is possible.

Arc discharges in sodium vapor produce a very distinctive light output because of their very narrow spectral output. Almost the entire output of a sodium vapor lamp is concentrated in the double yellow line located at 0.5890μ and 0.5896μ, which makes these lamps unsuitable for uses where color reproduction is important. Lamps of this type are normally used only for street lighting where a distinctive color is desired to indicate special hazards such as at intersections. The typical light output for such uses is on the order of 1.0×10^4 to 4.0×10^4 lm. While the available light output is not nearly as great as that of other arc lamps the narrow spectral output will allow use of a very narrow optical region thus reducing the background noise significantly.

Mercury vapor arc lamps are currently the most widely used enclosed arc lamp and find their main application in street lighting. For special applications water cooled types are available with an input power rating of over 12 kW and a light output of approximately 1.0×10^6 lm [42]. The spectral output of arc discharge lamps depends to a great degree on the pressure of the gas in which the discharge occurs. As the gas pressure is increased, the spectral distribution tends to become a continuum as the characteristic spectral lines tend to become wider. "The broadening

of the spectral lines is caused by the broadening of the energy levels due to the fields of neighboring atoms and colliding electrons ..." and "The continuous spectrum is due primarily to free electrons combining with ions, an event whose probability is significant under the conditions of high electron and ion densities existing in the arc" [40, p. 208]. The pressure used in most high pressure mercury arc lamps is such that the output radiation is almost evenly divided between the line spectra and the continuous spectra [40, p. 211].

For practical purposes all of the energy emitted by mercury vapor lamps can be assumed to lie in the 0.35 to 0.6μ region. The absence of any significant radiation above 0.6μ accounts for the characteristic blue-white color of mercury vapor lamps. While a significant amount of ultraviolet energy is produced the majority of this energy is absorbed by the glass enclosure. The location of the spectral lines of greatest significance is given in Appendix D. The large number of spectral lines which are present makes it impossible to construct a filter which would reject the background energy between the spectral lines and accept only the energy present in the spectral lines.

Xenon arc discharge lamps have a much smoother spectral output in the visible region and are used in applications such as motion picture projectors and solar simulators where color reproduction is important. Lamps with an input power rating of 20 kW and a light output of 1.15×10^6 lm are currently available [42]. The spectral output in the region 0.4 to 0.8μ is sometimes constant to within ± 15% depending on the pressure of the gas [40, p. 214] and makes the xenon arc lamp appear to be a white light source. In the region 0.8 to 1.0μ a number of spectral lines doubles the average spectral output as compared to the visible region.

The unenclosed carbon arc represents the highest power continuous light source available at the present time. The size of the reflectors used and the input power required for the largest carbon arcs would prevent their use on all but the largest ships as shown by the following example. A searchlight developed for the Army used a 120 inch parabolic reflector and produced a beam divergence of 4° by 6°. The peak light output of this searchlight was 2.7×10^9 cd and required an input power of 600 kW at a current of 4000 A [41, p. 18-10]. Some typical examples of carbon arcs of a more practical size are given in Table 5. The spectral output of a carbon arc lamp is approximately that of a black body at the color temperature listed in Table 5. In the visible region black bodies of the color temperatures given have a fairly flat spectral output which makes the carbon arc suitable for photographic and projection purposes which require a white light for true color reproduction.

The black body spectrum approximation holds only for those carbon arcs where the light is produced by the incandescent crater of the electrode and the luminous vapors created by the vaporization of the electrode. Another type of carbon arc lamp is the flame arc lamp which uses carbon electrodes but depends mainly on the vaporization of the electrodes for light production. The color temperature of flame type carbon arcs is two to four times that of the carbon arcs given in Table 5,

Table 5

TYPICAL DIRECT-CURRENT CARBON ARC CHARACTERISTICS
[41, pp. 8-101]

	A	B	C	D	
Use	Projector	Projector	Searchlight	Studio	
Arc Current	120	180	150	225	A
Arc Voltage	68	74	78	70	V
Power	8.2×10^3	1.33×10^4	1.17×10^4	1.58×10^4	W
Candlepower	4.4×10^4	7.8×10^4	6.8×10^4	9.9×10^4	cd
Total Lumens	1.54×10^5	4.1×10^5	3.74×10^5	5.21×10^5	lm
Color Temperature	~ 6000	~ 6000	5400	4100	^oK

and the spectrum no longer corresponds accurately to a black body spectrum at the color temperature. The spectrum of flame-type carbon arcs is usually modified to produce increased output in some desired region by adding rare earth elements to the electrodes.

3.6.1.3 Flashtubes: arc discharges (pulsed operation)

The arc discharges just described were used for continuous operation. Arc discharges can also be used for pulsed operation which is normally done by discharging a capacitor across a spark gap in a high pressure atmosphere. The gas-filled tubes which are used for this purpose are called flashtubes. Pulsed operation of carbon arc discharges is very difficult due to the fact that a stable arc cannot be obtained in the short time required.

The heat dissipation requirements for pulsed operation are much less severe and very high peak outputs can be obtained at very low power dissipation levels. Flashtubes are normally rated for both peak and average power levels. The peak power restriction is necessary because the severe shock of the arc discharge can shatter the glass enclosure of the flashtube if the walls of the tube are too thin. The peak power rating may be as much as four orders of magnitude larger than the average power rating, but this generally occurs only for very narrow pulse widths.

Flashtubes normally consist of three electrodes, two of which are used to conduct the arc current with the third being used to trigger the discharge. A typical circuit for use with flashtubes consists of a pulse forming network which is discharged through the flashtube with the energy for the discharge being provided by the charge stored in the

capacitors of the pulse forming network. The pulse forming network determines the shape of the current pulse, and hence the shape of the light output pulse. The output pulse is triggered by applying a high voltage pulse to the triggering electrode which initiates the electrical discharge. The voltage supplied to the pulse forming network must be less than that required to initiate electrical breakdown between the electrodes without a triggering pulse. The pulse duration is determined by the characteristics of the pulse forming network and typical values range from 1 μs to 10 ms.

Flashtubes are classified into types according to the physical configuration of the light emitting section and four different shapes are commonly used; helical, linear, spherical, and U-shaped. Flashtubes are normally filled with the rare gas xenon, but argon, krypton, and other gases are also used. The spectral output of these tubes is usually a continuum and any spectral lines that are present are quite wide. When xenon is used the spectral output is fairly flat in the visible region with a slightly higher output in the 0.8 to 1.1μ region due to the presence of several spectral lines. Some examples of the performance of currently available flashtubes are given in Table 6.

Arc discharges in unconfined gases have also been used as pulsed light sources but the capabilities of such discharges are normally below those of the flashtube and will not be discussed.

Table 6

TYPICAL FLASHTUBE CHARACTERISTICS [38, p. 49; 43, 44]

Type	Peak Energy Input (joules)	Average Power Input (watts)	Operating Voltage (kV)	Light Emission (cd-s)	Peak Emission (10^6cd)	Pulse Duration (ms)	Arc Resistance (ohms)
U-shaped	120	12	0.3	250	0.25	1.0	0.8
Spherical	8×10^4	1350	6.0	2.8×10^6	36.0	6.0	2.3
Linear	1.5×10^4	1250	2.4	5.0×10^4	1.1	45.0	18.0
Helical	2.6×10^4	110	7.5	1.05×10^5	10.5	10.0	1.2
Linear	2.5×10^4	125	5.0	1.0×10^5	30.0	3.3	0.28

3.6.1.4 Lasers

All the light sources discussed so far, with the exception of the sodium vapor lamp, produced energy over a wide spectral region which make it impossible to filter out a significant portion of the background energy. The laser has a distinct advantage in that its spectral output occupies only a very narrow spectral region so a significant portion of the background energy can be removed. Very narrow beamwidths make it

possible to concentrate the energy available in the desired region to a much greater extent than is possible with incoherent sources. While the average power of most present laser systems is much less than that of other light sources, the peak power available is much greater. Peak powers on the order of 10 TW (1×10^{13} W) have been reported for narrow pulses [45, 46]. One important disadvantage of laser systems is the relatively high cost compared to other light sources.

A summary of the majority of commercially available lasers has been compiled [39]. The results of this study, which are representative of the various types of lasers available, are presented in the following tables. In general the data presented show that the maximum CW power level ranges from a few watts up to the kilowatt level depending on the wavelength, and hence the material used in the operation of the laser. In pulsed operation the peak power depends on the pulse width but for extremely narrow pulses, on the order of 10^{-12} s, power levels in the gigawatt range are available. The data presented are representative only of present commercial lasers and the great amount of research currently being done in this area will provide higher powers and more wavelengths in the near future. A study has recently indicated that a CO_2 laser which operates at 10.6μ with a continuous power output of 8.8 kW has been constructed and an order-of-magnitude increase in the power could be expected in the near future [47]. While this wavelength is much too long for use with present television camera tubes, it indicates the potential power available from gas lasers is much greater than the power now available. In addition to changing the wavelength of a laser by changing the elements used, it is also possible to tune a laser over a given region. Experiments have already shown that a laser can be tuned to a certain extent and it seemed likely that some lasers could be tuned to cover half the visible region [48].

Table 7

GAS LASERS

No.*	Output Spectrum**	Multimode Power Output (W)	Pulse Length or CW	Maximum Rep. Rate	Beam Divergence (mrad)
1	Ar	20	50 μs	5 p/s	1
2	Ar	25	10 μs	120 p/s	2
3	Kr	1.2	50 μs	100 p/s	2
4	0.3371(N_2)	100 kW	10 ns	100 p/s	2 × 30
	0.5401(Ne)	10 kW	3 ns	100 p/s	2 × 30
5	Ar + Kr	20	CW		1
6	10.6 (CO_2)	1000	CW		1
7	0.6328	0.08	CW		0.8

* Identified in Appendix E.

** See Appendix D for location of specific spectral lines.

Table 8

SOLID-STATE LASERS

No.*	Output Spectrum	Output Power	Pulse Length Or CW	Maximum Rep. Rate	Beam Divergence (mrad)
1	0.6943 or 1.06	100 MW	10 ns	30 p/min	3
2	0.6943	750 MW	~ 50 ns	2 p/min	3-5
3	1.06	16 GW	30 ns	8 p/min	0.1
4	1.06	60 MW	0.5-3.0 ms	5 p/min	18
5	0.6943	0.9 W	CW		-
6	1.06	25 W	CW		1-2

Table 9

INJECTION LASERS

No.*	Output Spectrum(μ)	Width of Output(μ)	Peak Power (kW)	Pulse Width (μs)	Maximum Rep. Rate (Hz)	Beam Divergence
1	0.8540	0.0015	0.015	5	500	230 mrad
2	0.9040	0.0100	0.2	0.1	1000	260 mrad
3	0.9160	0.0050	0.8	0.1	1000	0.1 srad
4	0.9040	0.0075	10.0	0.2	500	--

3.6.2 Optical Filters

The generation of an optical signal with well-defined spectral limits immediately presents the problem of recovering that signal from any background noise that may be present when the signal is received. If an optical filter which will recover the original signal while rejecting the background noise is not available, then nothing has been accomplished by using a spectrally well-defined signal that could not have been accomplished by using a higher power source. The problem of choosing an optical energy source for information transmission is thus inherently related to the availability of filters to recover the source energy while rejecting a significant portion of the background energy.

Optical filters are constructed in a variety of ways. The determination of the best optical filter to do a specific task is dependent on how well the problem is specified. The simplest optical

* See Appendix E.

filters are those which consist of some type of optical material. Optical materials, such as glass and plastic, have different inherent transmission characteristics, which can be changed by changing the composition of the material. Considering the many different glass and plastic compositions which are available a large variety of filter characteristics can be obtained. Many optical materials have the property that light above a certain wavelength or below a certain wavelength is absorbed. A bandpass filter can then be constructed by combining two materials of the type just mentioned. Optical filtering can also be accomplished by using special coatings applied to the lenses of an optical system. The ability of an optical coating to provide a filtering action is dependent on the actual transmission characteristics of the coating, the thickness of the coating, and the wavelength dependent reflectance of the coating material. Filters constructed by these methods generally have a passband transmission of approximately 50% and a stopband transmission of 0.1%. The number of specific combinations of optical materials and coatings is so large that only by considering a specific problem or application can the actual filter characteristics be determined.

Another type of optical filter is the filter which operates using the interference phenomena and is generally known as an interference filter [3, p. 286]. The performance of this class of filters is much better than those discussed previously and filters can be constructed which will select a single spectral line. The performance of a set of commercially available interference filters for selecting some typical laser lines is given in Table 10 [49]. The extremely narrow passband of these filters allows almost complete rejection of all light energy except the desired signal. Interference filters can also be constructed with wider bandwidths. Filters which have a bandwidth greater than 1% of the passband center wavelength have transmissions which are usually on the order of 60% while the stopband transmission is less than 0.01% [50].

Table 10

INTERFERENCE FILTERS FOR COMMON LASER WAVELENGTHS

Wavelength (μ)	Bandwidth (μ)	Transmission at Center of Passband	Transmission in Stopband
0.4880	0.001	50%	0.001%
6.5145	0.001	50%	0.001%
0.6328	0.001	50%	0.001%
0.6943	0.001	60%	0.001%
1.060	0.005	45%	0.001%

In general optical filters can be constructed which will have at least 50% transmission in the passband and at most 0.01% transmission in the stopband using one of the methods previously described.

3.6.3 A Comparison of Various Light Sources Using An Example

In order to evaluate the various types of light sources, some uniform means of comparison must be found. Since the optical navigation system being considered will make use of a television camera, one method of comparison would be to choose an actual television system and determine which source will give the best results. The television system that will be used in the comparison is the Surveyor television system. The Surveyor 7 spacecraft has already detected optical signals transmitted to the surface of the moon from earth [51] and should provide a good basis for comparison. Since optical signals have already been detected using one type of source (a laser) one method of comparison would be to determine what other types of sources could also have been used in this experiment.

The optical signal which the Surveyor 7 spacecraft television camera detected had a stellar magnitude of about -3 [51] which gives an equivalent illumination level of 3×10^{-6} lm/ft^2 (f_c) [3, p. 107]. In the experiment in which Surveyor detected the optical signals, a total of six lasers were aimed at the moon and two were detected. The detected signals were located within the moon's shadow, while the others were located in the sunlit portion of the earth. The illumination level on the moon for the portion of the image corresponding to the region of the earth in the moon's shadow was between 10^{-10} and 10^{-8} lm/ft^2. The illumination level on the moon resulting from the earth-reflected sunlight ("earthshine") has been estimated at between 1.2 and 1.7 lm/ft^2 [37, 52]. Thus the signal-to-noise ratio for the received images of the lasers located on the earth but in the moon's shadow was much greater than one. While the signal-to-noise ratio for the lasers located in the sunlit portion of the earth was several orders of magnitude less than one. It should be noted that no optical filters were used to specifically select the laser signals since the camera was not designed for this purpose.

In order to compare the various light sources, they will be evaluated on the basis of the illumination resulting on the moon when the total light output is concentrated into a beamwidth of 10 mrad (0.5°). A beamwidth of this size was considered as reasonably easy to obtain by means of parabolic reflectors or Fresnel lenses. While beamwidths as small as 1 mrad have been reported [38, p. 213], it was not considered practical to assume such a small beamwidth since this could only be accomplished for very small light sources which could be accurately positioned at the focus of the lens or reflector. If the light output is uniformly distributed over the beamwidth and the total luminous flux is concentrated into the beam, then by (3.6-1) the intensity of the source is

$$I = \frac{F}{\Omega} \qquad (3.6\text{-}2)$$

where Ω = solid angle of beam.

If instead of the total luminous flux, F, the light output is specified as the intensity for a given beamwidth, then under the same assumptions used previously, the intensity and beamwidth (in the sense of the solid angle) are related by

$$\Omega_1 I_1 = \Omega_2 I_2 \tag{3.6-3}$$

In other words, the total luminous flux is constant and the beamwidth and intensity are inversely proportional, i.e., their product is a constant.

The above two formulas can be used to calculate the intensity of the beam which would be produced from a specified source when the desired beamwidth is known. The plane angle beamwidth is related to the solid angle of the beam by

$$\Omega = 4\pi \sin^2\left(\frac{\theta}{4}\right) \tag{3.6-4}$$

where Ω = solid angle of the cone formed by rotating a plane angle θ

θ = plane angle in radians.

When θ is small, (3.6-4) reduces to

$$\Omega \approx \frac{\pi\theta^2}{4} \tag{3.6-5}$$

The illumination level at a distance d from a point source of intensity I is

$$E = \frac{I}{d^2} \tag{3.6-6}$$

where E = illuminance in lm/ft^2

I = luminous intensity in cd

d = distance in ft.

Using the distance to the moon as d, (3.6-6) reduces to

$$E = 6.3 \times 10^{-19} I \tag{3.6-7}$$

Using the above simplifications and assuming a beamwidth of 10 mrad, the illumination level produced by a source with a luminous flux output of F lm is

$$E = 8 \times 10^{-13} F \qquad (3.6\text{-}8)$$

where E = illumination level on the surface of the moon in lm/ft^2

F = luminous flux output in lm.

In the case where the light output of the source is specified in terms of the intensity over some given beamwidth, the illumination level is

$$E = 8 \times 10^{-13} \Omega I \qquad (3.6\text{-}9)$$

where Ω = solid angle of the original beam in sr

I = average intensity of the original beam in cd.

Using (3.6-8) or (3.6-9) with the data presented previously on high power light sources gives various values for the illumination level which are presented in Table 11 along with other pertinent data.

Table 11

ILLUMINATION LEVELS OF SIGNALS RECEIVED ON THE MOON FROM VARIOUS HIGH POWER LIGHT SOURCES

Source	Input Power	Light Output	Illumination Level (signal power) lm/ft^2 *	Spectral Region
Incandescent	10 kW	3.5×10^5 lm	2.8×10^{-7}	Visible Region **
Sodium Vapor	400 W	4.0×10^4 lm	3.2×10^{-8}	0.55μ to 0.65μ
Mercury Vapor	12 kW	1.0×10^6 lm	8.0×10^{-7}	0.35μ to 0.6μ
Xenon Vapor	20 kW	1.15×10^6 lm	9.2×10^{-7}	Visible Region
Carbon Arc	600 kW	2.7×10^9 lm/sr ($\sim 5^\circ$ beamwidth)	1.8×10^{-5}	Visible Region
Carbon Arc (D, Table 5)	15.8 kW	5.2×10^5 lm	4.1×10^{-7}	Visible Region

* Assuming 10 mrad beamwidth.

** $0.35\mu < \lambda < 0.77\mu$.

Comparing the illumination levels given in Table 11 with the illumination level of the signal detected (3×10^{-6} lm/ft^2) shows that there are various high power light sources which could be detected on the moon. It is quite significant to note that the lasers which were detected produced a total output of between 2 and 4 watts but, of course, at a much narrower beamwidth. In all cases the received signal intensity is over five orders of magnitude less than the intensity of the reflected sunlight, thus indicating a very small chance of detection for sources in the sunlit portion of the earth. Even in the case of the sodium vapor lamp the use of a filter would not improve the signal-to-noise ratio sufficiently to allow detection since the few percent of background energy that would still be present would be too much.

The inverse square law can be used to relate the calculations just made to the case of a synchronous satellite. The distance to the synchronous satellite is such that improvement of two orders of magnitude can be expected in the signal strength, but this also applies to the background noise. Hence, the conclusions made on the basis of the signal-to-noise ratio at the moon's surface apply equally as well to the synchronous satellite. In the case of pulsed light sources, the duration of the light pulse must be considered. However, if it is assumed that the camera shutter and source are synchronized, then only the light output must be considered. Under this assumption the illumination level for the pulsed light sources (e.g., Table 6) is slightly higher than those of Table 11, but not sufficiently different to change the results.

The following conclusions can be drawn from the results of this section. While there are a number of high power light sources that could be used to provide a detectable signal in the absence of reflected sunlight, none provides a sufficient signal-to-noise ratio for detection against a sunlit background. The laser represents the only light source which has a sufficiently narrow spectral output to permit filtering out a significant portion of the background noise which consists of reflected sunlight. By making use of interference filters such as those described in Table 10, it should be possible to eliminate almost all of the reflected sunlight. In the case of light in the center of the visible region ($\lambda \approx 0.55\mu$) and a filter bandwidth of 0.001μ the background energy present after the filter would be on the order of 0.1% of the incident energy assuming a 6000°K black body spectral distribution. All optical energy sources except the laser can therefore be rejected on the grounds of insufficient signal power in a sufficiently narrow spectral region to overcome the background noise present. An exact determination of the signal-to-noise ratio required will determine if lasers with sufficient power are available.

3.7 Acquisition, Tracking and System Configuration

The results presented in the previous section demonstrate that optical signals from earth-based users can be detected at synchronous altitude under certain conditions. The mere fact that optical signals could be detected does not imply that an optical navigation system is feasible, however. To demonstrate the feasibility of an optical navigation system, it is necessary to show that a system can be

constructed which will be able to detect users under sufficiently general conditions to permit navigation. In other words, the conditions required for detection will impose certain restrictions on when the user's optical signal can be detected, and these restrictions in turn will determine if it is feasible to use optical methods for navigation.

3.7.1 General System Considerations

The system configuration chosen is a television camera which will detect optical signals transmitted by the users. The output from the camera will be fed to a threshold detector which will perform binary detection on each resolvable image element. For such a system to perform reliably, the received signal must be sufficiently strong to ensure a high signal-to-noise ratio so that the detection of the optical signal can be performed under very general conditions. The possible user restrictions which will be imposed by the conditions required for detection of the signal will be illustrated by considering the example of the previous section.

The detection of optical signals described in Section 3.6.3 was accomplished under the following conditions:

1) the signal sources which were detected would have had to come from users operating at night in order to reduce the background energy;

2) very accurate aiming of the lasers used to generate the optical signals was necessary;

3) the resolution available during the experiment was only 200 TV lines [51].

While the performance of the Surveyor 7 television system was never meant to be even remotely connected with an optical navigation system, the conditions under which it operated have very definite implications on the operation of such a navigation system. Conditions 1 and 3 do not present serious restrictions, since it should be possible to use higher power sources and filters to overcome the background noise, and the development of high resolution camera tubes which can operate in space should be expected as a result of the earth resources program. While conditions 1 and 3 are present because of the type of equipment involved, condition 2 has further implications regardless of what type of equipment is used.

In the experiment in which Surveyor 7 detected laser signals transmitted from the earth, it was found that a pointing accuracy of 2-4 seconds of arc was required [51]. In terms of the position error from synchronous altitude, this would mean a maximum allowable position error of 0.7 km with no provision for inaccurate aiming of the laser beam. If a position accuracy such as that just calculated is required in order to aim a laser so that the beam can be detected, then such a system could not be used for navigational purposes. A system which requires an accurate knowledge of the position of the user in order to operate cannot be expected to serve as the basis of a navigation system. In

order to overcome this restriction, it will be necessary to either increase the beam divergence or have the source scan the region where the satellite is assumed to be located. Assuming the user has an a priori knowledge of his approximate position, perhaps from a much less accurate navigation system, this knowledge can then be used to predict the approximate region of the sky where the satellite will be located.

The feasibility of an optical navigation system will depend on the relationships among source power, beam divergence and position knowledge with the restriction that the optical energy received must be sufficient to provide the resolution required. In order to be feasible the optical system proposed must be able to tolerate a sufficiently large position error without requiring a source power greatly in excess of the currently available laser power. A reasonable estimate for the maximum position error which should be tolerated is the distance between two successive position fixes and depending on the user's velocity and time between position fixes, the position error could be on the order of several hundred kilometers. It is unlikely such a large position error could be tolerated by an optical navigation system, considering the source power that will probably be available. Even the simplest navigation equipment, however, should provide a more accurate estimate than that which could be obtained by dead-reckoning, which is what a position error of several hundred kilometers might represent. A reasonable value for the source power required should be less than 100 W if the development of the source is to be expected in the near future.

3.7.2 Search Techniques

In order to determine the section of the sky in which the satellite is located, it is necessary to know the approximate location of the user. The more accurate the estimated user position is, the smaller will be the section of the sky in which the satellite is located. For small position errors it may be possible to increase the beam divergence to compensate for the lack of knowledge of the user's exact location. Large position errors, however, will require that the user scan the region of the sky in which it is expected that the satellite will be located. In either case the uncertainty in the position of the user can be directly related to the size of the region of the sky which must be searched, and hence to the beam divergence required to search that region.

The uncertainty in the user's position will be expressed as a circle with some given great circle distance as the diameter (region of possible location) and the center of which is the estimated position. The estimated position will determine the expected location of the satellite, and the error in the estimated position will determine the beam divergence required so that no matter what the true position of the user, the satellite will intercept the transmitted beam. The geometry of the situation is illustrated in Fig. 26, where the expected position of the user is at the subsatellite point. As will be shown later the derivation of the beam divergence in this specialized situation represents no loss in generality. The situation illustrated in Fig. 26 is the following. The user has estimated his position and found that it is at

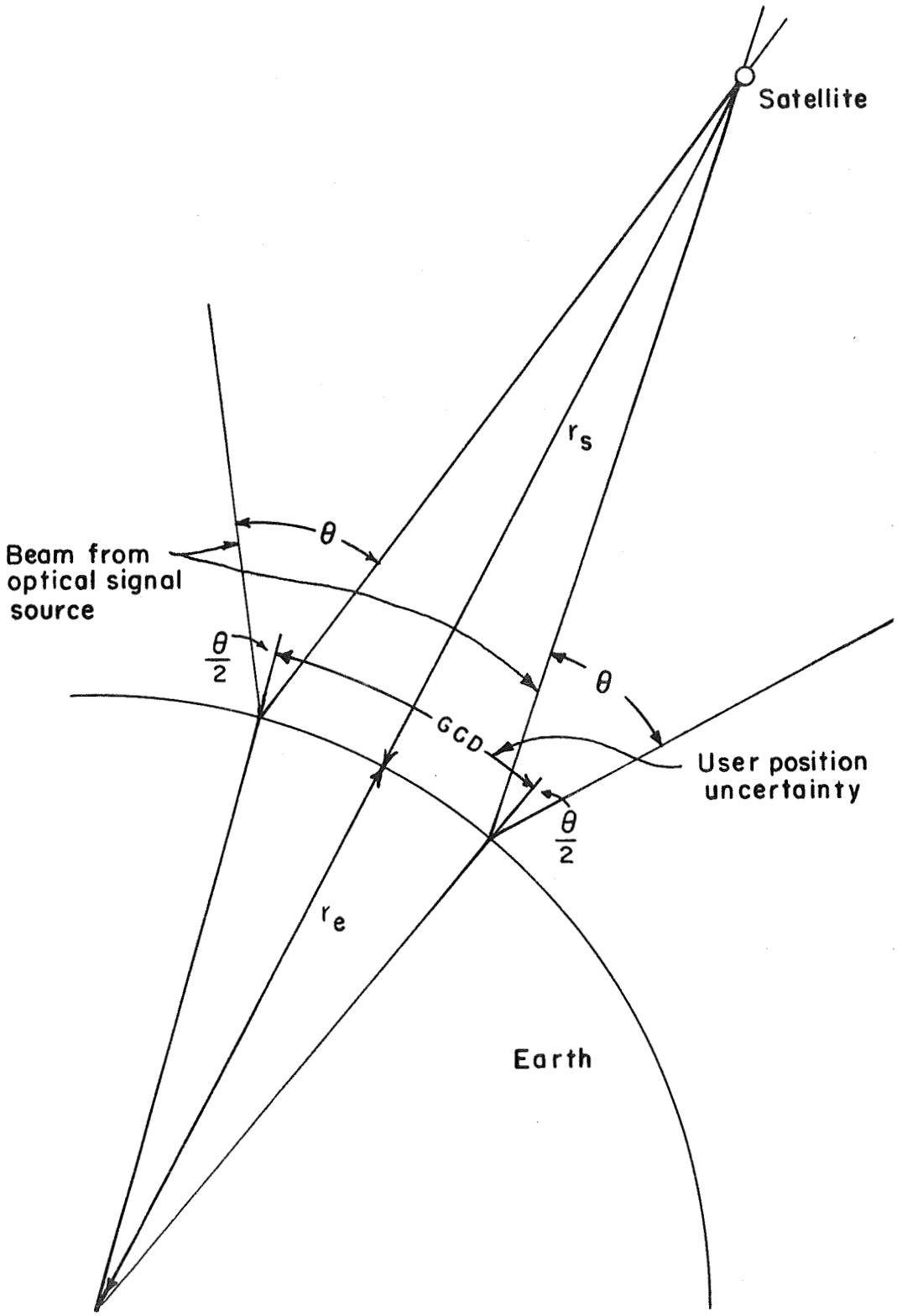

FIGURE 26 GEOMETRICAL RELATIONSHIP BETWEEN USER POSITION UNCERTAINTY AND BEAM DIVERGENCE.

the subsatellite point and the accuracy of this estimate is such that with a very small probability of error, the user is within a circle with great circle distance GCD as the diameter. Since the optical signal transmitted must be received by the satellite, the user position corresponding to the maximum possible error will determine the beam divergence. The angle θ corresponds to the beam divergence required in the worst case and is illustrated for two positions exactly opposite one another.

Geometrically the situation described in Fig. 26 is exactly the same as that described in Fig. 12 except that in the present situation θ and GCD have exactly half the value in Fig. 12. Using the previous result (2.7-4) and noting the relationship among the variables:

$$\frac{\theta}{2} = \tan^{-1}\left[\frac{r_e \sin\frac{d\Delta}{2r_e}}{r_s + r_e\left(1 - \cos\frac{d\Delta}{2r_e}\right)}\right] + \frac{d\Delta}{2r_e} \qquad (3.7\text{-}1)$$

where θ = beam divergence required

$d\Delta$ = GCD = diameter of the circle of uncertainty in the position expressed as a great circle distance

r_e = radius of the earth

r_s = synchronous satellite altitude.

A beam divergence (plane angle) of θ radians yields a beam of solid angle Ω:

$$\Omega = 4\pi \sin^2\left(\frac{\theta^2}{4}\right) \qquad (3.7\text{-}2)$$

which reduces to the following for very small angles:

$$\Omega \approx \frac{\pi\theta^2}{4} \qquad (3.7\text{-}3)$$

Using (3.7-1) and (3.7-2) the region of the sky where the satellite is located can be expressed in terms of a solid angle which is a function of the error in the estimated position.

$$\Omega = 4\pi \sin^2 \left\{ \frac{1}{2} \left(\tan^{-1} \left[\frac{r_e \sin \frac{d\Delta}{2r_e}}{r_s + r_e \left(1 - \cos \frac{d\Delta}{2r_e} \right)} \right] + \frac{d\Delta}{2r_e} \right) \right\} \qquad (3.7\text{-}4)$$

where Ω = solid angle of the portion of the sky in which the navigation satellite is located

$d\Delta$ = diameter of region of position uncertainty.

In the case of a very small error in the position estimate (3.7-4) reduces to

$$\Omega \approx \frac{\pi}{4} d\Delta^2 \left(\frac{r_e + r_s}{r_e r_s} \right)^2 \qquad (3.7\text{-}5)$$

or

$$\Omega \approx 2.7 \times 10^{-8} d\Delta^2 \qquad (3.7\text{-}6)$$

where $d\Delta$ is expressed in kilometers.

The results of (3.7-1) and (3.7-4) have been plotted in Fig. 27 for all possible values of the position uncertainty GCD or $d\Delta$. The results presented in Fig. 27 show that the size of the solid angle to be searched is directly proportional to the square of the position error except for extremely large values. Considering the relative magnitudes of r_e and r_s in (3.7-4), it is seen that for all practical purposes (3.7-6) can be used for all calculations and not just those in which $d\Delta$ is small. Note that the maximum $d\Delta$ is 18106 kM which corresponds to the case where the whole sky must be searched, i.e., the solid angle to be searched is 2π sr.

If the estimated position of the user is not at the subsatellite point then the size of the region of possible location must be such that it is not possible that the satellite is below the user's horizon. In terms of the distances involved the restriction necessary so that the satellite is never below the user's horizon for any position in the region of possible location is:

$$d\Delta \leq \frac{\pi}{2} r_e - 2d_{sp} \qquad (3.7\text{-}7)$$

where d_{sp} = great circle distance from the subsatellite point to the estimated position of the user.

Since the errors associated with an angular measurement navigation system become worse at low elevation angles the inequality (3.7-7) should be

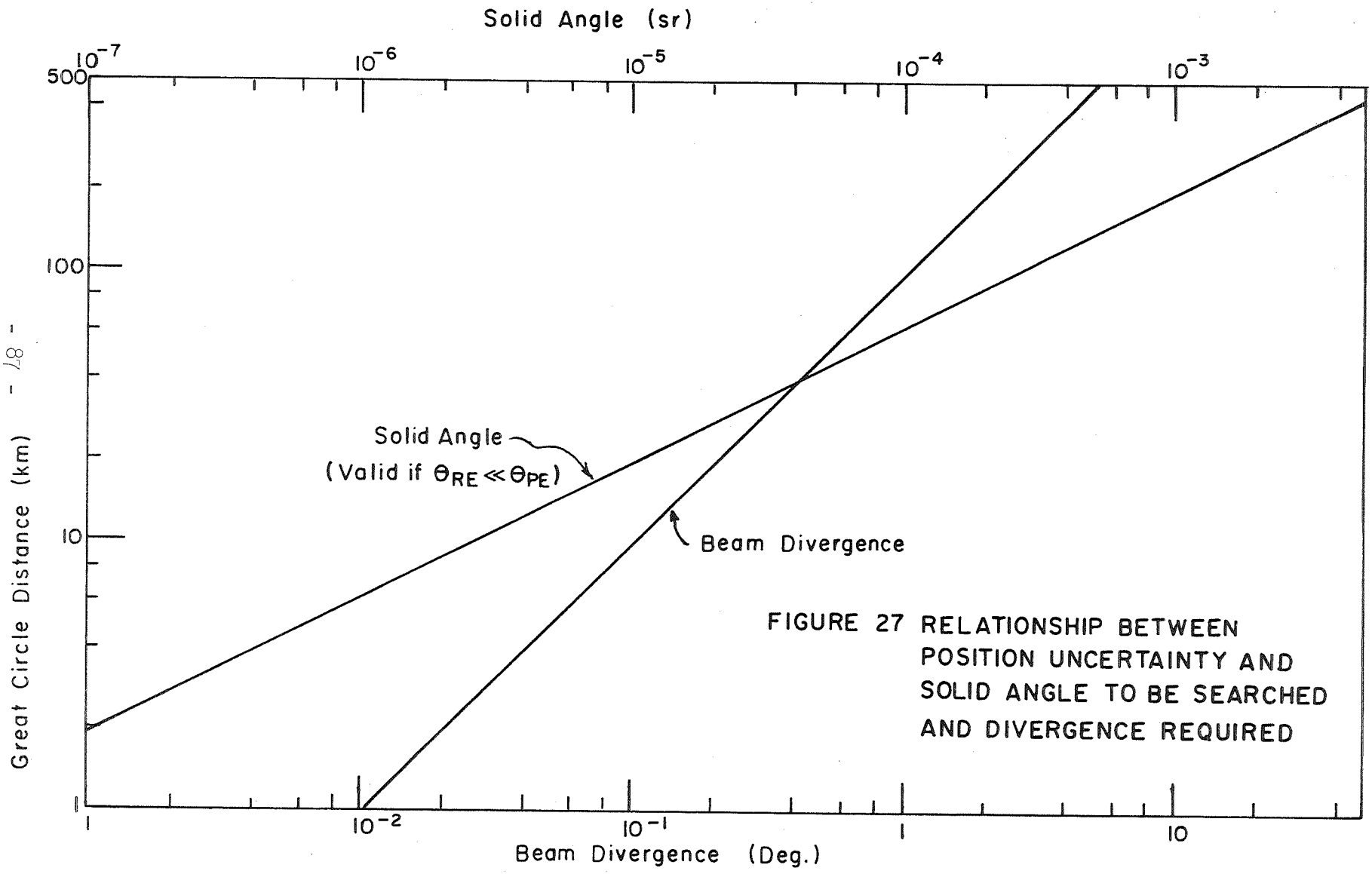

FIGURE 27 RELATIONSHIP BETWEEN POSITION UNCERTAINTY AND SOLID ANGLE TO BE SEARCHED AND DIVERGENCE REQUIRED

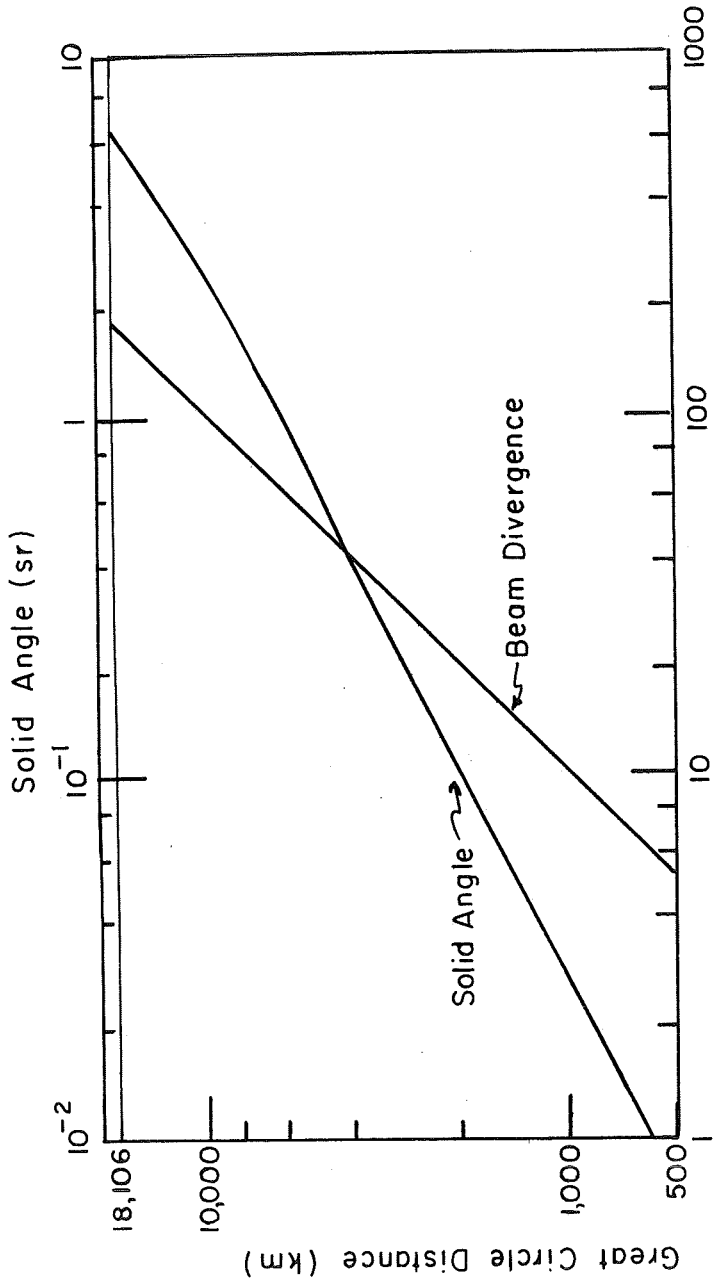

FIGURE 27 CONTINUED

made stronger by multiplying the right-hand side by some safety factor, say 0.85, for elevation angles below about 15°. The exact form of the restriction (3.7-7) and the value of the safety factor would depend on the performance of the optical system at the edges of the image. The factor $\pi\ r_e/2$ corresponds to a field-of-view of about 17° and the actual value of this factor would depend on the field-of-view of the actual optical system used.

The results in Fig. 27 represent the worst possible results for a given great-circle-distance since the angular resolution is best at the subsatellite point. The beam divergence required becomes less as the estimated position moves away from the subsatellite point since the effect of the possible position variation represents less of an angular variation than a similar position error at the subsatellite point. To a first approximation the size of the solid angle to be searched is inversely proportional to the square of the GDOP factor provided the size of the region of uncertainty or position location is small enough so that the elevation angle can be assumed to be constant in this region. Under these assumptions the results in Fig. 27 can be modified to account for estimated positions other than the subsatellite point by dividing the results of Fig. 27 by the GDOP factor or

$$\Omega(\epsilon) = \frac{\Omega}{(\text{GDOP})^2} \qquad (3.7\text{-}8)$$

where $\Omega(\epsilon)$ = solid angle to be searched as a function of the elevation angle

Ω = solid angle from Fig. 27 corresponding to the size of the region of uncertainty

GDOP = geometrical-dilution-of-precision corresponding to the elevation angle ϵ at the estimated user position.

From Appendix A, (A.6) can be used to evaluate the GDOP factor giving

$$\Omega(\epsilon) = \Omega \left(\frac{r_s}{r_1(\epsilon)\ \text{cosec}(\epsilon)} \right)^2 \qquad (3.7\text{-}9)$$

The elevation angle and the distance to the user from the satellite, $r_1(\epsilon)$, can both be evaluated in terms of the great circle distance from the subsatellite point to the estimated user position using (2.7-3) and (2.7-4) giving the approximation (3.7-10). Equation (3.7-10) is valid only if the elevation angle is approximately constant over the region of possible user position and this restriction becomes weaker as the estimated position approaches the subsatellite point where it is unnecessary.

$$\Omega(d\Delta,\ d_{sp}) = \frac{r_s^2\left\{4\pi \sin^2\left[\frac{1}{2}\left(\tan^{-1}\left[\frac{r_e \sin\frac{d\Delta}{2r_e}}{r_s + r_e\left(1 - \cos\frac{d\Delta}{2r_e}\right)}\right] + \frac{d\Delta}{2r_e}\right)\right]\right\}}{\left[r_s^2 + 2r_e r_s\left(1 - \cos\frac{d_{sp}}{r_e}\right) + 2r_e^2\left(1 - \cos\frac{d_{sp}}{r_e}\right)\right] \operatorname{cosec}^2\left\{\frac{\pi}{2} - \tan^{-1}\left[\frac{r_e \sin\frac{d_{sp}}{r_e}}{r_s + r_e\left(1 - \cos\frac{d_{sp}}{r_e}\right)}\right] - \frac{d_{sp}}{r_e}\right\}}$$

(3.7-10)

where $\Omega(d\Delta,\ d_{sp})$ = solid angle to be searched as a function of the distance from the subsatellite point and diameter of the region of uncertainty

d_{sp} = distance from the subsatellite point to the estimated user position

$d\Delta$ = diameter of the region of position uncertainty

r_e = earth radius

r_s = synchronous satellite altitude.

Using the same approximations as those used to obtain (3.7-5) the value of (3.7-10) can be approximated by

$$\Omega(d\Delta,\ d_{sp}) = \frac{\pi}{4}\, d\Delta^2 \left(\frac{r_e + r_s}{r_e\ r_s}\right)^2 \left[1 - \frac{1}{2}\left(d_{sp}\left(\frac{r_e + r_s}{r_e\ r_s}\right)\right)^2\right]^2 \qquad (3.7\text{-}11)$$

or

$$\Omega(d\Delta,\ d_{sp}) = 2.7 \times 10^{-8}\, d\Delta^2 \left[1 - 1.7 \times 10^{-8}\, d_{sp}^{\ 2}\right]^2 \qquad (3.7\text{-}12)$$

which is sufficiently accurate for most purposes except in regions of small elevation angles, i.e. 15° and below, and large values of $d\Delta$.

The size of the region of position uncertainty is not the only factor which determines the size of the region to be searched. In addition to knowing his position, the user must also have some orientation reference in order to know in which direction to aim the laser. The user's heading must be known and his horizontal reference must also be known and any error in these quantities will cause a corresponding error in the estimated position of the satellite. Such an error is not accounted for in the determination of the size of the region to be searched from the position error. The size of the region to be searched will have to be increased to allow for the possibility of an orientation error.

The user's orientation will be determined from his compass heading and a horizontal reference which will probably be the position of the horizon. If each of these directions has an associated angular error and the directions are assumed to be orthogonal, then the true position of any point in the sky will be within a projected rectangular region. The beam divergence will be increased so that no matter where the true location of a point is within the projected rectangle, it will still be within the region scanned by the user. Using the independence assumption, the maximum angular position error which can occur will be the hypotenuse of the right spherical triangle with sides $\Delta\theta_C$ and $\Delta\theta_H$. If the beam divergence is then increased by the maximum angular reference error then the system will operate regardless of the error. The total beam divergence, taking into account the angular reference error, is:

$$\theta_T = \theta_{PE} + \theta_{RE}$$

$$= \theta_{PE} + \cos^{-1}\left[\cos(\Delta\theta_C)\cos(\Delta\theta_H)\right] \qquad (3.7\text{-}13)$$

where θ_T = total beam divergence required

θ_{PE} = θ = beam divergence required as a result of position error (from Fig. 27)

θ_{RE} = beam divergence required as a result of reference errors

$\Delta\theta_C$ = maximum angular error in compass heading

$\Delta\theta_H$ = maximum angular error in horizontal reference.

The total beam divergence, θ_T, must be used when determining the size of the region to be searched (see Section 3.9.3).

Now that the relationship between the position uncertainty, the reference error and the size of the region to be searched has been found, the method used to search the region must be considered. At the beginning of this section two possible search methods were given. One method was simply to increase the beam divergence using a variable focus lens for example. The other was to actually sweep or scan the region to be searched in some predetermined manner. The point at which the switch should be made from an increasing beam divergence system to a scanning system will depend on the source power available. It would be preferable to simply increase the beam divergence since this would require a simpler mechanical system than a scanning system, but as the beam divergence is increased the power required to yield a detectable signal also increases. In order to compare the two methods the total received signal energy must be found since the signal duration will not be the same for the two cases.

The received signal energy in the case where the beam divergence is varied can be calculated from the energy distribution in the beam and the shutter speed. To calculate the received energy in the case of a scanning beam, the energy distribution in the beam must be known as a function of the time in which the beam is incident on the satellite. The method in which the beam is scanned over the desired region will determine the energy distribution of the received signal.

Since the region to be scanned is conical a spiral method of scanning will be used. This method is consistent with the shape of the beam and the shape of the region to be searched. Figures 28 and 29 illustrate the type of search method which will be used. The situation described in these figures is the following. The user has estimated his position and the accuracy of his position and found that the region to be searched corresponds to a total beam divergence of θ_T which includes any possible reference errors. The region must be searched with a source having a beam of θ_b. The search pattern to be used is a spiral with the center of the spiral corresponding to the estimated satellite position determined from the user's estimated position. The scanning motion is produced by a rotating lens system which rotates at a rate $\omega(\phi)$ and is aimed in a direction ϕ which is the deviation from the expected position of the satellite. If the probability distribution of the user's position within the region of uncertainty were known then the scanning motion could be modified to scan the most probable region. Since it is assumed that the user can be anywhere within the region of uncertainty, a uniform probability

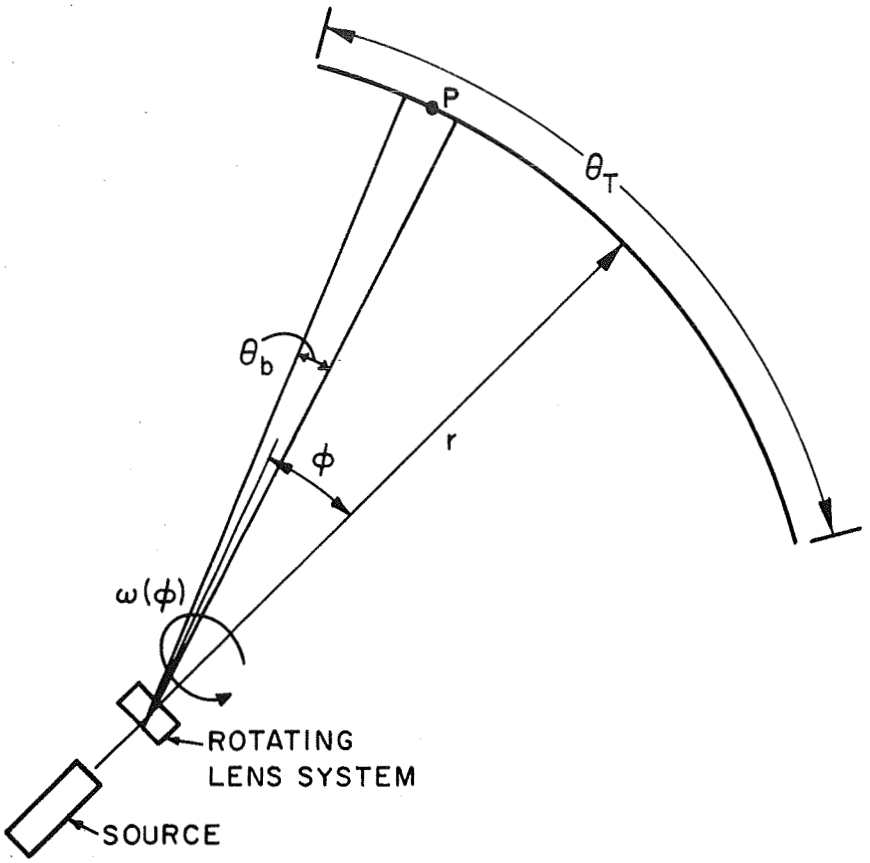

FIGURE 28 SCANNING SYSTEM CONFIGURATION

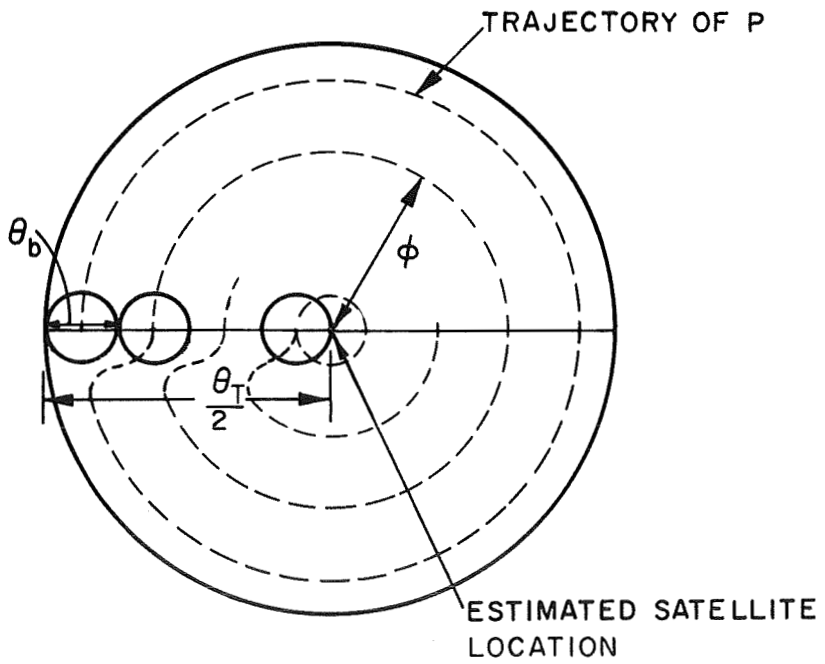

FIGURE 29 SEARCH PATTERN

distribution is implied. The source beam must therefore scan the region to be searched in such a way that the rotation rate $\omega(\phi)$ decreases as ϕ increases so as to illuminate each point in the region θ_T to be searched equally. An analysis of the scanning motion will be made to determine how the received signal energy varies with the scanning motion.

From Fig. 29 it can be seen that the total number of revolutions of the source beam required to cover the desired area is

$$R_T = \frac{\theta_T}{2\theta_b} \tag{3.7-14}$$

where R_T = number of revolutions required

θ_T = total divergence of total region to be searched

θ_b = beam divergence.

If R_T is large, then the scanning pattern illustrated in Fig. 29 can be approximated by a true spiral. The results which follow will then be applicable to a true sprial even though they are derived using Fig. 29. If the source beam is revolving at a rate $\omega(\phi)$ then the tangential velocity of the point P, the center of the search beam, is

$$v = \omega(\phi) r \sin \phi \tag{3.7-15}$$

assuming that the distance to the satellite does not change as a function of ϕ. This assumption is true if the user is stationary and the estimated user position is at the subsatellite point. If the received signal energy is to be constant at all points in the region to be searched, then the velocity of point P must be constant and the rate of rotation, $\omega(\phi)$, must be

$$\omega(\phi) = \frac{v}{r \sin \phi} \tag{3.7-16}$$

In order for the point P to move according to the search pattern illustrated in Fig. 29, the deviation angle, ϕ, must take on all odd multiples of $\theta_b/2$. The path length over which P moves in one revolution is

$$\ell(\phi) = 2\pi r \sin \phi \tag{3.7-17}$$

and the total path length travelled while scanning the entire region is

$$L_T = \sum_{\phi} \ell(\phi)$$

$$= \sum_{\phi} 2\pi r \sin \phi$$

$$= 2\pi r \sum_{n=1}^{n=\frac{\theta_T}{2\theta_b}} \sin \left\{ \frac{(2n - 1)\theta_b}{2} \right\} \qquad (3.7\text{-}18)$$

where L_T = total path length

r = distance to satellite (see (2.7-3))

θ_T = total divergence of region to be searched

θ_b = beam divergence of user's source.

Equation (3.7-18) can be simplified by evaluating the summation giving [53]

$$L_T = 2\pi r \sin^2 \left(\frac{\theta_T}{4}\right) \operatorname{cosec} \left(\frac{\theta_b}{2}\right) \qquad (3.7\text{-}19)$$

since P is moving at a constant velocity, the length of time it will take P to move a distance L_T is

$$T = \frac{L_T}{v} \qquad (3.7\text{-}20)$$

where T = search time

L_T = total path length

v = tangential velocity.

In order to find the minimum search time the minimum value of the path-length to velocity ratio must be found. The value of this ratio will depend on the minimum signal energy required. By evaluating (3.7-20) using various restrictions the feasibility of the system can be determined in terms of the search time and source power required.

3.7.3 System Configuration and Hardware

The description of the system and method of operation which has been given so far is sufficient to permit a description of a method of implementation. The hardware realization of the system which has been proposed is partially given in Figs. 30 and 31. A more exact hardware description could only be given after examining the trade-offs between hardware and software in the blocks which must perform the computations. In the receiver especially it might be possible to have one small computational block which would perform the various computations needed by changing the program used to perform the calculations. The increasing capability in the large-scale-integration of integrated circuits should make the blocks which perform only computations readily available as custom designed devices. The cost of such devices should be relatively small compared to the cost of the laser and scanning system components.

The navigation satellite, shown in Fig. 30, works in the following manner. The signals from the users and the reference stations are focused through a filter on to a high-resolution television camera. The output from the television camera is fed to a threshold device which makes a binary decision on each resolvable image element as to the presence of a user. The outputs from the threshold device and the deflection circuits are fed to a device which calculates the picture coordinates of the signals detected. One possible method of doing this is to feed the horizontal and vertical sweep signals into analog-to-digital converters which would yield a digital representation of the position of the detected signals. The conversion process is initiated by the presence of an output from the threshold device so only the coordinates of the detected signals are calculated. The picture coordinates of the detected signals are stored in a series of registers until the scanning process is complete. The picture coordinates of the reference stations and their locations will be used to compute the location of the users from the picture coordinate. In order to separate the reference stations from the users, the system will have to be calibrated at regular intervals. The interval between calibrations will depend on the stability of the satellite.

Several methods are available which could be used to calibrate the system and in addition some could be used to differentiate among users. Since the location of the ground reference stations is very well known, only a very narrow beam divergence is required thus giving a much larger signal energy. A second threshold detector also operating on the camera output could be used to distinguish the very large signals of the reference stations from the much weaker signals of the users. The threshold level of the reference station detector would be set much higher than that of the user level detector. A second method which could be used is to allot certain time segments to different classes of users. In such a system, users would be given a priority which would determine the time segment to be used and the velocity of the user would determine the length of time between segments. By making the segments very long compared to the time interval between observations by the satellite relatively inaccurate timing systems could be used. Another method which could be used is to use several filters for different wavelengths. Such a system could be implemented by placing the filters

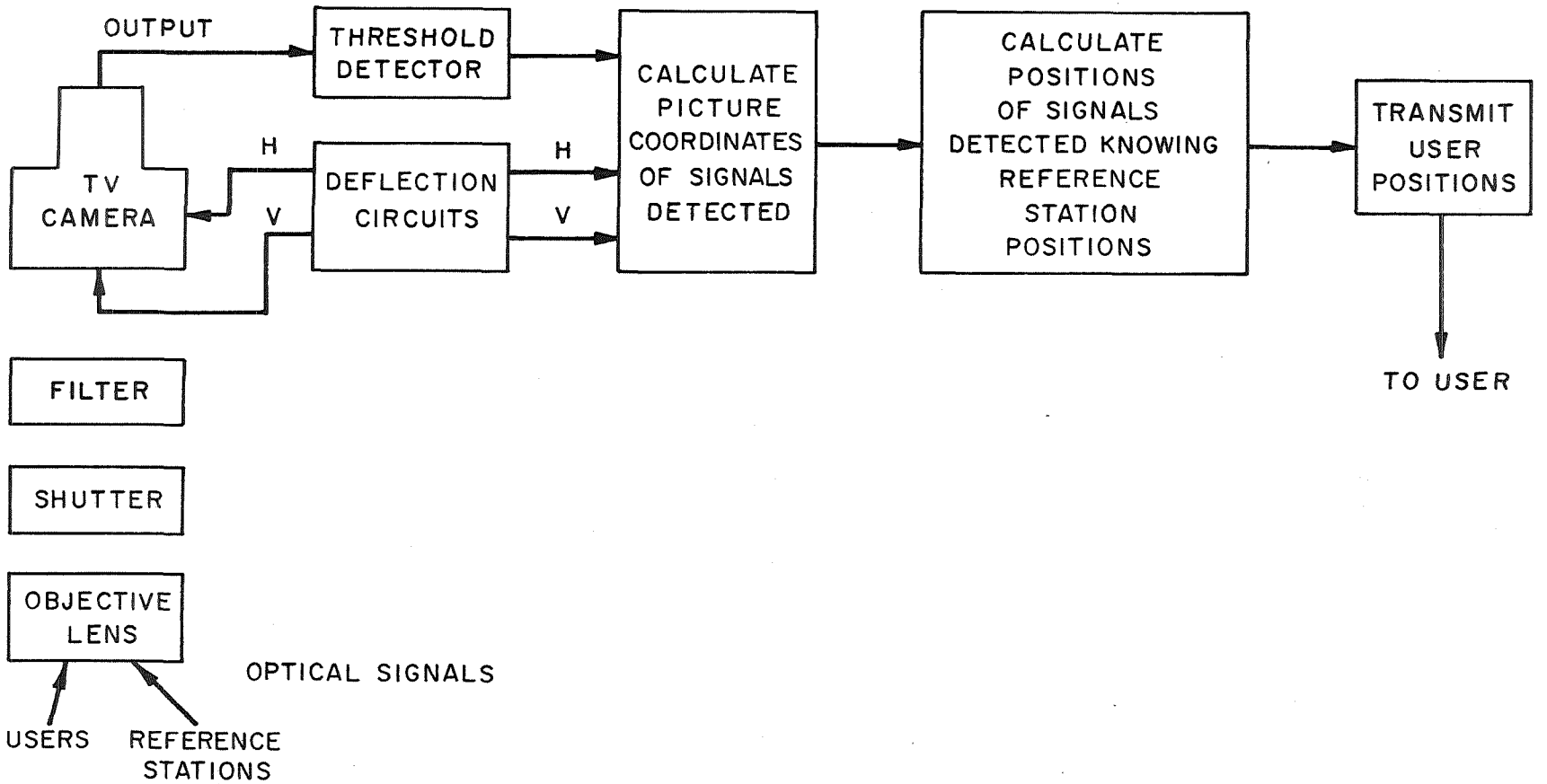

Figure 30 Simplified Block Diagram of an Optical Navigation Satellite

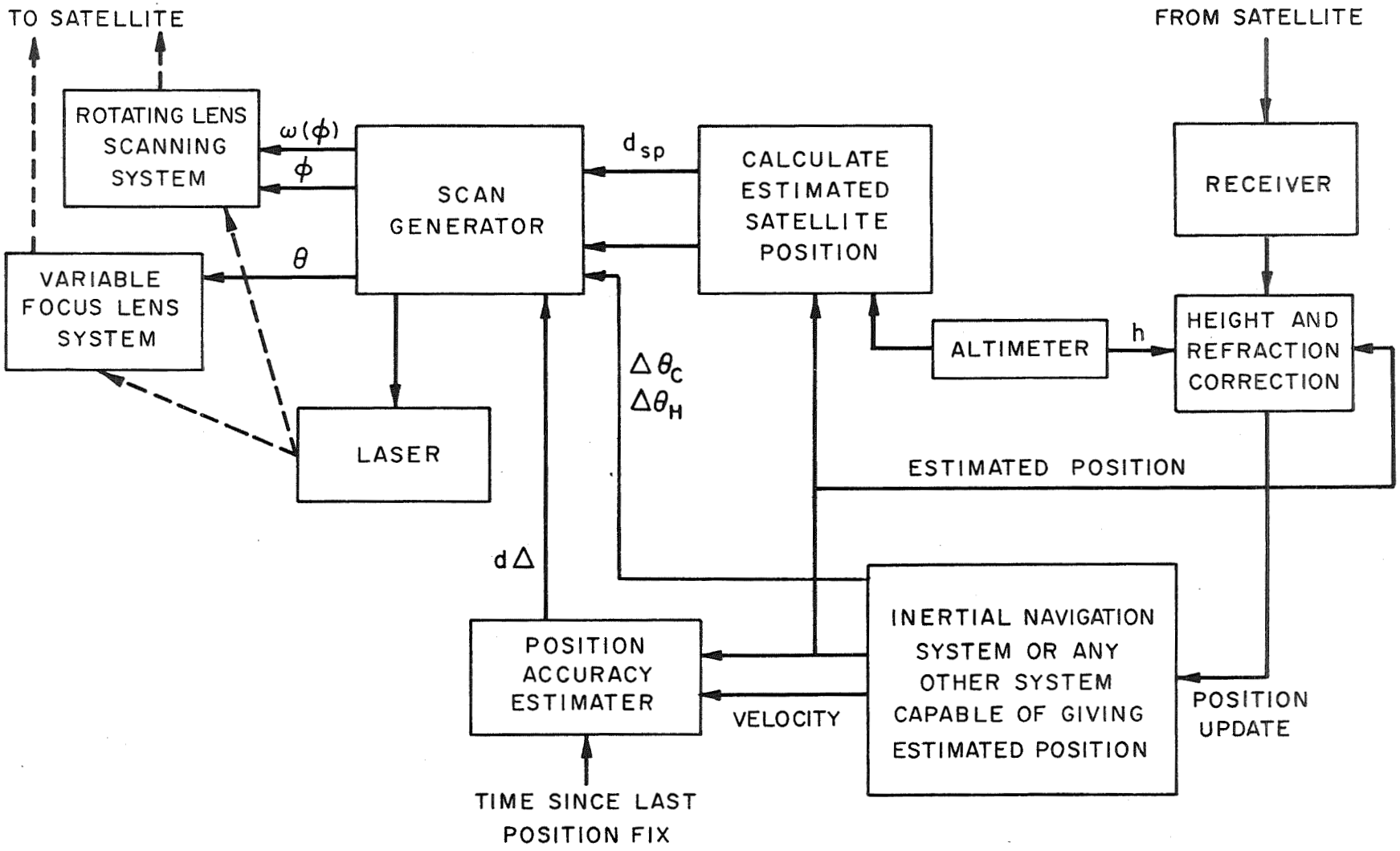

Figure 31 Simplified Block Diagram of User Equipment for an Optical Navigation System

on a wheel which rotated in front of the camera and would require that several different types of lasers be used. It might also be possible to use a combination of these methods at the same time in order to differentiate and identify particular users.

The users equipment, shown in Fig. 31, is based on the assumption that an estimate of the current position and its accuracy is available. While this position estimate may range from a simple estimate made by the pilot from the velocity and compass readings since the last position fix to the sophisticated estimate made by an inertial navigation system the principle of operation is the same. The estimated position and its accuracy is used to control the scanning circuits. Depending on the accuracy of the estimated position, one of the two proposed scanning systems would be chosen so that only one of the systems would be present in actual equipment.

The system shown operates in the following manner. The satellite transmits the calculated location of the observed signals and the receiver selects the one most likely to represent the user's position. If a time division system and/or wavelength division system is used then the user will have little trouble in recognizing his position among the others transmitted since these methods reduce the number of positions likely to be received by a given class of user. Once the new position fix is obtained it must be corrected to minimize the effects of altitude and refraction. Since the corrections must be done knowing the height of the user and the weather conditions (temperature and humidity are needed for refraction correction), the corrections can only be made by the user. Since the position must be known in order to make these corrections it may be necessary to make the corrections using the estimated position and then make them again using the position just calculated to get a more accurate correction. Depending on the field-of-view and the accuracy required these corrections may be unnecessary or so small that they could be estimated at the satellite and transmitted to the user to reduce the complexity of the user equipment. The corrected position is then transmitted to the inertial navigation system.

The remainder of the blocks in the user equipment diagram are connected with the determination of the scanning pattern parameters. The estimated position is used to determine the origin of the spiral search pattern and might be called the expected satellite position. The estimated position is also used to calculate the expected distance from the subsatellite point which is needed to evaluate the size of the region to be searched. The velocity, time, estimated position and type of navigation system providing the estimated position must all be considered in providing an evaluation of the accuracy of the position estimate. The estimated satellite position, the distance to the subsatellite point, and the position accuracy estimation are all fed into the scan generator which aims the beam and provides the scanning signals necessary to perform the search pattern described in Section 3.7.2. The complexity of the user's equipment will depend on how many of the calculations needed can be performed by equipment already existing in the present navigation system. If the present navigation system is complicated and has the computational capacity needed, then the additional

equipment will consist mainly of the laser and scanning system. Since few navigation systems have the computational capacity needed a more realistic approach would be to combine the navigation systems so as to have common components which would then reduce the cost.

The optical navigation system just described is intended to operate in conjunction with another navigation system. The feasibility of an optical navigation system will probably depend directly on the value of the estimated position accuracy, since this quantity will directly determine the size of the region to be searched. If the search time or signal energy required for the size of a typical region to be searched is too large for the systems which might be available in the near future, then an optical navigation system will not be feasible.

3.8 Signal Energy Received

In the passive case the signal-to-noise ratio could be determined from the irradiance (incident power) due to the source and the background. In the active case, however, the energy in the signal and the background noise must be used since the duration of the signal and the noise will not be equal.

3.8.1 Intensity Distribution of a Laser Beam

To calculate the energy received at the satellite the spatial energy distribution of the laser beam must be known. The intensity distribution in a laser beam is approximately the same as the Fraunhoffer diffraction pattern due to a plane wave incident on a circular aperture (e.g., a lens) [54]. The conditions under which this pattern is produced are illustrated in Fig. 32 and this situation corresponds to a laser which uniformly illuminates an ideal lens. The intensity distribution (or irradiance) on the plane at a given distance is given by [55, p. 396]

$$I(p) = \left[\frac{2J_1(k\theta a)}{k\theta a}\right]^2 I(0) \qquad (3.8\text{-}1)$$

$$k = \frac{2\pi}{\lambda} \qquad (3.8\text{-}2)$$

where $I(p)$ = irradiance at point P

θ = angular deviation from the center line

λ = wavelength of radiation incident on the aperture

a = aperture or lens radius

$I(0)$ = irradiance on the center line at a distance r_s from the source

J_1 = first order Bessel function.

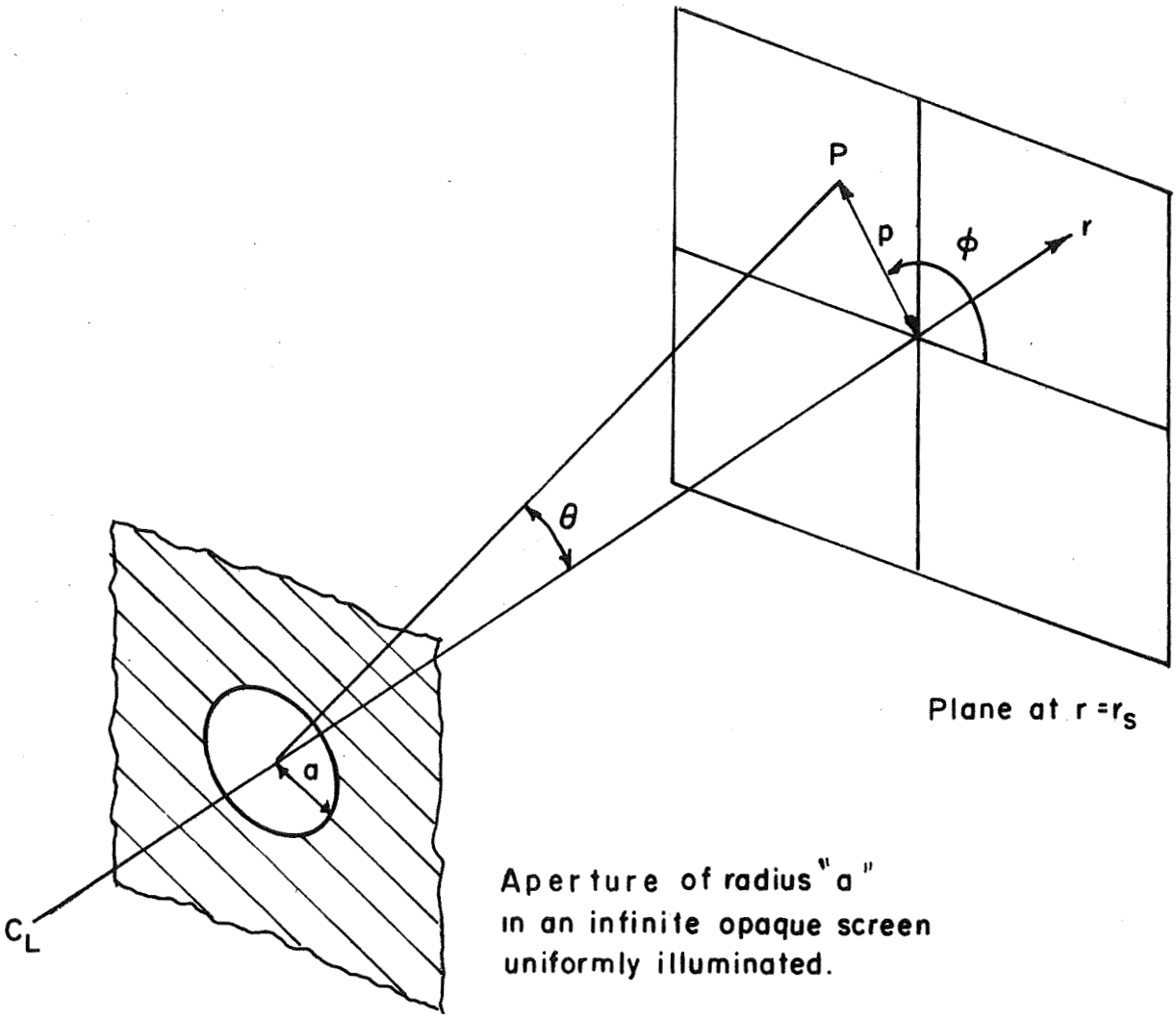

FIGURE 32 FRAUNHOFER DIFFRACTION BY A CIRCULAR APERTURE.

Equation (3.8-1) is plotted in Fig. 33. The use of polar coordinates is indicated by the geometry of the situation under consideration. The intensity distribution of Fig. 33 was qualitatively described in Section 2.3.1.

In order to avoid considering the wavelength of the light being used and the diameter of the lens these quantities will be related to the beam divergence. The term "beam divergence" can be defined in various ways but in this report it will be taken to be the plane angle between the 3 dB or half power points exactly opposite each other on the intensity distribution. The half power point is the point at which the intensity is equal to half the maximum value. Using this definition, the beam divergence can be found by solving the equation

$$\frac{I(p)}{I(0)} = \left[\frac{2J_1(k\theta a)}{k\theta a}\right]^2 = \frac{1}{2} \qquad (3.8\text{-}3)$$

for θ which will be equal to half the beam divergence when (3.8-3) is satisfied. The solution to (3.8-3) is

$$k\theta a = 1.61634 \qquad (3.8\text{-}4)$$

or

$$\frac{\theta_b}{2} = \frac{1.61634}{ka} \qquad (3.8\text{-}5)$$

By solving for ka this factor can be eliminated from (3.8-1) and θ_b introduced in its place. From (3.8-5)

$$ka = \frac{3.2327}{\theta_b} \qquad (3.8\text{-}6)$$

Substituting (3.8-6) into (3.8-1) and noting that

$$\theta \approx \frac{p}{r_s} \qquad (3.8\text{-}7)$$

for small angles gives

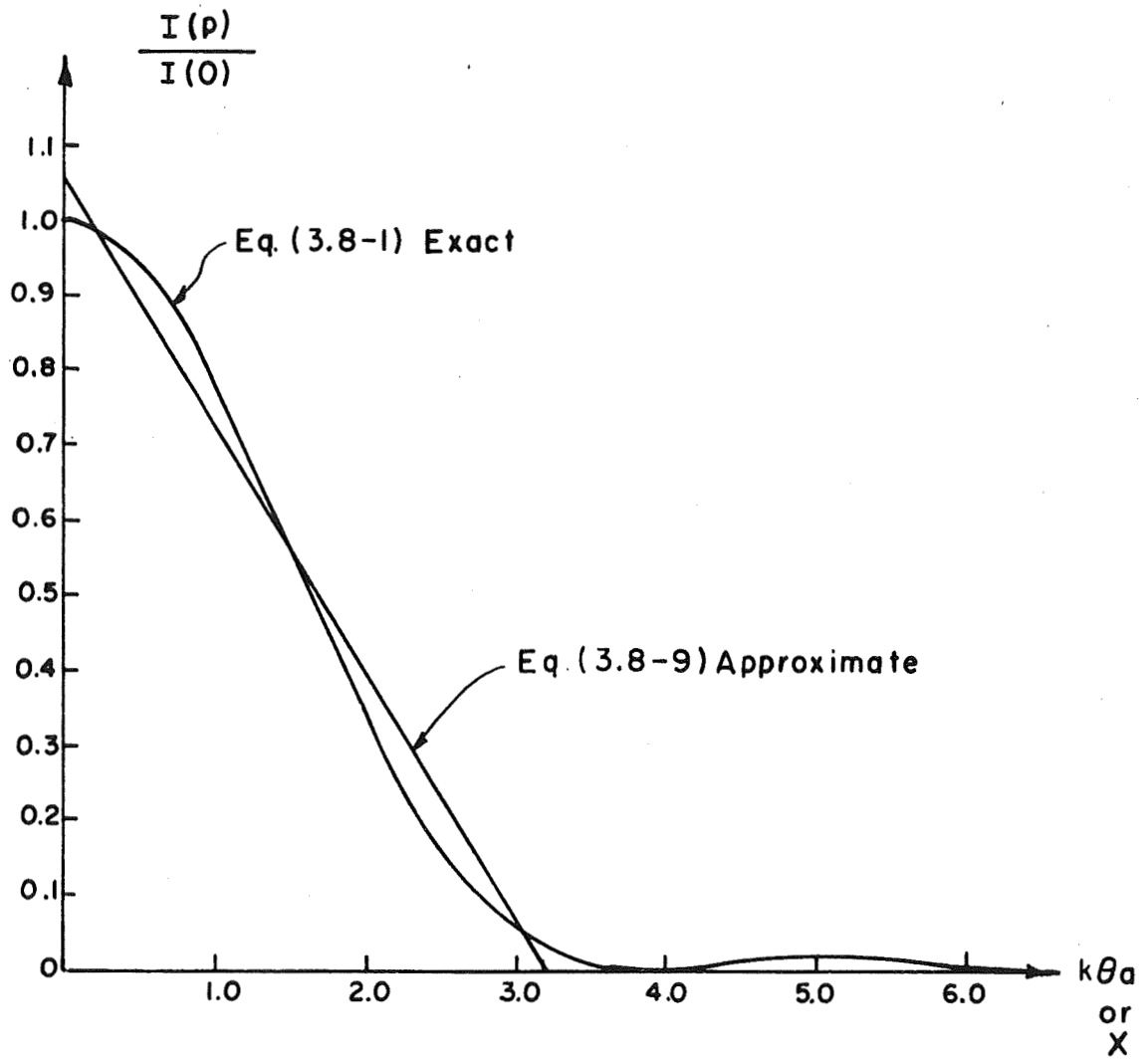

FIGURE 33 INTENSITY DISTRIBUTION OF THE FRAUNHOFER DIFFRACTION PATTERN OF A UNIFORMLY ILLUMINATED CIRCULAR APERTURE.

$$I_E(p) = \left[\frac{2J_1\left(\frac{3.2327\ p}{\theta_b\ r_s}\right)}{\frac{3.2327\ p}{\theta_b\ r_s}} \right]^2 I_E(0) \qquad (3.8\text{-}8)$$

where $I_E(p)$ = irradiance at a distance p from the center line and in a plane at a distance r_s from the source

θ_b = beam divergence

r_s = distance to the satellite.

It should be noted that if it is desired to increase the beam divergence while keeping the aperture diameter constant, a diverging lens could be placed in the aperture. However, it is not possible to reduce the beam divergence below the diffraction limit, i.e., the beam divergence which would be present with no lens.

In order to simplify the problem somewhat, it would be desirable to approximate the intensity distribution using simpler functions. From Fig. 33 it can be seen that when the diameter of the region under consideration is less than twice the beam divergence (i.e., $x \leq 3.2327$), the intensity distribution can be fairly well approximated by a straight line. The best straight line approximation (in the least-square sense) to (3.8-8) is

$$I_a(p) = (1.055 - 0.3264\ x) I_A(0) \qquad (3.8\text{-}9)$$

for $0 \leq x \leq 3.2327$ and zero otherwise.

$$x = \frac{3.2327\ p}{\theta_b\ r_s} \qquad (3.8\text{-}10)$$

Equation (3.8-9) is also plotted on Fig. 33 for comparison. A three-dimensional plot of the approximate intensity distribution would be cone shaped.

The fractional amount of power within a circle of radius x using the exact intensity distribution (3.8-8) is [55, p. 398].

$$L(x) = 1 - J_o^2(x) - J_1^2(x) \qquad (3.8\text{-}11)$$

Substituting $x = 3.2327$ into (3.8-11) shows that the amount of power within the region over which the approximation (3.8-9) is being made is 83.2% of the total power. Hence for practical purposes the assumption that the intensity is zero for $x > 3.2327$ corresponds to neglecting only a very small portion of the total incident power.

The actual power incident on a given region is found by integrating the irradiance over the desired region. The total power incident on the region over which the approximation (3.8-9) is being made is

$$W_T = \int_0^{2\pi} \int_0^{3.2327} I(p)\, p\, dp\, d\phi \qquad (3.8\text{-}12)$$

In the case when $I(p)$ is the exact irradiance (3.8-8)

$$W_T = 10.449\ I_E(0) \qquad (3.8\text{-}13)$$

and when $I(p)$ is the approximate irradiance (3.8-9)

$$W_T = 11.545\ I_A(0) \qquad (3.8\text{-}14)$$

Hence the replacement of the exact distribution by the approximate distribution implies that a larger amount of power is incident on the region being considered than is actually present. In order that the total incident power in each case be equal the intensity $I_A(0)$ of the approximate distribution will be reduced by the factor

$$T_1 = \frac{10.449}{11.545} = 0.9051 \qquad (3.8\text{-}14)$$

so that

$$I_A(0) = T_1\ I_E(0) \qquad (3.8\text{-}15)$$

which will make the total incident powers equal.

The maximum intensity $I_E(0)$ will first be calculated under the assumption that no diffraction occurs. If the diffraction phenomena did not occur, it would be expected that the power in the projected beam would be uniformly distributed if the power incident on the aperture was uniformly distributed. The assumption that both the power in the projected beam as well as the power incident on the aperture are uniformly distributed yields a very simple solution. Under this assumption the laser can be considered as a point source with radiant intensity

$$J = \frac{W}{\Omega} \tag{3.8-16}$$

where J = radiant intensity in W/sr

W = power of the laser in W

$\Omega \approx \frac{\pi}{4} \theta_b^{\,2}$ = solid angle subtended by a beam with divergence θ_b.

The irradiance at a distance r_s from the source is

$$I_U(0) = \frac{J}{r_s^{\,2}} = \frac{W}{r_s^{\,2}\,\Omega} \tag{3.8-17}$$

where $I_U(0)$ = irradiance in W/m^2 under the assumption that the energy in the beam is uniformly distributed.

Equations (3.8-16) and (3.8-17) are the radiometric equivalents of the photometric equations (3.6-2) and (3.6-6), respectively.

The intensity at the origin would be given by (3.8-17) if diffraction did not occur. Since diffraction does occur, the actual value of the intensity at the origin must be somewhat less than that given by (3.8-17). Using the conservation of energy, the maximum intensity can be found by equating the total power present in the diffraction pattern to the power of the laser which gives, using (3.8-8),

$$W_T = \int_0^{2\pi} \int_0^{\infty} I_E(0) \left[\frac{2J_1\left(\frac{3.2327\ p}{\theta_b\ r_s}\right)}{\left(\frac{3.2327\ p}{\theta_b\ r_s}\right)} \right]^2 p\ dp\ d\phi$$

$$= \frac{I_E(0) 4\pi}{\left(\frac{3.2327}{\theta_b\ r_s}\right)^2}\ 2 \int_0^{\infty} \frac{J_1^{\,2}\left(\frac{3.2327\ p}{\theta_b\ r_s}\right)}{p}\ dp \tag{3.8-18}$$

Substituting $x = \frac{3.2327\ p}{\theta_b\ r_s}$ gives

$$W_T = \frac{I_E(0)4\pi}{\left(\frac{3.2327}{\theta_b\ r_s}\right)^2}\ 2\int_0^\infty \frac{J_1^{\,2}(x)}{x}\,dx \qquad (3.8\text{-}19)$$

but [55, p. 398]

$$2\int_0^\infty \frac{J_1^{\,2}(x)}{x} = 1 \qquad (3.8\text{-}20)$$

Hence,

$$W_T = \frac{I_E(0)4\pi}{\left(\frac{3.2327}{\theta_b\ r_s}\right)^2} \qquad (3.8\text{-}21)$$

Solving for $I_E(0)$ gives

$$I_E(0) = \frac{W_T}{4\pi}\left(\frac{3.2327}{\theta_b\ r_s}\right)^2 \qquad (3.8\text{-}22)$$

Rearranging (3.8-22) slightly gives

$$I_E(0) = \frac{4W_T}{\pi(\theta_b\ r_s)^2}\ \frac{(3.2327)^2}{16} \qquad (3.8\text{-}23)$$

but the first factor is just $I_U(0)$ using (3.7-3) and (3.8-17), hence,

$$I_E(0) = T_2\ I_U(0) \qquad (3.8\text{-}24)$$

$$T_2 = \frac{(3.2327)^2}{16} = 0.6531 \qquad (3.8\text{-}25)$$

The above equation shows that the intensity at the center of the diffraction pattern is 65.3% of the intensity which would be present if the energy from the laser were uniformly distributed over a beam of angular width θ_b.

3.8.2 Approximate Intensity Distribution of the Laser Beam at the Satellite

The analysis just performed did not consider the effects of the atmosphere and the optical components, and these effects must be considered since the irradiance at the satellite will be reduced by absorption in these components. To determine the irradiance at the satellite, the total transmission factor, which is the product of all the individual transmission factors along the transmission path, will be determined. The irradiance at the satellite will then be the irradiance as determined in the loss-free case in Section 3.8.1 multiplied by the total transmission factor.

The total transmission factor, which is the ratio of the intensity distribution present to that which would be present in the absence of any absorption or attenuation along the transmission path, is

$$T_T = T_t \, T_a \, T_r \, T_f \qquad (3.8\text{-}26)$$

where T_T = total transmission factor

$T_t = 0.9$ = approximate transmission factor of the optical components of the source

$T_a = 0.1$ = atmospheric transmission factor from Section 3.3

$T_r = 0.9$ = approximate transmission factor of the optical components in the receiver

$T_f = 0.5$ = transmission factor of the optical filter (from Table 10).

Equation (3.8-26) becomes

$$T_T = 0.0405 \qquad (3.8\text{-}27)$$

Using the approximate intensity distribution (3.8-9) and the appropriate correction factors the intensity distribution at the satellite is

$$I_r(p) = T_T \, T_1 \, T_2 \, I_U(0) \, I_a(p) \qquad (3.8\text{-}28)$$

using (3.8-15) and (3.8-24). Substituting the values of each of the factors in (3.8-28) gives

$$I_r(p) = 0.0239\ I_U(0)\ I_a(p) \tag{3.8-29}$$

$$I_r(p) = 0.0239 \frac{W}{r_s^2 \frac{\pi\theta_b^2}{4}} (1.055 - 0.3264x) \tag{3.8-30}$$

Using (3.8-10) to eliminate x gives

$$I_r(p) = 0.0322 \frac{W}{r_s^2 \theta_b^2} \left(1 - \frac{p}{\theta_b r_s}\right) \tag{3.8-31}$$

where

$$p < \theta_b r_s \tag{3.8-32}$$

One of the assumptions that was made in arriving at this result was that the aperture or the lens on which the laser was focused was uniformly illuminated. If the illumination on the aperture is not uniform, then a different diffraction pattern will result. Since it might be expected that the illumination near the edges would be less than that at the center of the aperture, the diffraction pattern in this case will be examined. If the normalized illumination on the aperture has the form known as the inverted parabola type of illumination

$$F(p) = \left[1 - \left(\frac{2p}{D}\right)^2\right]^n \tag{3.8-33}$$

where F(p) = normalized irradiance on the aperture

p = radial distance from center of the aperture

D = diameter of the aperture

n = form factor,

then the diffraction pattern is given by [56]

$$I(x) = \left[C_n \frac{J_{n+1}(x)}{x^{n+1}} \right]^2 \qquad (3.8\text{-}34)$$

where $I(x)$ = normalized irradiance in the diffraction pattern

x = radial distance from the center of the pattern

C_n = a constant

($C_o = 2$, $C_1 = 8$, $C_2 = 48$, etc.).

In the case of uniform illumination n = 0. Each of these diffraction patterns is very similar to the one in Fig. 32. If the aperture illumination was significantly non-uniform, then a larger value of n could be chosen to more closely approximate the actual distribution. The choice of a larger value of n would only require changing the constants involved in the analysis and not the method used. As n increases the triangular approximation to the diffraction pattern would become wider and the intensity at the origin would decrease. When n = 2 for example the pattern would be about 33% wider at the half power points and the intensity at the origin would probably be reduced by a similar amount. The fact that the actual distribution of energy may be somewhat non-uniform would not introduce changes significant enough to change the conclusion on the feasibility of an optical navigation system, however.

3.8.3 Total Signal Energy Received

Now that the approximate form of the intensity distribution in the laser beam has been found, the total energy received can be calculated. The energy received per unit area is normally denoted as the "exposure" and is equal to the time integral of the irradiance. Assuming that the objective lens is small enough so that the irradiance is constant over the area of the lens the received energy is the product of the objective area and the exposure. The exposure will be determined from the approximate intensity distribution and the motion of the laser beam as it was described in Section 3.7.2.

To determine the signal energy received the motion of beam as it scans over the satellite must be known. Since the signal energy received will not be the same for all possible paths, the path which represents the worst case will be chosen. Each of the circular scanning paths (see Fig. 29) is separated by an angular separation of θ_b but since the actual width of each beam is $2\theta_b$ the energy distribution along each path overlaps with the previous and the following path. In Fig. 29 the beam from the laser was assumed to be uniform so that the circles representing the beam actually represent the half-power point of the actual energy distribution in the beam. The worst possible position at which the satellite could be located would be halfway between two of the circular scanning paths. In this position, illustrated

in Fig. 34, the beam intensity would be least and the beam would be incident on the satellite for the shortest period of time. If the beam scanned across the satellite in any other manner the intensity would be higher and the duration would be longer. A higher received signal energy would occur if the satellite were closer to the next scanning path since the intensity and duration would be greater on the following scanning path. The case in which the satellite is located halfway between two of the circular scanning paths thus represents the situation in which the signal energy received is the least and the system must operate in this situation in order to perform reliably.

To determine the exposure in the worst case, the irradiance along the path just described must be found. Since the irradiance has been determined in polar coordinates, if the radial distance to the center of the distribution is found as a function of the position along the worst-case path then the irradiance desired will be known.

If the beam divergence, θ_b, is much smaller than the size of the region to be searched, θ_T, then the worst-case path will approximately be a straight line and, from Fig. 35,

$$\frac{p}{\theta_b r_s} = \sqrt{0.25 + \left(\frac{p'}{\theta_b r_s}\right)^2} \qquad (3.8\text{-}35)$$

where p' = distance along the worst-case path.

And

$$\left|p'\right| < \frac{\sqrt{3}}{2} \theta_b r_s \qquad (3.8\text{-}36)$$

Substituting (3.8-35) into (3.8-31) gives the approximate irradiance distribution along the worst-case path.

$$I_r(p') = 0.0322 \frac{W}{\theta_b^2 r_s^2} \left(1 - \sqrt{0.25 + \left(\frac{p'}{\theta_b r_s}\right)^2}\right) \qquad (3.8\text{-}37)$$

Equation (3.8-37) represents the intersection of a plane (the straight line path) and a cone (the irradiance distribution) which is the hyperbola plotted in Fig. 36.

To calculate the exposure, the irradiance must be expressed as a function of time. The scanning motion was assumed to move with a constant tangential velocity in the plane of the satellite and under this assumption

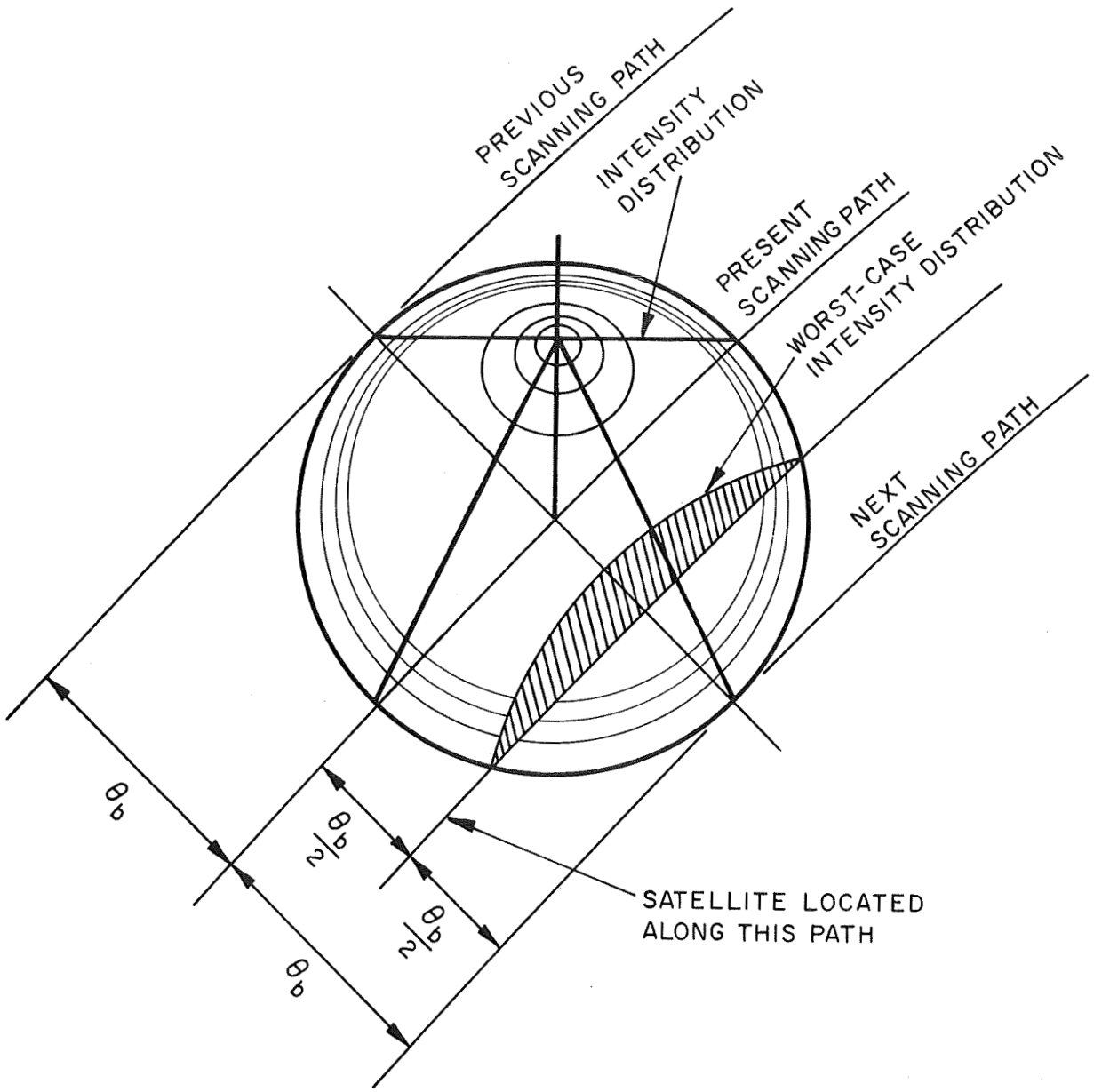

Figure 34 Intensity Distribution During Scanning of the Worst-Case Satellite Location

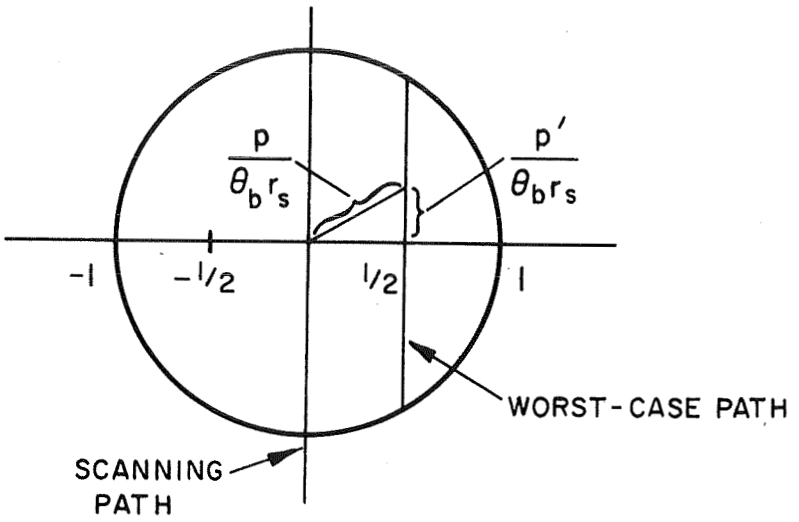

Figure 35 Geometrical Relationship In The Worst-Case Situation

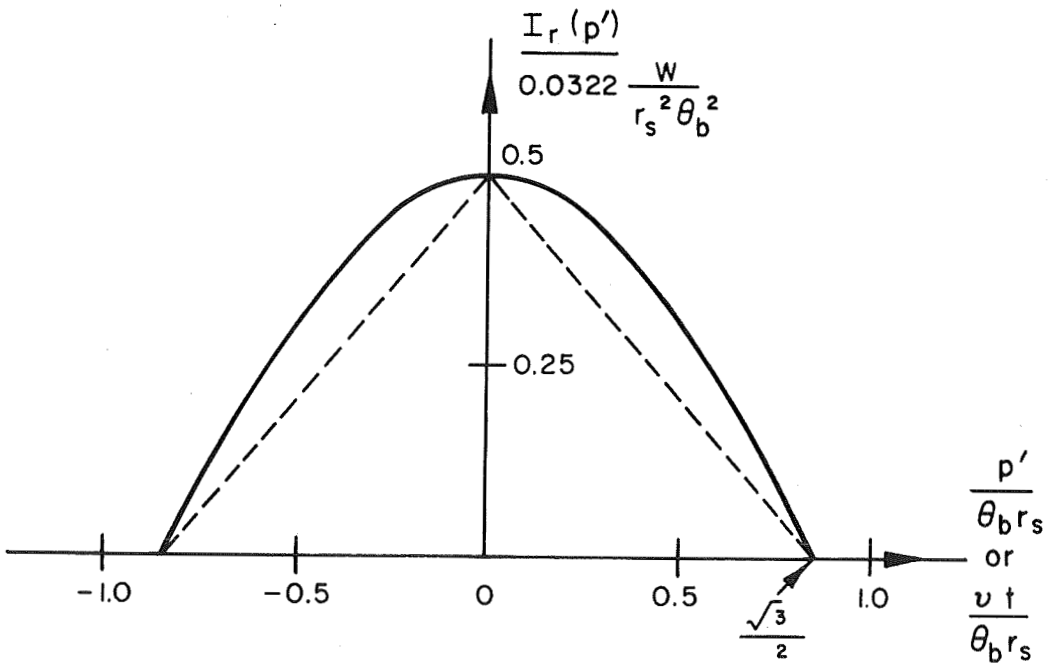

Figure 36 Intensity Distribution Along The Worst-Case Path

$$p' = vt \tag{3.8-38}$$

where p' = distance along worst-case path

v = velocity (see Section 3.7.2)

t = time.

The irradiance on the satellite is therefore

$$I_r(t) = 0.0322 \frac{W}{\theta_b^2 r_s^2} \left(1 - \sqrt{0.25 + \left(\frac{vt}{\theta_b r_s}\right)^2}\right) \tag{3.8-39}$$

and the exposure will be given by

$$E = \int I_r(t)\, dt \tag{3.8-40}$$

where the time integral must be evaluated over that period of time in which the beam is incident on the satellite. The total distance which the beam moves while it is incident on the satellite (along the worst-case path) is $\sqrt{3}\, r_s \theta_b$ and since the beam moves at a constant velocity the total duration of the signal is

$$T = \frac{\sqrt{3}\, r_s \theta_b}{v} \tag{3.8-41}$$

Since the irradiance is an even function over symmetric limits (3.8-40) becomes

$$E = 0.0322 \frac{W}{\theta_b^2 r_s^2}\, 2 \int_0^{\frac{T}{2}} 1 - \sqrt{0.25 + \left(\frac{vt}{\theta_b r_s}\right)^2}\, dt \tag{3.8-42}$$

Rearranging (3.8-42) slightly to simplify the integration

$$E = 0.0644 \frac{W}{\theta_b^2 r_s^2} \int_0^{\frac{T}{2}} \left(1 - \frac{v}{\theta_b r_s} \sqrt{\left(\frac{\theta_b r_s}{2v}\right)^2 + t^2}\right) dt \tag{3.8-43}$$

which can be evaluated using [57, p. 56]

$$\int (x^2 + a^2)^{1/2}\, dx = \frac{x(x^2 + a^2)^{1/2}}{2} + \frac{a^2}{2} \ln(x + (x^2 + a^2)^{1/2}) \quad (3.8\text{-}44)$$

Using (3.8-44) and (3.8-41) the integral (3.8-43) becomes, after some manipulation,

$$E = 0.0322 \frac{W}{v\theta_b r_s} \left[\frac{\sqrt{3}}{2} - \frac{\ln(2 + \sqrt{3})}{4} \right] \quad (3.8\text{-}45)$$

or

$$E = 0.0175 \frac{W}{v\theta_b r_s} \quad (3.8\text{-}46)$$

where E = exposure in J/m^2

W = laser power in W

v = tangential scanning velocity

θ_b = beam divergence at the half-power points

r_s = distance to the satellite in m.

As a check on the result the intensity distribution of Fig. 36 was approximated by a triangle (indicated by the dashed lines) and the exposure was determined. Using this approximation the constant in (3.8-46) was found to be 0.0139 which tends to confirm the result found using the exact distribution.

Using the assumption that the irradiance is uniform within the area of the objective lens the received signal energy in the worst-case is

$$J = EA \quad (3.8\text{-}47)$$

or

$$J = 0.0175 \frac{WA}{v\theta_b r_s} \quad (3.8\text{-}48)$$

where J is the signal energy received in J. Since the projected beams along adjacent scanning paths overlap the actual energy received in the worst-case would be twice that obtained by using (3.8-48), if the scanning motion were perfect. The motion of the user and imperfect

mechanical components, however, will tend to introduce perturbations in the circular scanning pattern so that instead of multiplying (3.8-48) by two, a value of 1.5 will be used to compensate for the perturbations of the scanning motion. Hence,

$$J = \frac{0.026\ WA}{v\ \theta_b\ r_s} \tag{3.8-49}$$

In order to introduce the parameters of the navigation system into (3.8-49), the tangential scanning velocity will be eliminated using (3.7-19) and (3.7-20) giving

$$J = \frac{0.026\ WAT}{2\pi\ r_s^2 \sin^2\left(\frac{\theta_T}{4}\right) \operatorname{cosec}\left(\frac{\theta_b}{2}\right)} \tag{3.8-50}$$

or

$$J = \frac{4.2 \times 10^{-3}\ WAT \sin\left(\frac{\theta_b}{2}\right)}{r_s^2 \sin^2\left(\frac{\theta_T}{4}\right)} \tag{3.8-51}$$

where T = search time

θ_T = divergence of the region to be searched given by (3.7-13)

θ_b = beam divergence.

This expression is valid provided the scanning path can be approximated by a straight line and this condition is satisfied if $\theta_b \ll \theta_T$. The implication of this requirement is that at least five or more revolutions of the source beam should be required in order to cover the region to be searched. If the region to be searched is so small that only a few revolutions of the source would be required then it would be more advantageous to increase the source power and beam divergence and eliminate the scanning equipment altogether.

In the case when the region to be searched is small enough to avoid scanning the region the irradiance incident on the satellite will be given by (3.8-31) but the value will be constant over the duration of the signal assuming a rectangular pulse. In order to give a reasonable signal strength over the entire region to be searched the beam divergence will be set equal to the divergence of the region to be searched, i.e., $\theta_b = \theta_T$, so that the region in which the satellite should be located is within the half-power points of the projected beam. The irradiance in the worst-case will be when the satellite is located at the half-power points so that, from (3.8-31)

$$I_r = 0.0161 \frac{W}{r_s^2 \theta_b^2} \qquad (3.8\text{-}52)$$

and assuming a rectangular pulse the received signal energy will be

$$J = \frac{0.0161WAT}{r_s^2 \theta_b^2} \qquad (3.8\text{-}53)$$

where J is the received signal energy in joules.

The fact that (3.8-51) implies that θ_b should be large and (3.8-53) implies that θ_b should be small in order to obtain the same result may seem contradictory. It should be noted, however, that these results were derived under two different sets of circumstances and (3.8-51) is applicable only when $\theta_b \ll \theta_T$ and (3.8-53) is applicable only when θ_b is greater than the diffraction limit. The implications of (3.8-51) are that if a scanning system is to be used then the value of θ_b should be chosen as large as possible. In other words in the trade-off between the number of revolutions of the scanning beam required and the beam divergence, a higher received signal energy will result if the beam divergence is increased to keep the number of revolutions required to a minimum. In a system in which the beam divergence is increased to cover the desired region of the sky the minimum value which the beam divergence can have is θ_T and in both systems the minimum beam divergence is given by the diffraction limit.

Now that the signal energy received can be determined in terms of the parameters of the navigation system, the signal-to-noise ratio can be determined. The feasibility of the active optical navigation system will be determined from the signal-to-noise ratio which can be expected for a typical set of navigation system parameters. As in the passive case this analysis will illustrate the interdependence between the various system parameters and determine which are critical.

3.9 Analysis of the Signal-to-Noise Ratio in the Active Case

To analyze the feasibility of an active optical navigation system the signal-to-noise ratio under typical conditions will be examined as it was in the passive case. The signal-to-noise ratio which will be used is the ratio of the variation in the energy received on a resolvable image element due to the presence of a signal to the variation in the energy on an image element due to variations in the background. The same definition was used in the analysis of the passive case.

3.9.1 Image Analysis

As was done in the passive case and will be done in the active case the method of analysis will be based on an analysis of the image

available to the detector and not the combination of the two. While technological advances are continually improving the detectors available, e.g., [59, 60], if the image available does not have sufficient quality then no detector improvements will change the situation. An extensive analysis of the relationship between the image and the image detector has been made by Schade [25,62]. It is shown that the presence of noise in the detector and the quantum limitations of the photosensitive surfaces used for detection will reduce the resolution in the resulting signal which represents the original image. In a detector which consists of a number of cascaded stages of the same type, such as an electronic image intensifier, the resolution will deteriorate directly with the square root of the number of stages used [62, p. 84]. Hence in a system in which resolution is very important, the least number of photosensitive surfaces possible should be used in the detector. In addition special consideration must be given to uniformity in the photosensitive surfaces so that an image of uniform quality is produced.

An optical image can be analyzed in several ways but in this situation the analysis will be based on the changes which occur in the nonuniform background. Since background variations presented a major problem in the passive case it is reasonable to suspect that background variations will also cause problems in the active case. It is also reasonable to expect that clouds will again be the major cause of variations in the background because of their radically different optical properties. A major problem in designing optical systems which operate in the presence of nonuniform backgrounds is to provide sufficiently strong signal, "... so that the peak signal due to the field moving from one element of background to another will exceed the target contrast signal only in some minor, acceptable portion of the time... It is to be realized in the foregoing that no consideration has been given to optical gain, cell noise, cell sensitivity, system noise, etc. The above is a criterion only for the ability to recognize a probable target signal from background clutter." [63] Thus to analyze an optical system with a nonuniform background the magnitude of the signal variation must be compared to the magnitude of the variations in the background and this is exactly what the signal-to-noise ratio defined previously is expected to do.

3.9.2 Albedo Variations and the Variational Noise Power

In order to determine the variational noise power on each resolvable image element the causes of the variation must be known. The primary variations in the background are due to the changing reflecting properties of the weather formations which are present in the image background. Although the steady-state solar irradiance is modulated by 0.1% [64] due to changes in the sun's surface the primary variations in the background are due to changes in the albedo, the average reflectance, and these changes are caused by both spectral and spacial variations. "It is important to note that for a receiver with spectral widths of 100 angstroms or less, looking at only part of the planet, the published (albedo) values may be considerably in error, perhaps by as much as a factor of three, as a result of geographical and spectral

variations in albedo" [37, pp. 269-270]. It is important to note that the reflectance values given for various backgrounds may or may not be the same as the planet albedo, depending on the type of measurements, due to the properties of the intervening atmosphere.

A study of the data available on the spectral and spacial variations of the albedo indicates that a very wide range of values will be encountered, but that the greatest variations will exist between clear and cloudy areas [65]. One source states that the albedo varies linearly from 0.17 to 0.70 according to the fractional amount of cloud cover with the larger albedo value being associated with 100% cloud cover [66]. The simple linear relationship is only valid for moderate amounts of cloud cover and represents the average value over large areas. In a recent series of articles, the albedo of clouds was calculated theoretically and under various conditions it was found that the albedo can vary from almost zero to over 0.8 [67-69]. Similar variations in the cloud albedo were reported previously [32, p. 7-5]. A summary of the measured data on the albedo of various types of clouds and for clear areas is given in Fig. 37 [70, p. 75]. Theoretical calculations have given an even larger range of values for the albedo over clear areas [71] but satellite measurements seem to confirm the results of Fig. 37 which give relatively low values for the albedo over clear areas [72]. So far no mention has been made of the spectral variations of the albedo but it has been found that the reflectance of clouds is relatively constant spectrally [73, p. 30] so that the variations given in Fig. 37 can also be assumed to indicate the magnitude of the spectral variations.

From the data presented it is justified in assuming that the variation in the albedo can be taken as 0.8 for small spectral regions and small observed areas. The variation in the background noise power on an individual image element can then be determined using (3.5-6) by replacing α_λ by $\Delta\alpha_\lambda$ which is the variation of the albedo at a given wavelength. Using the same assumptions as were used to derive (2.7-10) the variational background noise power on each resolvable image element can be determined from (3.5-6) by multiplying by the objective area and dividing by the number of resolvable image elements. Since a very narrowband filter will be used to filter out as much of the background noise as possible, the variational background noise power will be the sum of the variation of the energy in the filter passband plus the variation of the energy in the filter stopband. Under these assumptions the variational background noise power on an individual resolvable image element is:

$$P_N = \frac{A}{N^2}\left[I_T f_p \rho_s \frac{\Delta\alpha_\lambda}{\alpha} \sin^2\left(\frac{GCD}{2r_e}\right) + I_T f_s (1-\rho_s) \frac{\Delta\alpha_\lambda}{\alpha} \sin^2\left(\frac{GCD}{2r_e}\right)\right] \tag{3.9-1}$$

or

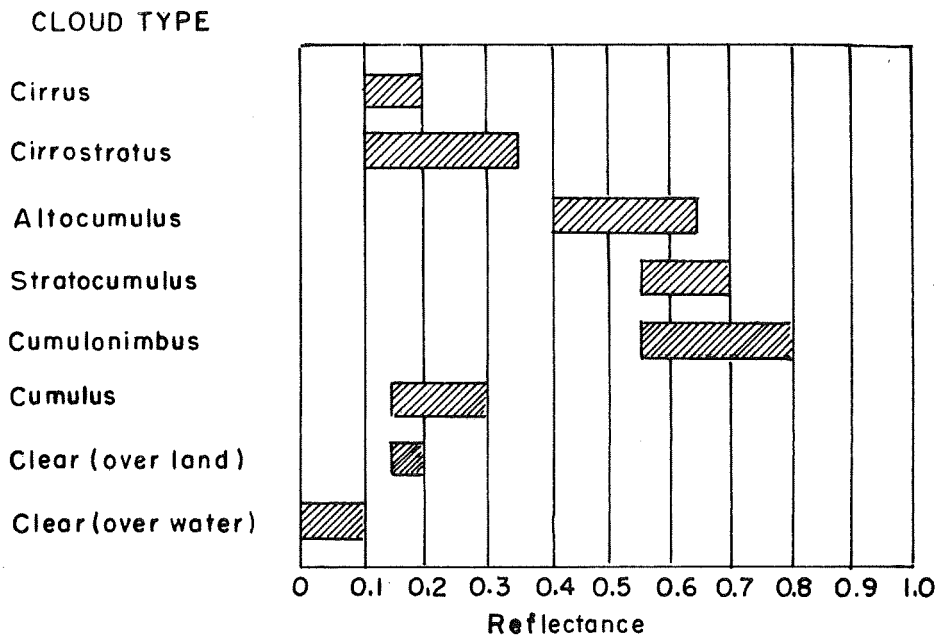

FIGURE 37 SUMMARY OF THE PROBABLE SPREAD OF REFLECTANCE FOR VARIOUS CLOUDS.[70]

$$P_N = \frac{A}{N^2} I_T \frac{\Delta\alpha_\lambda}{\alpha} \sin^2\left(\frac{GCD}{2r_e}\right)\left[f_p \rho_s + f_s(1-\rho_s)\right] \qquad (3.9\text{-}2)$$

where P_N = variational noise power on an individual resolvable image element

A = area of the objective lens

I_T = total noise irradiance from Fig. 23

$\Delta\alpha_\lambda$ = 0.8 = change in the albedo which can be expected for different backgrounds

α = 0.4 = average albedo used to derive results in Fig. 23

GCD = diameter of the observable region

r_e = radius of the earth

f_p = fractional amount of energy passed for wavelengths in the filter passband

ρ_s = fractional amount of I_T which is present in the passband (from Fig. 22 or (2.5-1))

f_s = fractional amount of energy passed for wavelengths in the filter stopband.

Since the worst-case value will be used for this calculation $I_T = 10\ W/m^2$ and substituting for f_p and f_s, the values found in Table 10 gives

$$P_N = \frac{20A}{N^2} \sin^2\left(\frac{GCD}{r_e}\right)\left[0.5\rho_s + 1.0 \times 10^{-5}(1-\rho_s)\right] \qquad (3.9\text{-}3)$$

Note that ρ_s is the only wavelength dependent quantity so that the expression in the brackets can be evaluated as a function of wavelength and the worst-case value chosen. A conversion factor can then be found to convert the worst-case value to the value at the desired wavelength. The wavelength dependent quantity

$$q(\lambda) = 0.5\rho_s + 1.0 \times 10^{-5}(1-\rho_s) \qquad (3.9\text{-}4)$$

was calculated for the typical filter found in Table 10 and assuming that the background noise had a spectral distribution corresponding to that of a 6000°K blackbody. The results of this calculation are given in Fig. 38.

The wavelength at which the worst-case value occurs can be found by using (2.2-3) which gives $\lambda = 0.48\mu$ for the wavelength at which the

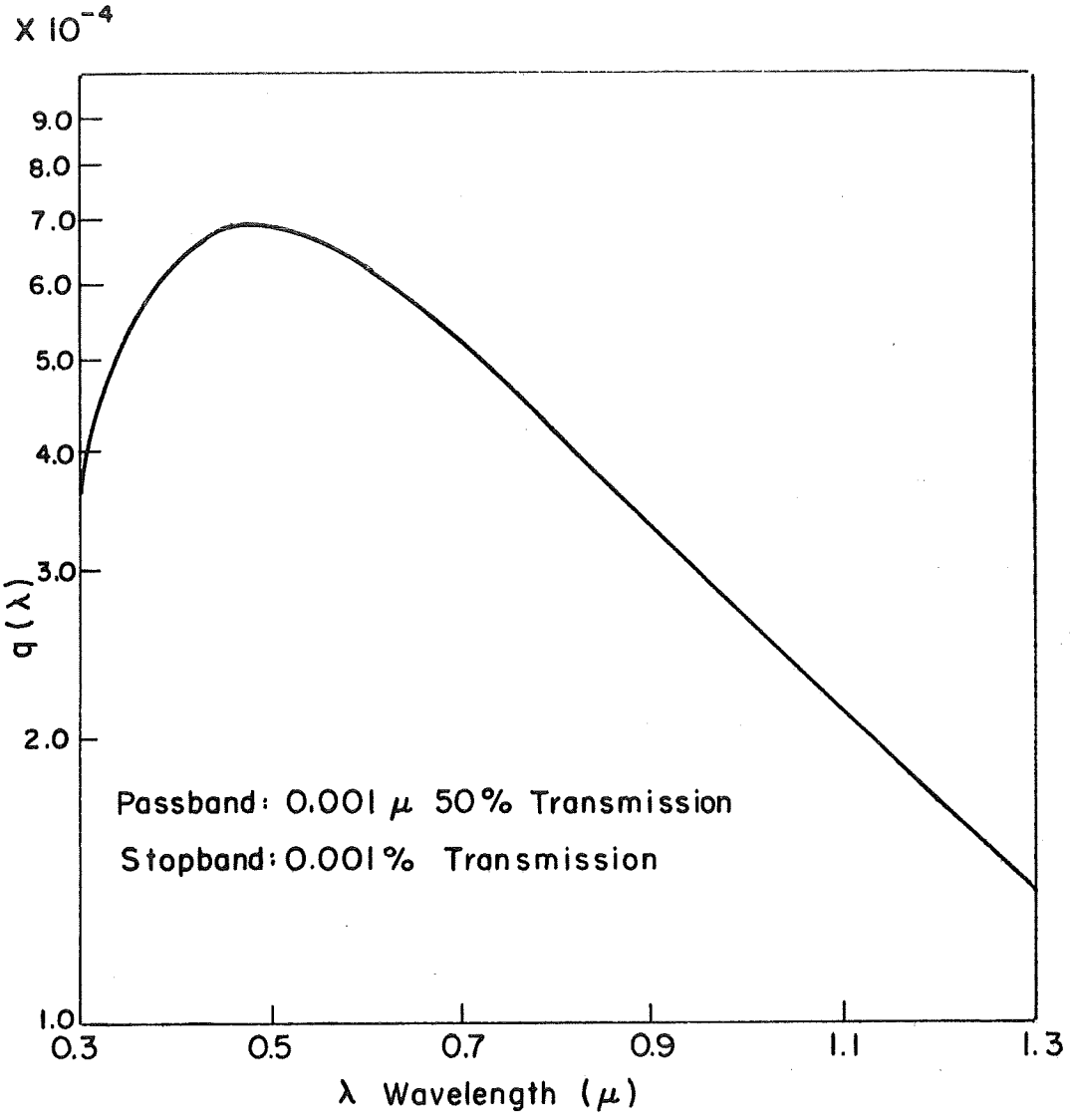

FIGURE 38 FRACTIONAL AMOUNT OF ENERGY TRANSMITTED THROUGH A TYPICAL INTERFERENCE FILTER FOR A 6000°K SPECTRAL DISTRIBUTION.

maximum noise power occurs. All calculations will therefore be made using the value q(0.48) and a conversion factor will be used for different wavelengths. Hence,

$$P_N = \frac{20A}{N^2} \sin^2 \left(\frac{GCD}{2r_e}\right) q(0.48) \qquad (3.9\text{-}5)$$

or

$$P_N = \frac{1.38 \times 10^{-3} A}{N^2} \sin^2 \left(\frac{GCD}{2r_e}\right) \qquad (3.9\text{-}6)$$

Since the ultimate use of (3.9-3) and (3.9-4) will be to evaluate the signal-to-noise ratio and the noise power appears in the denominator, the conversion factor will be defined for converting the signal-to-noise ratio rather than the noise power. The conversion factor, k, is defined as

$$k = \frac{q(0.48)}{q(\lambda)} \qquad (3.9\text{-}7)$$

and is plotted in Fig. 39. The signal-to-noise ratio as a function of wavelength is found by multiplying by the conversion factor, k, while to find the variational noise power as a function of wavelength, it is necessary to divide by the conversion factor k.

3.9.3 The Signal-to-Noise Ratio Under Typical Operating Conditions

One use of an optical navigation system would be to provide checks on the less accurate navigation systems carried by the users. A typical example of this would be to provide position up-dates to inertial navigation systems. Another use would be to eliminate blunder errors or cycle-slipping errors which occur in electronic navigation systems. To calculate the signal-to-noise ratio some assumptions must be made on the accuracy of the a priori knowledge the user has of his position.

Three sets of navigation system parameters have been chosen to represent low, medium and high accuracy systems. The choice of these parameters has been made so that they realistically represent some of the navigation systems now in use. The three systems which will be considered are given in Table 12 along with the parameter values which will be used. Actual navigation systems which might be used in conjunction with the optical navigation system to give the parameter values stated are also given. For simplicity the angular error in the heading, $\Delta\theta_C$, and the angular error in the horizontal reference, $\Delta\theta_H$,

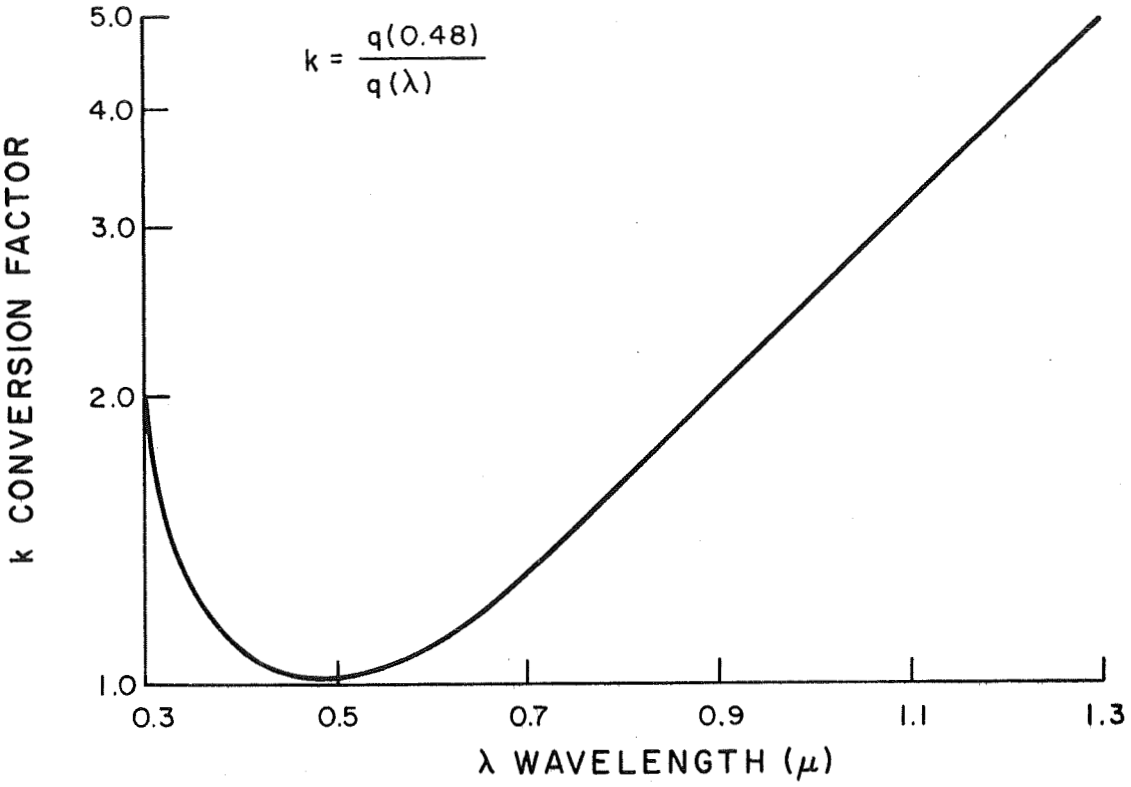

FIGURE 39 CONVERSION FACTOR TO FIND SNR FROM WORST-CASE VALUE

System Accuracy	Parameters	Systems Which Might Produce This Accuracy +	References
Low	$d\Delta$ = 30 km	Inertial*	74
		Doppler	75
		CONSOL	77
	$\Delta\theta_C, \Delta\theta_H = 1.5^o$	Doppler	75
		Optical and Infrared Techniques	61, pp. 554-563; 80
Medium	$d\Delta$ = 10 km	Inertial*	74
		LORAN-C	78
		Dectra	79
	$\Delta\theta_C, \Delta\theta_H = 0.3^o$	Optical and Infrared Techniques	61, pp.554-563;81;82
High	$d\Delta$ = 1 km	Inertial*	74
		Decca	76, p. 345
		Omega	76, p. 347
	$\Delta\theta_C, \Delta\theta_H = 0.05^o$	Optical and Infrared Techniques	61, pp.554-563; 83

Table 12

NAVIGATION SYSTEM PARAMETERS

will be considered to be equal. Note that the error in the horizontal reference could actually be the error in the determination of the local vertical since either of these could be used as a reference. In addition it is also assumed that the errors given are the maximum errors which can be tolerated by the optical navigation system and that they occur independently with no preferred values.

Now that the accuracy of the a priori knowledge of the user's position has been determined by specifying the navigation system parameters, the signal-to-noise ratio can be calculated. The two cases which will be considered are the circular scanning pattern, where the received signal energy is given by (3.8-51), and the case where the beam divergence is varied and the received signal energy is given by (3.8-53). The variational noise energy is equal to the variational noise power (3.9-6) multiplied by the shutter time

$$E_N = \frac{1.38 \times 10^{-3}}{N^2} AT_o \sin^2\left(\frac{GCD}{2r_e}\right) \qquad (3.9\text{-}7)$$

* Depending on length of time between position up-dates.
\+ Many other methods are also in use (e.g. magnetic compasses).

where T_o is the shutter time in sec. The signal-to-noise ratio in each case can be found by dividing the received signal energy by the variational noise energy to give:

$$SNR = \frac{3.0\ WTN^2 \sin\left(\frac{\theta_b}{2}\right)}{T_o\left[r_s \sin\left(\frac{\theta_T}{4}\right) \sin\left(\frac{GCD}{2r_e}\right)\right]^2} \qquad (3.9\text{-}8)$$

in the scanning beam case and

$$SNR = \frac{11.7\ WTN^2}{T_o\left[r_s\ \theta_b \sin\left(\frac{GCD}{2r_e}\right)\right]^2} \qquad (3.9\text{-}9)$$

in the variable beam divergence case. Since the signal energy and noise energy are both directly proportional to the area of the objective lens, this factor does not appear in the signal-to-noise ratio. It should be noted, however, that it was assumed that the majority of the signal energy would be focused on one individual image element so that the resolution of the objective lens must be greater than that of the television camera. . The same situation was encountered in the passive case where the lens diameter was restricted by (2.2-8). In the active case this restriction is given by (3.4-2), which is plotted in Fig. 21, and the lens diameter must be equal to or greater than the value that satisfies (3.4-2).

In the scanning beam case it will be assumed that the scanning motion is completed during the length of time the shutter remains open. Normally, this would require synchronization between the user and the satellite, but if the scanning motion is repeated many times, then synchronization is not required. This statement is equivalent to saying that the spiral scanning motion depicted in Fig. 29 can start at any point on the spiral but the entire spiral must be covered once within the shutter time. Under this assumption the time factors in (3.9-8) can be cancelled to give

$$SNR = \frac{3.0\ WN^2 \sin\left(\frac{\theta_b}{2}\right)}{\left[r_s \sin\left(\frac{\theta_T}{4}\right) \sin\left(\frac{GCD}{2r_e}\right)\right]^2} \qquad (3.9\text{-}10)$$

which is valid provided the user and satellite motion is small (see Section 2.4). In the variable beam divergence case it is also possible to make the same assumptions provided the laser is on for a period much longer than the shutter time. In this case, however, the time factors will be retained since it would also be possible to use a very high power pulse laser. If the signal duration were much smaller than the shutter time, then the problem of synchronization would be minimal.

This would be especially true of the shutter time were on the order of 0.1 sec (as in Section 2.4) since relatively low accuracy clocks could be used, and considering that many of the high power pulse lasers put out pulses as short as 10^{-12} sec.

To determine the total beam divergence required (3.7-13) will be used but if $\Delta\theta_c$ and $\Delta\theta_H$ are small then this equation can be approximated by

$$\theta_T = \theta_{PE} + \sqrt{(\Delta\theta_c)^2 + (\Delta\theta_H)^2} \qquad (3.9\text{-}11)$$

where θ_{PE} is obtained from Fig. 27 or (3.7-1). Substituting in the values from Table 12, the following results are obtained:

$$\begin{aligned} &\text{Low:} && \theta_T = 0.317 + 2.12 = 2.437^\circ \\ &\text{Medium:} && \theta_T = 0.106 + 0.424 = 0.53^\circ \\ &\text{High:} && \theta_T = 0.0106 + 0.0707 = 0.0813^\circ \end{aligned} \qquad (3.9\text{-}12)$$

Note that the major component of the total beam divergence is due to the angular reference errors so the restriction on the solid angle to be searched in Fig. 27 is not satisfied. In this case θ_T must be substituted in (3.7-2) or (3.7-3) to find the solid angle to be searched. In deriving (3.9-8), it was assumed that $\theta_b \ll \theta_T$ but to increase the signal energy θ_b should be as large as possible. As a reasonable compromise in this case θ_b will be taken as

$$\theta_b = \frac{\theta_T}{10} \qquad (3.9\text{-}13)$$

so that θ_b is much less than θ_T, but is as large as possible. This result was reached by considering that when θ_b and θ_T are related by (3.9-13) a total of five revolutions of the search beam will be required and this is the minimum number required for the assumptions used for (3.9-8) to hold (see Section 3.8.3).

The signal-to-noise ratio in the scanning beam case, given by (3.9-10), is plotted in Fig. 40 for the three navigation systems being considered. Note that from Fig. 21 an objective diameter of 1 m is sufficient to satisfy (3.4-2) for all values of the parameters used in Fig. 40. The signal-to-noise ratios given in Fig. 40 were derived

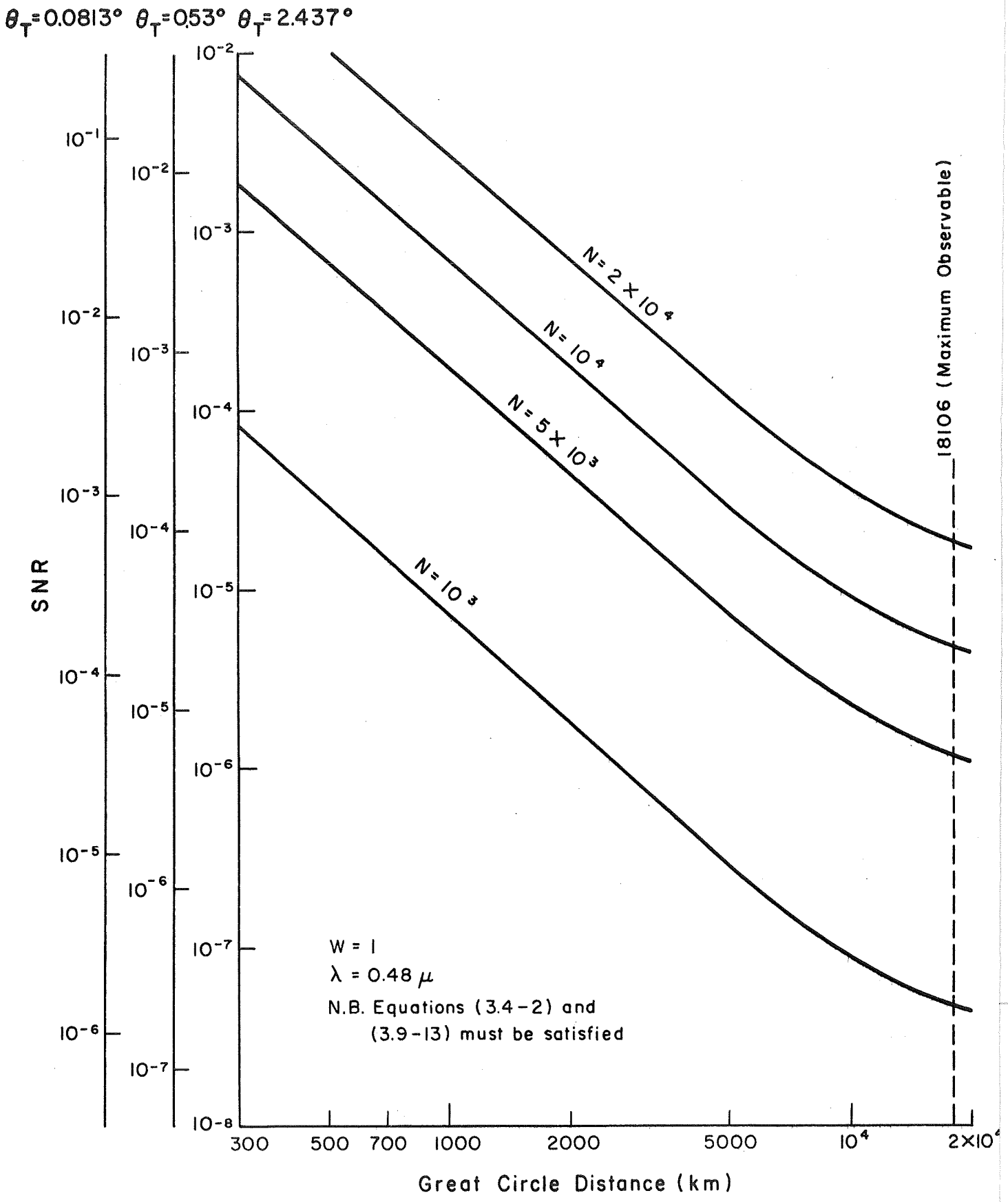

FIGURE 40 SIGNAL-TO-NOISE RATIO (Scanning Beam)

under the assumption of a 1 watt source operating at a wavelength of 0.48μ. Operation at a longer wavelength can improve the signal-to-noise ratio by a factor of 5 (Fig. 39) and a laser power of 20 watts is not unreasonable so that the signal-to-noise ratios in Fig. 40 can be improved by a factor of 100. Even this improvement, however, is insufficient to yield an image of sufficient quality for any reasonably large area.

The signal-to-noise ratio for the variable beam divergence case is plotted in Fig. 41. By comparing the results in Figs. 40 and 41 (or by dividing (3.9-8) by (3.9-9))it will be found that the signal-to-noise ratio for the scanning beam case is always less than the signal-to-noise ratio for the variable beam divergence case for equal system parameters. Hence, it has been shown that spiral scanning will always be less efficient than increasing the beam divergence when a given conical region must be covered. If it is assumed, as in the previous case, that the signal-to-noise ratio can be improved by a factor of 100, then a sufficiently high quality image can be obtained for the medium accuracy navigation system if $N = 10^4$ and $GCD = 5 \times 10^3$. The values chosen for N and GCD correspond to the number of television lines which can be expected for the high resolution television cameras which will be available in the near future and the great circle distance corresponds to a field-of-view of about 8^o which is sufficient to cover most of the North Atlantic. These parameter values correspond to the values of the typical optical navigation system which was postulated in the passive case. To use Fig. 41 to find the signal-to-noise ratio in the case of a pulsed signal, it is necessary to multiply the results in Fig. 41 by the source energy (WT) and divide by the shutter time T_o.

3.9.4 The Signal-to-Noise Ratio at the Detector Output

The results obtained in the previous section indicate that under certain conditions the image received at the satellite is of sufficient quality to consider whether or not a detector is available which could reliably reproduce the received image. To answer this question the signal-to-noise ratio at the detector output will be examined to see if a reliable determination could be made as to the presence or absence of a user's signal. Note that the definition of the signal-to-noise ratio which will be used in this section is not the same as that used previously and will correspond much more closely to the commonly accepted definition of a signal-to-noise ratio.

The signal-to-noise ratio will be defined as the ratio of the peak-to-peak signal divided by the rms noise which is [84]:

$$S = \left(\frac{I}{2eB} \right)^{1/2} F_2 \qquad (3.9\text{-}14)$$

where I = current generated at the photocathode

e = 1.6×10^{-19} c = electronic charge

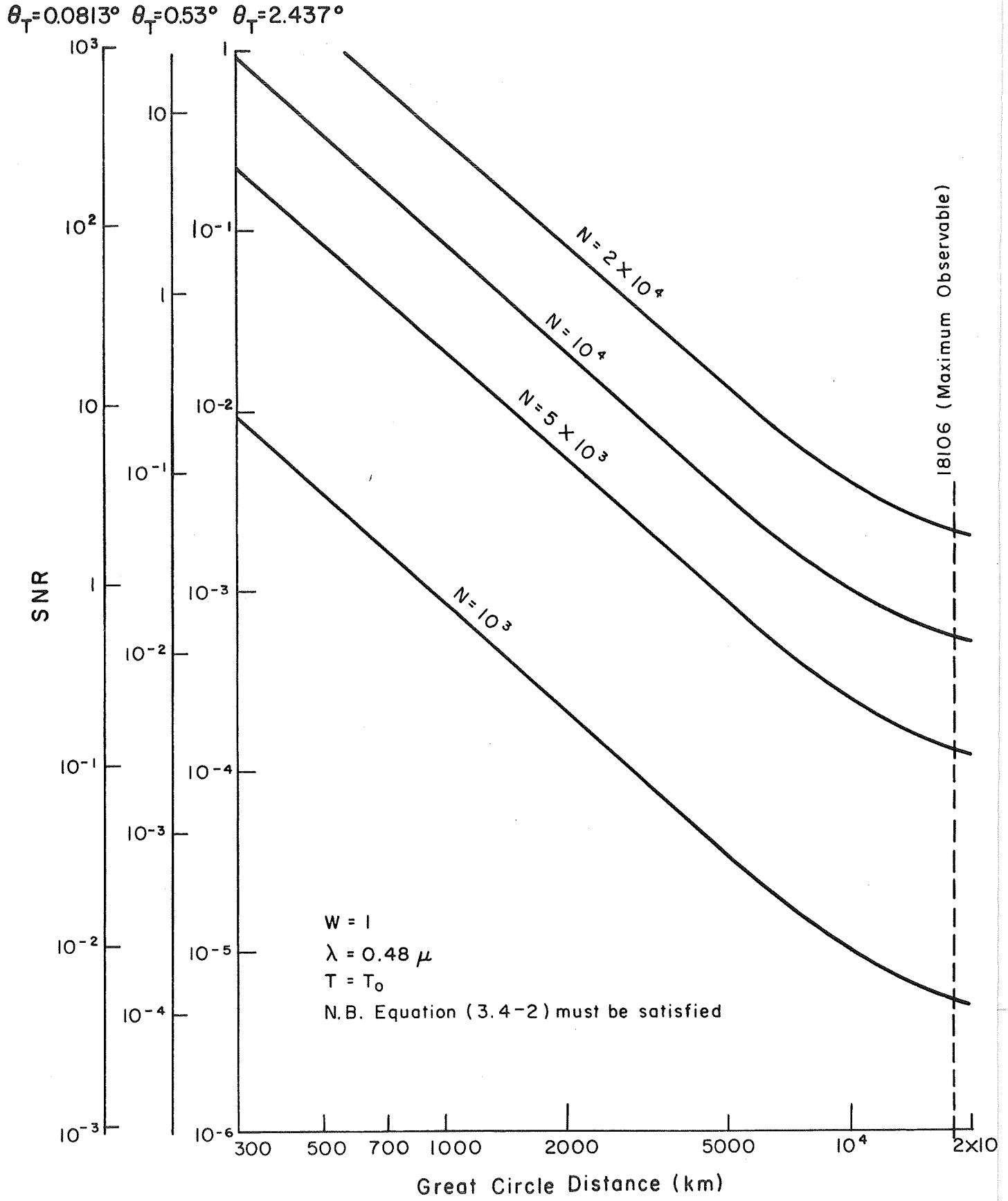

FIGURE 41 SIGNAL-TO-NOISE RATIO (Variable Beam Divergence)

B = bandwidth of the video amplifier

F_2 = a function of the detector parameters.

The photocurrent can be determined from the irradiance using the radiant sensitivity of the photosensitive surface.

$$I = \beta I_r A \tag{3.9-15}$$

where β = radiant sensitivity in A/W

I_r = incident irradiance given by (3.8-52)

A = area of the objective lens.

The parameter F_2 is a function of the detector's ability to store the information present in the image and derive a useful video signal from that information. The maximum value of F_2 is one and a typical value for practical detectors is 0.5 [84]. Using (3.9-15), (3.8-52) and the values of F_2 and e, the signal-to-noise ratio becomes

$$S = \frac{8.85 \times 10^8}{r_s \theta_T} \left(\frac{\beta AW}{B}\right)^{1/2} \tag{3.9-16}$$

A typical value for the radiant sensitivity of a relatively high sensitivity photosensitive surface in the region 0.4μ to 0.8μ might be 0.05 A/W [85, p. 88] but values four times this can be achieved. It will be assumed as it was previously that the objective lens diameter is on the order of 1 meter so that the signal-to-noise ratio becomes, after substitution of the synchronous altitude,

$$S = \frac{4.9}{\theta_T} \left(\frac{W}{B}\right)^{1/2} \tag{3.9-17}$$

Since it was found that a reasonably high quality image could be obtained for the medium accuracy navigation system, the value of θ_T will be taken to be 0.01 rad ($\sim 0.57^o$). Since the images will not change significantly during a period of several seconds the total time taken to scan the image can be relatively long. It will be assumed that the time required to scan the image is 10 sec and with $N = 10^4$ TV lines the bandwidth required is 5 MHz (from Fig. B1). The signal-to-noise ratio under these assumptions is

$$S = 0.22 \sqrt{W} \tag{3.9-18}$$

In order for a binary detection system to work reliably the signal-to-noise ratio must be much greater than one which implies, using (3.9-18), that an average power on the order of several kilowatts would be required. Even the high accuracy system with θ_T an order of magnitude lower would require several hundred watts of power for a reliable signal.

The very simple analysis used to obtain the signal-to-noise ratio is probably not very accurate for small signals. However, the use of a more sophisticated analysis would probably yield an even worse result since the more complicated models take into account additional sources of noise which were not considered in the equation used. In addition the more complicated models require an increase in the signal strength as the spacial resolution in the image is increased whereas in the simple model used to derive (3.9-14) the resolution entered the problem only through the bandwidth. It should be noted that the 2W laser which was detected on the moon by the Surveyor spacecraft had a beamwidth on the order of microradians and the video bandwidth was of the order of a few kHz so that a useable signal-to-noise ratio was obtainable with very little power.

In the case of very high peak power signals the total energy received must be considered. Using (3.8-53) and recognizing WT as the source energy the received energy is

$$J = \frac{0.0161\ J_s\ A}{r_s^2\ \theta_T^2} \tag{3.9-19}$$

or, using $\theta_T = 0.53^o$,

$$J = 1.46 \times 10^{-15}\ J_s A \tag{3.9-20}$$

where J_s is the output energy of the source and A is the objective lens area. It has been reported that it is possible to detect a signal with an energy density of 2×10^{-10} J/m^2 [86]. The energy density of the signal at the input to the image detector may be found by dividing the total energy received (3.9-20) by the area of the detector

$$U = \frac{J}{A_d} = \frac{1.46 \times 10^{-15}\ J_s A}{A_d} \tag{3.9-21}$$

where U is the energy density and A_d is the area of the detector. Considering the area of typical components, the ratio A/A_d may be on the order of 150 so that

$$U = 2.2 \times 10^{-13} J_s \qquad (3.9\text{-}22)$$

and a detectable signal might be produced with a laser energy output on the order of several hundred joules. While pulsed lasers are available with an output energy of this order of magnitude, their cost is likely to be on the order of $25,000 and up [39, p. 123]. In addition the wavelength at which many of the very high energy lasers operate is 1.06μ and the radiant sensitivity of most of the photosensitive surfaces available is about two orders of magnitude less than the sensitivity in the visible region.

3.10 Conclusions on an Active Optical Navigation System

The feasibility of using an optical navigation satellite with active users can be evaluated using the results presented in Sections 3.9.3 and 3.9.4. First of all it must be pointed out that the active optical navigation system cannot be considered as a replacement for existing navigation systems. The optical navigation system is only capable of improving the accuracy of an existing navigation system because the source power required to provide a usable signal when the user does not have a fairly good idea of his position is much too large to be practical. The success which has been achieved in using low power optical sources to transmit signals over very long distances has required extremely accurate aiming of the source. In the case of the laser which the Surveyor spacecraft detected, the accuracy required in aiming the laser was on the order of 2-4 secs of arc [51]. For the purpose of navigation it must not be a requirement that the laser be aimed very accurately since this would imply the user already knew his position.

The operation of the active optical navigation system depends on the ability of the user to estimate his position with some known degree of accuracy and then increasing the beam divergence of the optical source to overcome this inaccuracy. One of the major results of this section was the development of the relationship between the accuracy of the a priori knowledge of the user's position and the beam divergence of the source required to overcome this inaccuracy to ensure reliable reception of the user's signal. In order to be practical the optical navigation system must be able to take a relatively inaccurate estimate of the user's position and refine it to a much more accurate result and do this with equipment that would cost less than other types of equipment capable of achieving the same final accuracy.

The emphasis on the analysis used in this section has been to analyze the image available to the detector in terms of the various system parameters. The problem as in the passive case was to achieve a sufficiently high quality image so that the user's signal could be reliably distinguished from changes in the background. The results of this analysis showed that if a region of given angular size must be considered then a larger received signal energy will result if the beam divergence of the source is increased to cover the desired region rather than

scanning the desired region with a beam of smaller size. After determining the conditions under which a reasonably high quality image could be obtained the detector required to convert the image into electrical signals was considered. The video bandwidth required to reproduce the image was very large and a considerable amount of internal noise was present which caused a large reduction of the signal-to-noise ratio at the output of the detector.

The results obtained in this section showed that the maximum possible beam divergence which could be used and still obtain a reasonable signal was on the order of 0.5^{o}. This is the beam divergence required when the user already knows his position to be within a 10-km diameter circle and has a vertical reference and compass heading accurate to within 0.3^{o}. Although it was found that it would be impossible to detect the signal from CW lasers of average power under these conditions it would probably be possible to detect the user's signal with a pulsed laser with an output of several hundred joules. Although such lasers are available their wavelength of operation is not in the region where the highest sensitivity photosensitive surfaces operate. With the resolution obtainable in the television cameras which will be available in the near future it should be possible to reduce the error in the user's position from 10 km to 1 km if the user's signal can be detected. The cost of the user's equipment for such a system would probably be in excess of $100,000. The limited conditions under which any improvement in the position accuracy might be obtained make the use of an active optical navigation system economically unjustifiable.

4.0 ADDITIONAL AREAS OF STUDY

The primary purpose of this study has been to analyze the problem of detecting the user's signal. The lack of suitable detectors has made it unnecessary to investigate certain other problems which would have been considered if the optical navigation system was feasible.

4.1 System Calibration and Distortion

All television cameras and optical systems have certain inherent distortions and nonlinearities. In order to use a preselected set of signals as reference points in the television picture, these nonlinearities and distortions must be removed. Since the position of the user is assumed to be related to the position of the signal in the image by some ideal geometrical relationship any deviations from this ideal relationship must be recognized and corrected. The removal of distortion and nonlinearities from television pictures has been accomplished using calibrated reference images [87, 88]. A detailed study would be necessary to determine if the residual errors were small enough to be neglected and the relationship between the various errors and the total system error would have to be determined.

4.2 Beam Broadening

Since scattering and atmospheric turbulence produce a spreading of the laser beam [89], the beam divergence used for calculations in the ideal case may have to be increased to take into account the beam divergence which is actually present at the satellite. For high altitude users it is not expected that any correction of the beam divergence would be necessary.

4.3 Computational Scheme and Refraction Correction

In order to compute the position of the user a relationship must be found between the user's position coordinates on the earth and the position coordinates of the user's signal in the television camera image. The reference signals in the image and the position of the reference stations would provide a common reference point in each coordinate system. The complexity of this coordinate system transformation will determine to a great extent the computational capacity which must be built into the satellite. Since the image at the satellite will contain no information as to the altitude of the user the coordinate transformation will have to be made on the basis of one reference altitude and the user will have to correct the position received according to the deviation from this reference altitude. It will also be necessary to determine the amount of atmospheric refraction which will occur at the reference altitude under standard conditions of temperature, humidity and pressure. It would then be necessary for the user to correct the amount of atmospheric refraction assumed in the calculations if significant deviations from the reference altitude and standard atmospheric conditions occured. In this case it is also expected that high altitude users would not have to make any significant corrections.

4.4 Identification

The operation of the optical navigation system described is dependent only on the detection of the user and not identification. Under these conditions the user would be required to determine which of the detected signals, and corresponding locations, correspond to a particular user. Assuming that there are only a few users and that position determinations are not required very frequently then the probability of having more than one user detected at a time is small. If the positions of the users detected are sufficiently far apart then a particular user should be able to decide which position is his. If the users are close together or separated in altitude only then the identification problem becomes more important. One possible solution would be to assign particular users a certain time block to use the satellite or to use several different wavelengths along with a corresponding filter at different times. The solution to this problem for many users requiring frequent position determinations is not evident and may not be readily solved.

4.5 Other Systems

The active system being considered is not the only possible system configuration which could be used. One possible alternative would be to put the optical source in the satellite and have a camera in the user which detects the signal produced. This possibility was rejected since the background noise problem would be much worse and would require the user to have the more expensive equipment which is a definite disadvantage. Although optical signals have been detected from satellites it was only possible to detect these signals at night [90].

Another possible alternative would be to have a retroreflector mounted in the satellite similar to the laser reflector left on the moon during the Apollo mission. The user would then aim a laser at a portion of the sky and look for a reflection from the satellite whose position is accurately known. The return signal from the satellite, however, would be extremely hard to detect since only a very small fraction of the energy transmitted would be reflected; the reflected energy would be inversely proportional to the fourth power of the distance from the user to the satellite. The aiming of the laser would have to be extremely accurate for such a system to work. It would also have the additional disadvantage that the user needs two expensive components, the optical detector and the laser, while the satellite would be relatively inexpensive. Other optical system configurations might be possible but in each case if a laser is used then it must be aimed as accurately as possible and if an incoherent source is used then the background radiation from the sun will almost certainly obscure the signal during daylight hours. The use of low-altitude satellites has not been considered because of the number of satellites that would be required for continuous coverage and the fact that both the signal and the external noise would increase in the same proportion as the altitude of the satellite was decreased.

5.0 RESULTS AND CONCLUSIONS

5.1 Resume of the Principal Objectives of This Study

The objective of this report has been to analyze the use of infrared and optical techniques in a navigation system using synchronous satellites. The method of analysis has been to analyze the optical image which would be available to the detector under typical operating conditions to determine if a user's signal could be reliably detected. By concentrating the analysis on the image available and not the detector itself, it was hoped that it would be possible to determine the feasibility of an optical navigation system from a theoretical viewpoint without relying too heavily on the current state of optical technology. This goal was realized to a certain extent but it was necessary to assume that the detector could resolve a certain number of individual image elements.

Two different situations were considered. First, it was assumed that the satellite would detect the infrared energy emitted by the user's engines and use this information to determine the user's position. In the second case the users would be equipped with high-power optical sources which would be aimed in the general direction of the satellite and these signals would be used by the satellite to compute the user's position. The two cases were denoted, respectively, as the passive case and the active case. The satellite is equipped with a high resolution television camera and a binary decision is made on each resolvable image element as to the presence of a user's signal. A number of ground stations will provide reference signals so that the relative position of the signals in the image can be used to compute the user's location. Since the image which would be processed by the detector will only contain a few signals of interest the binary detection system represents a method of reducing the amount of data which must be processed.

5.2 Passive Navigation System

In the passive case the source of the signal energy is assumed to be the infrared energy emitted by the exhaust system of a jet engine. The background noise in this case consists of the infrared energy emitted by the earth and clouds which are normally much colder than the earth. The analysis was based on a determination of the effect which changes in the effective background temperature would have on the detection of the user's signal. By assuming that the resolution of the optical system was high enough so that the user's signal would be present on only one resolvable image element, it was possible to derive a signal-to-noise ratio which described the quality of the image.

The resolution of the satellite optical system is limited by the diameter of the objective lens so that associated with every resolvable image element will be an area on the earth whose energy is focused on that image element. If the variation in the energy on an individual image element due to the presence of a user is less than the variation due to changes in the effective background temperature then it will not be possible to detect the presence of the user's signal. The ratio of these variations, that is the variation of the power incident on an

individual image element due to a signal divided by the variation in the power due to changes in the effective background temperature, was chosen as a measure of the quality of the image. It was found that for objective lenses of practical size it was not possible to realiably discriminate between changes in the energy on an image element due to the presence of a signal and changes due to different background temperatures. Under typical conditions the signal variation might be several orders of magnitude less than the variation due to changes in the effective background temperature. The reason for this situation is found in the size of the resolvable image element. Even though the temperatures of the source and background are quite different the small percentage of energy from the background that falls in the spectral region of the source can be much greater than the desired signal because the relative size of the resolvable area and the source are so different. For example the signal might be generated by a source of several square meters at a temperature of 600° to 1000°K while the background energy on the same image element is generated by an area of several thousand square meters at a temperature of 250° to 280°K. Although the spectral distribution of the energy generated at these two temperatures is quite different, the absolute amount of energy generated by the low temperature is sufficient to exceed that generated by the high temperature source in the desired spectral region because of the relative size of the areas involved is so different. The problem presented by the variations in the background is that it becomes impossible to distinguish whether the large amount of energy on one image element is due to the presence of a user or to a very warm region. A very large objective lens diameter is necessary to ensure that the variations in the effective background temperature of a resolvable area are much less than the variation due to the presence of a user.

Certain additional problems besides the detection of the user's signal were also examined. It was found that for high altitude users the atmospheric attenuation likely to be encountered could be neglected. For low altitude users however the presence of even a slight amount of water vapor (in the form of clouds or fog) along the transmission path would cause a severe reduction in the signal level and would make the system inoperative. Modifications to increase the infrared energy produced by the plane were considered but the increases that could be produced by passive means would not be significant.

In addition to the background variations in the image another problem is that there are no high sensitivity detectors capable of producing a two-dimensional image for the spectral region in which most of the source energy is located. A large number of point detectors are available for the desired spectral region but these must be mechanically scanned to produce an image. The lack of a suitable detector would not present such a great problem if it were merely a matter of improving the detectors already available. However this is not the case since the infrared sensitive camera tubes which have been developed for the spectral region under consideration have been little more than laboratory curiosities (except for the possibility of classified developments). It was concluded that the large amount of background noise present and the lack of a suitable detector would make passive detection at synchronous altitude impossible.

5.3 Active Navigation System

In the active case each of the users is equipped with an optical power source which is aimed in the general direction of the satellite. The user aims the source to the best of his ability considering the accuracy of the a priori knowledge of his position. For the active case the major source of background noise is the sunlight reflected from the earth and the atmosphere. A problem similar to the temperature variations encountered in the passive case arises because the amount of reflected energy varies greatly according to the type of background present, e.g., clouds, sea, land, etc., and this variation causes the same problem in distinguishing the user's signal from changes in the background of the image.

Since a variety of high power optical sources are available an analysis was made to determine what type of source would best meet the requirements of the optical navigation system. It was found that although many sources could easily be detected in the absence of any background noise the laser was the only source which could be detected in the presence of the background noise by using a filter before the detector. The narrow spectral region in which the majority of the laser energy is located allows a significant amount of any background noise present to be removed by filtering. The optical filters which are presently available are capable of eliminating a very large percentage of the undesired background energy while having a minimal effect on the desired signal. The use of a signal with a very narrow spectral range will not be advantageous unless a filter is available which can extract that signal from any background noise present. Although the primary advantage of the laser is its narrow spectral output there are two other important advantages. The laser has a much smaller input power requirement than many of the other sources considered and the wavelength of operation can be chosen to a certain extent to minimize the effects of atmospheric attenuation. An analysis showed that it would be best to use wavelengths in the near infrared if possible, but the quantum efficiency of many detectors is not very good in this region so that the final choice of wavelength will depend on the spectral response of the detectors available and the wavelength of the laser rather than the atmospheric attenuation present.

The problem of atmospheric attenuation in the active case is similar to that in the passive case but there is an important difference. Although it will still not be possible to overcome the attenuation introduced by clouds or fog along the transmission path it will be possible to increase the source power to overcome some attenuation. The question now becomes what level of attenuation is it reasonable to try to overcome and how much will the navigation system performance be improved? To answer this question an analysis was made of the attenuation levels which could be expected in fair weather. It was found that by increasing the source power an order of magnitude above the zero attenuation level it should be possible to overcome the atmospheric attenuation which would be found under normal operating conditions.

The definition of the signal-to-noise ratio used in the active case to analyze the quality of the image is the same as that used in the

passive case. The discussion about the signal-to-noise ratio in the previous section could almost be used here except for the reason for the variations in the background. As was stated previously the predominant form of background noise in this case is the sunlight reflected from the atmosphere and various types of clouds. The reflectance of the various weather formations can vary from almost zero to over 80% so that significant differences can occur between the background noise present on various image elements. As in the passive case it was only possible to reliably detect the user's signal from the background variations under very limited circumstances. It was concluded that the limited circumstances under which the user's signal could be detected would not justify the cost of the equipment involved. Even under the limited circumstances when the image received was of sufficient quality to distinguish the user's signal, it was questionable whether or not the internal noise of the detector could be reduced enough to allow reliable detection. There is not only a significant amount of noise present in the image but the resolution required in this system is such that a very wide video bandwidth would be required. The shot noise and thermal noise generated internally in the detector may present a major problem because of the large video amplifier bandwidth. The high resolution television camera tubes available have required special construction techniques to minimize the internally generated noise.

After considering the conditions under which an active optical navigation system could operate it is concluded that the use of such a system would not be economically justifiable considering the limited improvement in position accuracy which might be obtained. Even if there were no reference errors in the heading or vertical reference, the user would have to know his position to within several tens of kilometers in order to get the optical navigation system to operate and such accuracy is better than some of the present radio navigation systems provide. The successful experiments using laser beams transmitted over long distances have required extremely accurate aiming of the sources. One important implication of this is that to make use of one of the most important properties of a laser, namely its narrow beamwidth, it must be possible to aim the device properly. If it is required to increase the beamwidth to compensate for the lack of ability to accurately aim the laser, then one of the important properties of the device is destroyed. It is apparent that the operation of a navigation system depends on the ability of the transmitter to produce a useable signal over a large region without accurately knowing beforehand in what direction to transmit the energy. The laser does not fit the requirements of the navigation system considered and it is concluded that at the present time it would be much less expensive and a much better system could be obtained through the use of radio frequency equipment.

The results obtained in this study indicate that optical techniques are not capable of providing the performance required for a synchronous navigation satellite system. In the passive case the detectors available have neither the sensitivity nor the resolution required to provide adequate performance. In the active case the conditions under which such a system could operate are so restrictive and the cost so high that it must be concluded that radio frequency techniques would give much better performance at a significantly lower cost. Considering the

stringent detector requirements necessary in both the active and passive cases and the detectors presently available it seems unlikely that any technological improvements will change the results presented to any great extent. It should also be pointed out that since wavelengths in the visible and near infrared regions do not penetrate clouds, an optical system would be restricted to users operating at high altitudes above the majority of clouds or to users which could operate without the optical navigation system for a time or had a backup system to navigate in periods of bad weather.

REFERENCES

1. Electronics, Vol. 41, No. 13, June 24, 1968, p. 25.

2. Sollfrey, W., Earth Coverage Patterns with High-Gain Antennas on Stationary Satellites, Rand Corporation Memorandum RM-4894-NASA, February 1966.

3. Wolfe, W. L., editor, HANDBOOK OF MILITARY INFRARED TECHNOLOGY, Government Printing Office, Washington, D. C., 1965.

4. Hackforth, H. L., INFRARED RADIATION, McGraw-Hill, New York, 1960.

5. Stall, V. R., and G. N. Plass, "Emissivity of Dispersed Carbon Particles," Journal of the Optical Society of America, Vol. 50, No. 2, February 1960, p. 121.

6. Jamieson, I. A., et al, INFRARED PHYSICS AND ENGINEERING, McGraw-Hill, New York, 1963.

7. Driggs, I. V., and O. E. Lancaster, GAS TURBINES FOR AIRCRAFT, Ronald Press, New York, 1955.

8. BASIC AND ADVANCED INFRARED TECHNOLOGY, Technical Assistance Division, Redstone Arsenal, AD 634 535, April 1965.

9. Shortley, G., and D. Williams, ELEMENTS OF PHYSICS, Third Edition, Prentice-Hall, Inc., Englewood Cliffs, N. J., 1961.

10. Pivovonsky, M., and M. Nagel, TABLES OF BLACKBODY RADIATION FUNCTIONS, MacMillan, New York, 1961.

11. Hannan, H. J., L. J. Nicastro and C. W. Reno, Doppler Optical Navigator, First Quarterly Progress Report, Contract AF 33(657)-11458, AD 420 000, September 1963.

12. McCartney, E. J., "Optical System Performance and Atmospheric Attenuation," Navigation, Vol. 14, No. 2, Summer 1967, p. 221.

13. Yates, H. W., and J. H. Taylor, Infrared Transmission of the Atmosphere, NRL Report 5453, AD 240 188, June 1960, pp. 32-33.

14. Observations from the Nimbus I Meteorological Satellite, 1965, NASA Special Publication No. SP-89, Goddard Space Flight Center.

15. Johnson, A. W., "Weather Satellites: II", Scientific American, Vol. 220, No. 1, January 1969, p. 62.

16. Soule, H. V., ELECTRO-OPTICAL PHOTOGRAPHY AT LOW ILLUMINATION LEVELS, John Wiley and Sons, Inc., New York, 1968.

17. Radio Corporation of America, RCA Vidicons, Publication CAM-700A.

18. Lasser, M. E., Chalet, P. H., and R. B. Emmons, "Electronic Scanning for Infrared Imaging," Proc. of the IRE, Vol. 47, No. 12, December 1959, p. 2069.

19. Artemyev, N. L., et al, "A New Camera Tube, The Infracon," Translated from the Russian, April 1966, U. S. Army Engineers, Research and Development Laboratories, T-1829-66, AD 630 687.

20. Redington, R. W., and P. J. VanHeerden, "Doped Silicon and Germanium Photoconductors as Targets for Infrared Television Camera Tubes," Journal of the Optical Society of America, Vol. 49, No. 10, October 1959, p. 997.

21. Electronic Design, Vol. 16, No. 21, October 10, 1968, p. 32.

22. Electronics, Vol. 42, No. 1, January 6, 1969, pp. 56-58.

23. Ruth, S. B., "Solid State TV Camera Eliminates Vidicon Tube," The Electronic Engineer, Vol. 25, No. 11, November 1966, p. 24.

24. Marton, L., Editor, "Television Pickup Tubes and the Problem of Vision," by A. Rose, Advances in Electronics, Vol. 1, Academic Press, New York, 1948, pp. 135-141.

25. Schade, O. H., "The Resolving-Power Functions and Quantum Processes of Television Cameras," RCA Review, Vol. 28, No. 3, September 1967, pp. 460-535.

26. Fink, D. G., TELEVISION ENGINEERING HANDBOOK, McGraw-Hill, New York, 1957, p. 3-15.

27. Berry, F. A., et al, HANDBOOK OF METEOROLOGY, McGraw-Hill, New York, 1945.

28. Solomon, I., Estimates of Altitudes with Specified Probabilities of Being Above All Clouds, Tech. Report 159, Air Weather Service (MATS), U. S. Air Force, 1961.

29. Elterman, L., Atmospheric Attenuation Model, 1964, in The Ultraviolet, The Visible, and The Infrared Windows for Altitudes to 50 km, Environmental Research Paper No. 46, Air Force Cambridge Research Laboratories, L. G. Hanscom Field, Bedford, Mass., 1964.

30. U. S. Standard Atmosphere, 1962, U. S. Government Printing Office, Washington, D. C.

31. Minzner, R. A., Champion, K. S. W., and H. L. Pond, The ARDC Model Atmosphere, 1959, Air Force Surveys in Geophysics No. 115, AFCRC-TR-59-267, AD 229 482, Air Force Cambridge Research Center, L. G. Hanscom Field, Bedford, Mass., August 1959.

32. Valley, S. L., Ed., Handbook of Geophysics and Space Environments, Air Force Cambridge Research Laboratories, L. G. Hanscom Field, Bedford, Mass., 1965, pp. 7-1 to 7-36.

33. Montgomery, A. J., Analysis of Optical Wavefront Distortions Caused by The Atmosphere, Technical Report AFAL-TR-68-167, AD 837 222, Air Force Avionic Laboratory, Wright-Patterson Air Force Base, Ohio, July 1968.

34. Fried, D. L., "Optical Resolution Through a Randomly Inhomogeneous Medium for Very Long and Very Short Exposures," Journal of the Optical Society of America, Vol. 56, No. 10, October 1966, pp. 1372-1379.

35. Fried, D. L., "Limiting Resolution Looking Down Through the Atmosphere," Journal of the Optical Society of America, Vol. 56, No. 10, October 1966, pp. 1380-1384.

36. Meisenholder, G. W.,Planet Illuminance, Jet Propulsion Laboratory Report JPL-TR-32-361, NASA N63-13443, November 1962.

37. Ross, M., LASER RECEIVERS: DEVICES, TECHNIQUES, SYSTEMS, John Wiley and Sons, Inc., New York, 1966, Chapter 7.

38. Frungel, F., HIGH SPEED PULSE TECHNOLOGY: OPTICAL PULSES, LASERS, AND MEASURING TECHNIQUES (Vol. 2), Academic Press, New York, 1965.

39. "Laser Technology," Microwaves, Vol. 7, No. 11, pp. 101-143.

40. Levi, L., APPLIED OPTICS, A GUIDE TO OPTICAL SYSTEM DESIGN, Vol. 1, John Wiley and Sons, Inc., New York, 1968, Chapters 5 and 7.

41. IES LIGHTING HANDBOOK, Illuminating Engineering Society, Third Edition, New York, 1959.

42. PEK Laboratories, Sunnyvale, California, "Product Reference Guide to High Intensity Light Sources," General Catalog No. 901-1.

43. Xenon Corporation, Medford, Mass., "High Energy Helical Flashtubes," Data Sheet 968E.

44. EG and G, Inc., Boston, Mass., "Linear Xenon Flashtubes," Data Sheet 1002-B.

45. DeMaria, A. J. and H. A. Heynau, Investigation of Means for Generating High Energy and Extremely Narrow Laser Pulses, United Aircraft Corp., East Hartford, Conn., Report No. F920475-5, March 1967, AD 809 590.

46. "Ten-Trillion-Watt Laser Developed by Sandia," Electronic Design, Vol. 17, No. 7, April 1, 1969, p. 44.

47. Horrigan, F. A., et al, High Power Gas Laser Research, Raytheon Co., Waltham, Mass., Report 5-1084, July 1968, AD 676 226.

48. Carman, R. L., J. Hanus, and D. L. Weinberg, "A New, Widely and Continuously Tunable, High Power Pulsed Laser Source," Applied Physics Letters, Vol. 11, No. 8, October 15, 1967, pp. 250-253, AD 667 875.

49. The Ealing Corporation, Ealing Optical Services, Cambridge, Massachusetts, 1968-1969 Catalog, p. 144.

50. Spectrum Systems, Inc., Visible and Near Infrared Filters, Waltham, Mass., Bulletins 55-14 and 55-11.

51. Hunter, G. S., "Surveyor Receives Earth Laser Beams," Aviation Week and Space Technology, Vol. 88, No. 5, January 29, 1968, p. 27.

52. Blanchard, L. E., "Television Pictures of the Lunar Surface by Earthshine," Journal of the Society of Motion Picture and Television Engineers, Vol. 77, No. 4, April 1968, pp. 351-353.

53. Gradshteyn, I. S., and Ryzhik, I. M., Table of Integrals, Series and Products, Academic Press, New York, 1965, p. 30.

54. Oliver, B. M., "Some Potentialities of Optical Masers," Proc. of the IRE, Vol. 50, No. 1, February 1962, pp. 135-141.

55. Born, M. and Wolf, E., Principles of Optics, Second Edition, The MacMillan Co., New York, 1964.

56. Ramsay, J. F., "Tubular Beams From Radiating Apertures," in Advances in Microwaves, Vol. 3, Edited by L. Young, Academic Press, New York, 1968, pp. 127-221.

57. Dwight, H. B., Tables of Integrals and Other Mathematical Data, Fourth Edition, The MacMillan Co., New York, 1961.

58. Rosenblatt, A., and Dickson, P., "At Long Last, ERTS Is On the Way," Electronics, Vol. 42, No. 10, May 12, 1969, pp. 98-106.

59. Livingston, W. C., "Resolution Capability of the Image-Orthicon Camera Tube Under Nonstandard Scan Conditions," Journal of the Society of Motion Picture and Television Engineers, Vol. 72, No. 10, October 1963, pp. 771-785.

60. Gray, S., Murray, P. C., and Ziemelis, O. J., "Improved High Resolution Electron Gun for Television Cameras," Journal of the Society of Motion Picture and Television Engineers, Vol. 72, No. 10, October 1963, pp. 792-794.

61. Hudson, R. D., INFRARED SYSTEM ENGINEERING, John Wiley and Sons, Inc., New York, 1969.

62. Schade, O. H., "An Evaluation of Photographic Image Quality and Resolving Power," Journal of the Society of Motion Picture and Television Engineers, Vol. 73, No. 2, February 1964, pp. 81-119.

63. Biberman, L. M., "Background Considerations in Infrared System Design," Applied Optics, Vol. 4, No. 3, March 1965, pp. 343-345.

64. Wischina, H. F., Hemstreet, H. S., and Atwood, J. G., "Determination of Optical Technology Experiments for a Satellite," NASA Contractor Report CR-252, July 1965, p. 3-39.

65. Wexler, R., "Infrared and Visual Radiation Measurements from Tiros III," Applied Optics, Vol. 3, No. 2, February 1964, pp. 215-219.

66. Brunt, D., PHYSICAL AND DYNAMICAL METEOROLOGY, Cambridge University Press, London, Second Edition, 1944, p. 113.

67. Plass, G. N., and Kattawar, G. W., "Influence of Single Scattering Albedo on Reflected and Transmitted Light from Clouds," Applied Optics, Vol. 7, No. 2, February 1968, pp. 361-367.

68. Plass, G. N., and Kattawar, G. W., "Monte Carlo Calculations of Light Scattering From Clouds," Applied Optics, Vol. 7, No. 3, March 1968, pp. 415-419.

69. Kattawar, G. W., and Plass, G. N., "Infrared Cloud Radiance," Applied Optics, Vol. 8, No. 6, June 1969, pp. 1169-1178.

70. Barnes, J. C., and Chang, D., "Accurate Cloud Cover Determinations and Its Effects on Albedo Computations," Allied Research Associates, Inc., Concord, Mass., NASA-CR-98596, Oct. 1968, N69-14336, p. 75.

71. Coulson, K. L., "Characteristics of the Radiation Emerging from the Top of a Rayleigh Atmosphere-II," Journal of Planetary and Space Science, Vol. 1, No. 4, 1959, pp. 277-284.

72. Whitehill, L. P., "Survey of Earth Albedo," Lincoln Laboratory Technical Note 1966-53, October 1966, AD 643 649.

73. Bartman, F. L., "The Reflectance and Scattering of Solar Radiation by the Earth," Michigan University Report 05836-11-T, NASA-CR-83954, February 1967, N67-25962.

74. Hirshon, S., "Inertial System Capabilities Applied to SST Operation," Navigation, Vol. 11, No. 3, Autumn 1964, pp. 237-249.

75. White, R. N., "Airborne Doppler Radar Navigation of Jet Transport Aircraft," IRE Trans. on Aerospace and Navigational Electronics, Vol. ANE-9, March 1962, pp. 11-20.

76. Bowditch, N., American Practical Navigator, Hydrographic Office Publication No. 9, U.S. Government Printing Office, Washington, D. C., 1966.

77. Air Navigation, Hydrographic Office Publication No. 216, U.S. Government Printing Office, Washington, D. C., 1963, Chapter 13.

78. DeGroot, L. E., "Navigation and Control from LORAN-C," Navigation, Vol. 11, No. 3, Autumn 1964, pp. 213-227.

79. Johnson, T. D., "Status of Dectra," Navigation, Vol. 5, No. 2, Summer 1957, pp. 303-310.

80. Chin, T. H., "Spacecraft Stabilization and Attitude Control," Space/Aeronautics, Vol. 38, June 1963, p. 88.

81. LaFond, C. D., "Infrared Horizon-Mapping Urged in Space," Electronic Design, Vol. 15, September 27, 1967, p. 22.

82. Schwarz, F., and Falk, T., "High Accuracy, High Reliability Infrared Horizon Sensors for Earth, Lunar and Planetary Use," Navigation, Vol. 13, No. 3, Autumn 1966, pp. 246-257.

83. Greene, J., "A Daylight Astro Tracker for Supersonic Transports," Navigation, Vol. 11, No. 3, Autumn 1964, pp. 228-236.

84. Cope, A. D. and Borkan, H., "Isocon Scan--A Low-Noise, Wide-Dynamic-Range Camera Tube Scanning Technique," Applied Optics, Vol. 2, No. 3, March 1963, pp. 253-261.

85. Radio Corporation of America, RCA Phototubes and Photocells, Technical Manual PT-60, 1963.

86. Ascoli-Bartoli, U., DeAngelis, A., and Nardi, N., "Use of the Image Orthicon Tube for Detecting Low Intensity Pulsed Light Signals," Applied Optics, Vol. 8, No. 1, January 1969, pp. 59-64.

87. Lackman, R. L., "Utilization of a Reseau for Reducing Electronic Scanning Nonlinearity in Surveyor Television Space Systems," Journal of the Society of Motion Picture and Television Engineers, Vol. 77, No. 4, April 1968, pp. 299-303.

88. Blanchard, L. E., "Design Considerations for Television Camera Reseau for the Reduction of Geometric Distortion on Planetary Missions," Journal of the Society of Motion Picture and Television Engineers, Vol. 77, No. 4, April 1968, pp. 303-306.

89. Subramanian, M., "Atmospheric Limitations for Laser Communications," 1968 Electronic and Aerospace Systems Convention, 1968 EASCON Convention Record, pp. 125-133.

90. Abby, D. G., and T. E. Wirtanen, "Photomultiplier Reception of Satellite Beacon Flashes," Applied Optics, Vol. 8, No. 3, March 1969, pp. 627-631.

Appendix A

THE GDOP FACTOR AND OPTICAL RESOLUTION

The geometrical dilution of precision effect (GDOP) arises from the projection of the minimum angular resolution on the curved surface of the earth as shown in Fig. A1. As the elevation angle to the satellite increases the accuracy of the position fix deteriorates until the point at which the satellite is on the user's horizon and the system has become inoperative. The best resolution is always obtained at the subsatellite point as would be expected for an angle measurement system. The position error is given by

$$PE = r_1 \, \delta\theta(\epsilon) \, \text{cosec} \, \epsilon \qquad (A.1)$$

where PE = position error

r_1 = distance to user from satellite (see (2.7-3))

$\delta\theta(\epsilon)$ = angular resolution of the optical system in rad as a function of the elevation angle

ϵ = elevation angle to satellite.

The GDOP factor is defined as the position error as a function of the elevation angle normalized with respect to the smallest position error which occurs at the subsatellite point hence

$$GDOP = \frac{r_1 \, \delta\theta(\epsilon) \, \text{cosec} \, \epsilon}{r_g} \qquad (A.2)$$

where r_g = ground resolution (position error) at the subsatellite point.

Simplification of this formula is possible by making a suitable assumption on the angular resolution. The ground resolution is given by

$$r_g = \delta\theta(0) \, r_s \qquad (A.3)$$

where $\delta\theta(0)$ = angular resolution at the subsatellite point

r_s = synchronous altitude.

If it can be assumed that the angular resolution is constant over the entire image then (A.2) reduces to

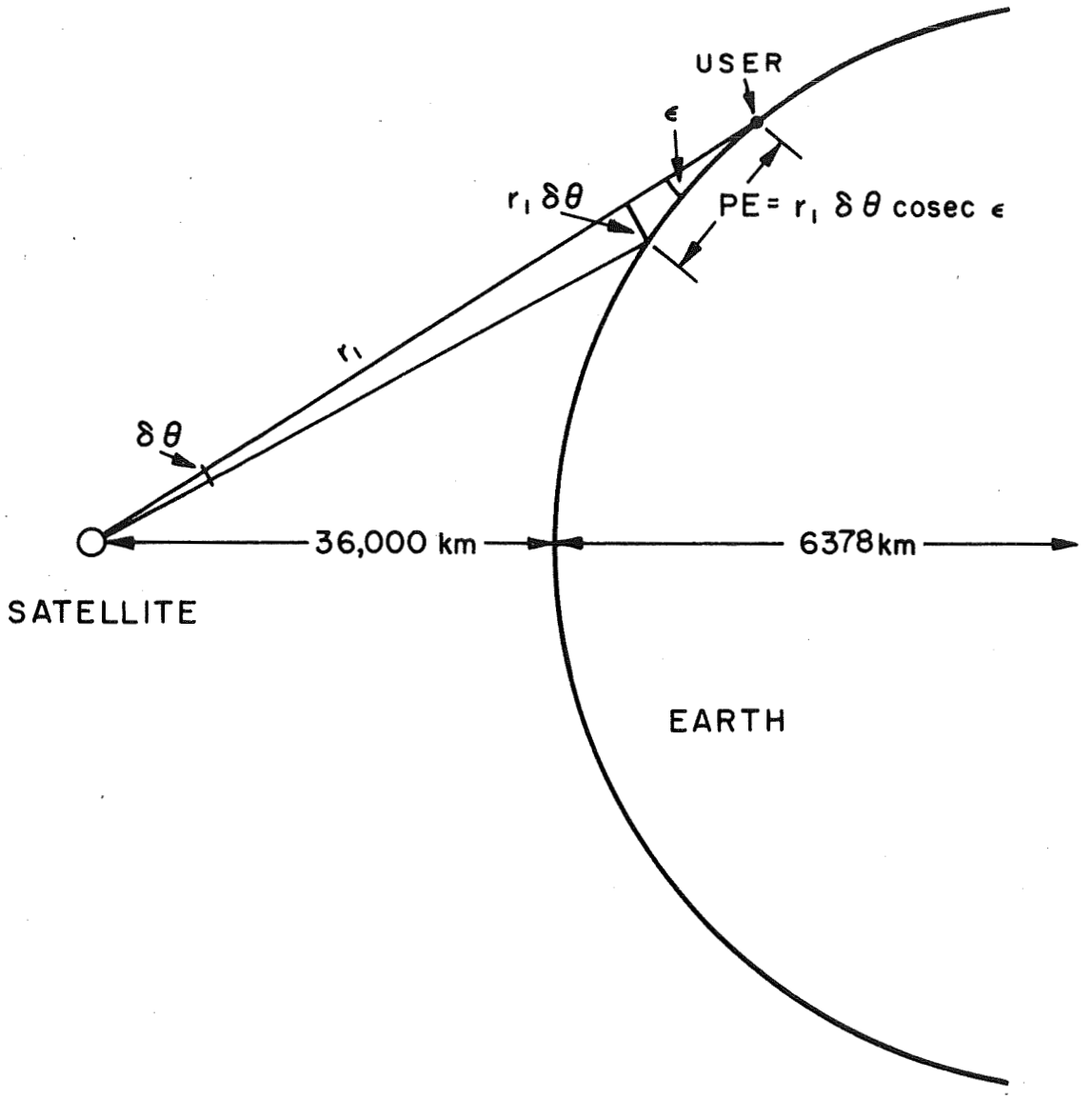

FIGURE AI THE GEOMETRICAL DILUTION OF PRECISION EFFECT

$$GDOP = \frac{r_1 \text{ cosec } \epsilon}{r_s} \qquad (A.4)$$

where r_s = 36,000 km = synchronous altitude.

The GDOP factor, (A.4), is plotted in Fig. 3 of Section 2.3.1. For an optical system using a television camera as a detector the assumption that the angular resolution is constant is somewhat questionable. Not only does the diffraction limited resolution become worse near the edges of the image but the effect of aberrations or departures from a perfect image also become worse near the edges. The effect of the aberrations on the image is sometimes proportional to the seventh power of the distance from the center of the image which means very high distortion for users near the edge of the field-of-view.

In addition to the decreased resolution at the image edge due to imperfect lens construction, the resolution of the television camera also decreases away from the image center. The operation of television camera tubes normally involves some form of electromagnetic field which is used for deflection and acceleration of the electron beam. Uniform fields are often required over a given volume and the uniformity will depend on the precise placement and construction of the tube elements. In many cases the uniformity over the entire image area cannot be maintained and the resolution at the edge is often 40% less than at the center of the image.

The increase in the position error given by the GDOP factor can only be considered as a lower limit on the position error which might be two or three times that predicted by the GDOP factor. Of course it is possible to reduce the effect of the optical distortions by providing correction factors for positions near the edge of the image. The reduction in the resolution or position accuracy can thus be attributed to the following interacting factors:

1) the geometrical dilution of precision due to poor user-satellite geometry

2) optical distortions which increase near the image edges

3) reduced television resolution near the edge of the photo-sensitive surface

4) the increased atmospheric path length which will make it more difficult to correct for atmospheric refraction.

In addition the vertical angular measurement and the horizontal angular measurement form an orthogonal coordinate system in which case:

$$r_t = \sqrt{r_h^2 + r_v^2} \qquad (A.5)$$

where r_t = total position error

r_h = horizontal resolution

r_v = vertical resolution.

Since the vertical and horizontal resolutions are assumed to be equal, the maximum position error for any user position is

$$r_t = \sqrt{2}\ r_g\ \text{GDOP} \qquad \text{(A.6)}$$

and the maximum position error occurs along a user path which is at a 45° angle to the projection of the scanning lines on the earth's surface. The term "maximum position error" is meant to mean the position error in the case where the only decrease in resolution is that due to the GDOP factor and the optical system and television camera are distortionless.

Appendix B

TELEVISION CAMERA RESOLUTION

The resolution of a television camera can be expressed in a number of ways. The number of television lines, as used in this report, means the actual number of raster lines which are present in the image or equivalently the number of horizontal scanning lines.

The resolution of a photosensitive surface can be derived from a statistical analysis of the quantum processes which take place [24,25,62]. A number of different units are employed to express the spacial resolution capability of a photosensitive surface which is known as the resolving power (f_r). The units of f_r are

$$\frac{\text{cycles}}{\text{mm}} = \frac{\text{line-pairs}}{\text{mm}} = \frac{\text{lines}}{\text{mm}} \qquad \text{(B.1)}$$

and are used interchangebly in many reports. The number of TV lines is a function of the scanning circuits used and the spacial resolving power is a function of the photosensitive surface and the energy incident on that surface. The number of TV lines can be related to the resolving power by noting that by the sampling theorem, two samples are required to give a spacial resolution of one cycle and here the samples are the raster lines which means that two TV lines are required for every cycle of resolving power. [59].

$$\frac{\text{cycles}}{\text{mm}} = \frac{\text{line-pairs}}{\text{mm}} = \frac{\text{lines}}{\text{mm}} = \frac{1}{2}\,\frac{\text{TV lines}}{\text{mm}} \qquad \text{(B.2)}$$

The resolution capability of a television camera tube is normally given in terms of the maximum number of TV lines but for special purpose cameras the resolution is sometimes given in terms of the maximum resolving power which is half the number of TV lines. The resolution can be expressed in terms of the total number of TV lines (or cycles) or in terms of the TV line (or cycle) density, i.e., TV lines (or cycles)/mm.

The spacial resolving power of a photosensitive surface is limited by the incident energy and the quantum properties of the surface up until the point at which the spacial resolution begins to exceed the size of the granules making up the surface. At present most photosensitive, i.e. TV, surfaces are not capable of resolutions exceeding 100 lines/mm although higher resolutions are possible by performing special smoothing operations on the cathode oxide [59, 60]. No increase in resolution is possible by having the number of scan lines greater than twice the spacial resolution limit whether the spacial resolution limit is quantum

limited or limited by the granularity of the surface.

It was assumed in Section 2.7 that there was equal resolution in the horizontal and vertical directions. The resolution in the vertical direction is a function of the number of TV (scan) lines while the horizontal resolution is obtained from the image information read-out during the scanning process. The resolution in the horizontal direction is directly proportional to the ability of the video amplifier to reproduce closely spaced pulses which is directly proportional to the amplifier bandwidth. The horizontal resolution is related to the amplifier bandwidth by [26]:

$$R_H = \frac{2aB}{f_f N} \qquad (B.3)$$

where R_H = horizontal resolution in TV lines

a = aspect ratio = height/width

B = bandwidth in Hz

N = number of TV lines

f_f = frame rate.

The aspect ratio is 1.0 since it is assumed that the vertical and horizontal sides of the image are equal. The frame frequency is simply the picture rate.

The bandwidth determined by (B.3) is not the bandwidth required to transmit the position information but only the bandwidth required of the video amplifier. The output of the video amplifier will be fed to a threshold device which will quantize the output. Since the bandwidth required of the video amplifier may determine the feasibility of the system it should be calculated for a typical system. Assume that the frame rate is either one per second, one every five seconds, or one every ten seconds, which is reasonable to assume from the calculations made in Section 2.4. If the vertical and horizontal resolutions are equal, then $R_H = N$ which when substituted in (B.3) gives:

$$B = \frac{N^2 f_f}{2} \qquad (B.4)$$

The results of this calculation are shown in Fig. B1. If the camera resolution is 10^4 lines, then the maximum bandwidth required would be 50 MHz. Since distributed video amplifiers have been constructed with bandwidths in excess of 400 MHz, the amplifier bandwidth will not present any serious limitations until the resolution is better than 3×10^4 lines.

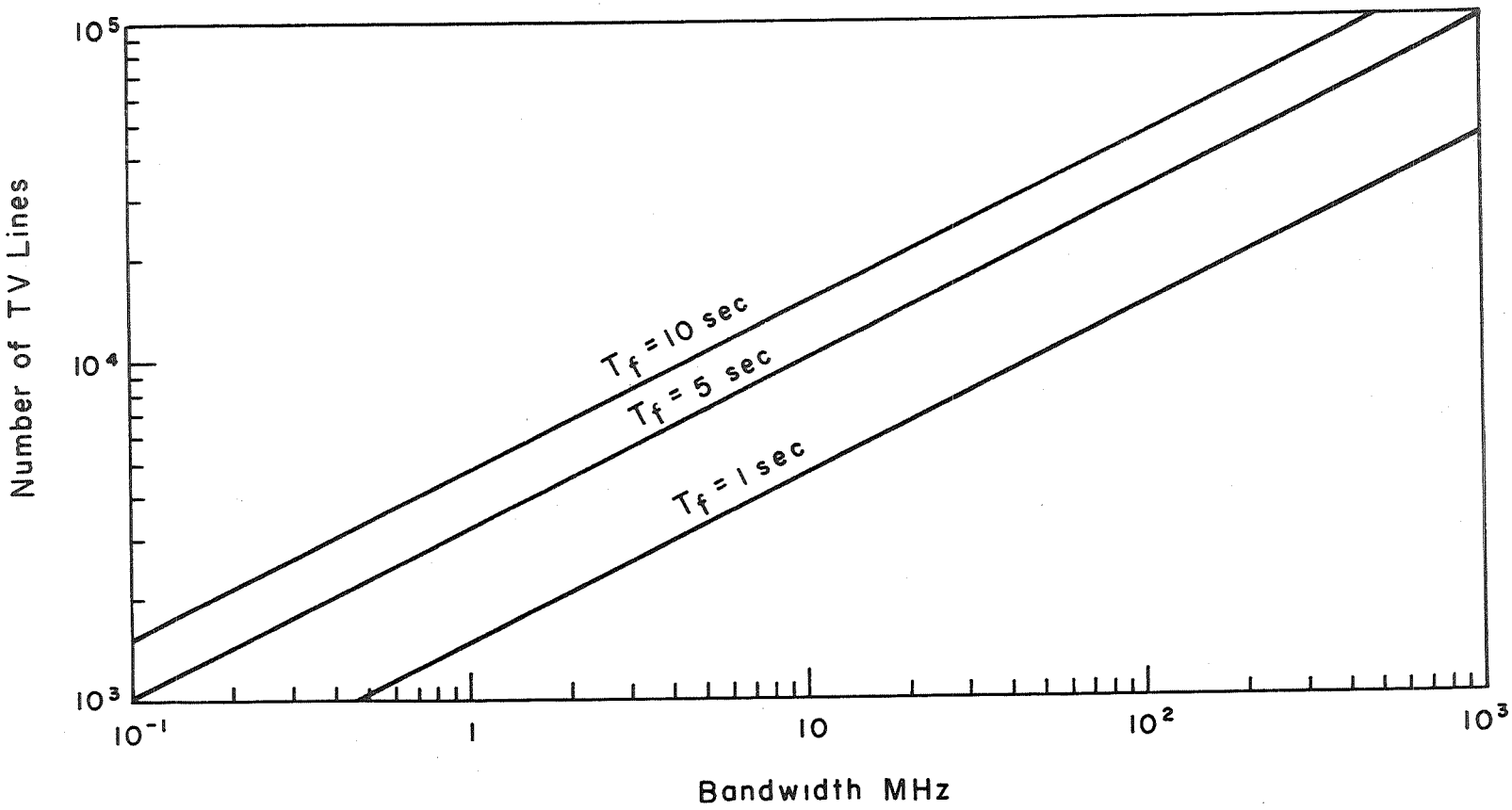

FIGURE B1 VIDEO AMPLIFIER BANDWIDTH

Appendix C

COMPUTER PROGRAM

The following computer program computes the irradiance (incident power density) on a satellite at synchronous altitude due to a circular region of diameter GCD. The earth is assumed to be a black body at 250°K and the center of the circular region is the subsatellite point.

```
C       PROGRAM TO CALCULATE INFRARED NOISE BACKGROUND POWER FOR THE      NGCD  10
C       EARTH AS A BACKGROUND AND USING LAMBERTS LAW OF COSINES  FOR CAL  NGCD  20
        DATA RE,RS,PI,SIG,TEMP,DA/6378.4,35900.0,3.141593,5.673E-8,250.0,  NGCD  30
       1100.0/                                                            NGCD  40
C       W IS TOTAL RADIANT EMMITTANCE AT TEMP(WATTS/SQ METER)              NGCD  50
        W=SIG*TEMP**4.0                                                   NGCD  60
C       VERTICAL AND HORIZONTAL INCREMENTS ARE 10 KM HENCE AREA INC IS 100NGCD  70
        C1=W*DA**2.0/PI                                                   NGCD  80
        WRITE(6,10) TEMP,RE,RS,DA                                         NGCD  90
10      FORMAT(1H1,' DATA USED IN CALCULATION OF NOISE POWER DENSITY',/,5X,NGCD 100
       1'TEMPERATURE',14X,F8.1,2X,'K',/,5X,'EARTH RADIUS',13X,F8.1,2X,'KM'NGCD 110
       2,/,5X,'SYNCHRONOUS ALTITUDE',5X,F8.1,2X,'KM',/,5X,'INCREMENTAL ARENGCD 120
       3A',5X,F8.1,2X,'SQ KM',///)                                        NGCD 130
C       N IS NUMBER OF DATA CARDS                                         NGCD 140
        READ(5,15) N                                                      NGCD 150
15      FORMAT(I2)                                                        NGCD 160
        DO 20 I=1,N                                                       NGCD 170
C       GCD IS MAX GREAT CIRCLE DISTANCE COVERED (KM)                     NGCD 180
        READ(5,16) GCD                                                    NGCD 190
16      FORMAT(F10.1)                                                     NGCD 200
C       COMPUTE MAX NUMBER OF 10 KM VERTICLE INCREMENTS FOR 0.5GCD        NGCD 210
        L=GCD/20.0                                                        NGCD 220
        K=L                                                               NGCD 230
C       INITIALIZE TOTAL ENERGY DENSITY INTEGRAL                          NGCD 240
        AJD=0.0                                                           NGCD 250
C       BEGIN TWO DIMENSIONAL NUMERICAL INTEGRATION OF LAMBERTS LAW OF COSNGCD 260
        DO 30 IH=1,K                                                      NGCD 270
        FIH=IH-0.5                                                        NGCD 280
        DO 30 IV=1,L                                                      NGCD 290
        FIV=IV-0.5                                                        NGCD 300
```

```
      GD=SQRT(FIV*FIV+FIH*FIH)*10.0                                        NGCD 310
      C2=GD/RE                                                             NGCD 320
      C3=1.0-COS(C2)                                                       NGCD 330
      BOT=RS*RS+2.0*RE*RS*C3+2.0*RE*RE*C3                                  NGCD 340
      TOP=COS((ATAN((RE*SIN(C2))/(RS+RE*C3)))+C2)                          NGCD 350
20    WJD=WJD+C1*TOP/BOT                                                   NGCD 360
C     CALCULATE LENGTH OF NEXT VERTICAL STRIP AND COMPUTE L                NGCD 370
      CL=K*K-(FIH+0.5)*(FIH+0.5)                                           NGCD 380
      IF(CL.LT.1.0) GOTO 30                                                NGCD 390
      L=SQRT(CL)                                                           NGCD 400
30    CONTINUE                                                             NGCD 410
      WRITE(6,40) GCD,WJD                                                  NGCD 420
40    FORMAT(1HO,4X,'GREAT CIRCLE DISTANCE',5X,F8.1,2X,'KM',15X,'NOISE PNGCD 430
     1OWER DENSITY',5X,1PE12.3,2X,'WATTS/SQ METER',/)                      NGCD 440
50    CONTINUE                                                             NGCD 450
      STOP                                                                 NGCD 460
      END                                                                  NGCD 470
```

Appendix D

SPECTRAL LINES OF SOME IMPORTANT ELEMENTS USED IN ARC DISCHARGE LAMPS AND LASERS

The spectral output of lasers and arc discharge lamps is dependent on the elements used in their construction. All elements have characteristic spectral lines corresponding to the various possible transitions within the structure of the atom. The transition of an electron from one level to another can produce light energy with a wavelength corresponding to the change in energy which occurred. Lasers and the light produced by arc discharges have strong emission lines corresponding to these atomic level changes.

In the case of arc discharge lamps using mercury vapor there are spectral lines at the locations given in the following list. Where several lines occur in a small region, only the region is listed with the predominant line in parenthesis if there is a predominant line in that region. All wavelengths are in microns.

0.302
0.312 - 0.314
0.334
0.365 - 0.367
0.404 - 0.407 (0.4047)
0.434 - 0.436 (0.4358)
0.5461
0.577 - 0.579

Two of the popular gases used in lasers are argon and krypton. The important wavelengths produced by these gases are listed below in order of decreasing power.

Argon	Krypton
0.4880	0.6471
0.5145	0.5682
0.4765	0.5309
0.4965	0.5208
0.4579	0.4762
0.5017	

The elements and compounds which are currently used in a majority of the lasers available are listed in the table below.

Material	Wavelength (μ)
Cr (Ruby)	0.6943
Nd (Doped glass or YAG)	1.06
HeNe	0.6328 or 1.15
Ar	0.45 - 0.52
CO_2	10.6
Kr	0.47 - 0.65
GaAs (Injection laser)	0.84 - 0.92

Table D1
COMMON LASER MATERIALS AND THEIR CORRESPONDING SPECTRAL OUTPUT

Appendix E

LASERS USED AS EXAMPLES IN SECTION 3.6.1.4

Table	No.	Manufacturer	Model
7	1	Hughes	3041H
	2	Resalab	3355
	3	Hughes	3043H
	4	Avco	C530
	5	Orlando Research	AB20
	6	Korad	K-G1000
	7	Resalab	3340
8	1	Biorad	QLPM
	2	TRG	302-1
	3	Biorad	VD640
	4	American Optical	20
	5	Siemens	SLR-3C1
	6	General Laser	--
9	1	Seed Electronics	S-40(15)
	2	Seed Electronics	S-55
	3	Sperry	0800-01
	4	Laser Diode Labs	LD440

DISTRIBUTION LIST

for report: "An Analysis of the Use of Optical Techniques in Synchronous Navigation Satellites"

under NASA Grant NGL-39-010-087

by

University of Pennsylvania

Addressee	Copies
National Aeronautics and Space Administration Washington, D. C. 20546 Attn: Eugene Ehrlich, Chief, Navigation and Traffic Control Programs, Code SCN	5
Winnie M. Morgan, Code US	5 (+ Repro.)
Electronics Research Center National Aeronautics and Space Administration 575 Technology Square Cambridge, Massachusetts 02139 Attn: Leo Keane, Code GSE	1
Goddard Space Flight Center National Aeronautics and Space Administration Greenbelt, Maryland 20771 Attn: Charles R. Laughlin, Code 733	1
Marvin Maxwell, Code 731	1
Director of Defense Research and Engineering Office of the Secretary of Defense Pentagon, Washington, D. C. 20310 Attn: Asst. Director (Communication and Electronics)	1
Department of the Navy Naval Air Systems Command Washington, D. C. 20360 Attn: Astronautics Division	1
Langley Research Center National Aeronautics and Space Administration Hampton, Virginia Attn: Mr. Fred Morel	1

Addressee	Copies
Federal Aviation Agency 800 Independence Avenue, S. W. Washington, D. C. 20553 Attn: Alexander Winick, Chief, Navigation Division, RD 300	1
The Rand Corporation 1700 Main Street Santa Monica, California 90406 Attn: J. Hutcheson	1
Stanford Research Institute Menlo Park, California 94025 Attn: E. J. Fremouw	1
Johns Hopkins Applied Physics Laboratory 8621 Georgia Avenue Silver Spring, Maryland 20910 Attn: Dr. Robert Newton	1
Lincoln Laboratory Massachusetts Institute of Technology Lexington, Massachusetts 02173 Attn: Dr. Thomas Goblick	1
The Boeing Company Aero-Space Division Seattle, Washington	1
General Electric Company Advanced Technology Laboratories P. O. Box 43 Schenectady, New York 12301 Attn: Roy Anderson	1
Smithsonean Astrophysical Observatory Cambridge, Massachusetts 02138 Attn: Dr. George Weiffenbach	1
International Business Machines Corporation Federal Systems Division 18100 Frederick Pike Gaithersburg, Maryland 20760 Attn: John Mafane, Jr.	1
Philco-Ford Corporation Western Development Laboratories 3825 Fabian Way Palo Alto, California Attn: Reiss Jensen	1

Addressee	Copies
TRW Systems One Space Park Redondo Beach, California 90278 Attn: David Otten	1
Radio Corporation of America Defense Electronic Products Systems Engineering, Evaluation and Research, 127-310 Moorestown, New Jersey 08057 Attn: Mike Mitchell	1
Hughes Aircraft Company Aerospace Group Culver City, California 90232 Attn: Guidance and Controls Division, R. S. Boucher	1
Westinghouse Electric Company Defense Space Center/Aerospace Division Box 1693 Baltimore, Maryland 21203 Attn: Ed Mueller	1
Cubic Corporation 9233 Balboa Avenue San Diego, California 92123 Attn: James Reid	1
U. S. Naval Research Laboratory Washington, D. C. 20390 Attn: Roger Easton, Code 5160 Leo Young, Code 5403	1 1
Aerospace Corporation Los Angeles, California Attn: Dr. James Woodford	1
Communications and Systems, Inc. 6565 Arlington Boulevard Falls Church, Virginia 22046 Attn: Howard Lefkowitz	1
Communications Satellite Corporation 950 L'Enfant Plaza So., S. W. Washington, D. C. 20024 Attn: Ed Martin	1
Tom Benham Havorford College 5 College Lane Havorford, Pennsylvania	1

Addressee		Copies
Donald Jansky Office of Telecommunications Management Executive Office of the President Washington, D. C. 20504		1
Perry I. Klein Communications Satellite Corporation 950 L'Enfant Plaza So., S. W. Washington, D. C. 20024		10
Dr. F. Haber	Moore School of Electrical Engineering University of Pennsylvania	2
G. Thomas	"	1
R. Lefferts	"	15
Dr. H. Kritikos	"	1
Dr. P. L. Bargellini		2
David Kurjan	"	1
Dr. J. Bordogna	"	1
Richard A. Hrusovsky MS62 RCA Defense Electronics Products Astro-Electronics Division P. O. Box 800 Princeton, New Jersey 08540		1

Security Classification

DOCUMENT CONTROL DATA - R & D

(Security classification of title, body of abstract and indexing annotation must be entered when the overall report is classified)

1. ORIGINATING ACTIVITY *(Corporate author)*
University of Pennsylvania
The Moore School of Electrical Engineering
Philadelphia, Pennsylvania 19104

2a. REPORT SECURITY CLASSIFICATION
UNCLASSIFIED

2b. GROUP

3. REPORT TITLE

AN ANALYSIS OF THE USE OF OPTICAL TECHNIQUES IN SYNCHRONOUS NAVIGATION SATELLITES

4. DESCRIPTIVE NOTES *(Type of report and inclusive dates)*
Interim technical report

5. AUTHOR(S) *(First name, middle initial, last name)*
Robert E. Lefferts

6. REPORT DATE	7a. TOTAL NO. OF PAGES	7b. NO. OF REFS
May 1970	166	90

8a. CONTRACT OR GRANT NO.	9a. ORIGINATOR'S REPORT NUMBER(S)
Grant NGL-39-010-087	Moore School Report # 70-10
b. PROJECT NO.	
c.	9b. OTHER REPORT NO(S) *(Any other numbers that may be assigned this report)*
d.	

10. DISTRIBUTION STATEMENT

Distribution of this report is unlimited

11. SUPPLEMENTARY NOTES	12. SPONSORING MILITARY ACTIVITY
	National Aeronautics & Space Administration Space Applications Programs Office Washington, D.C. 20546

13. ABSTRACT

The feasibility of using optical and infrared technology for use in synchronous navigation satellites is examined. The analysis is based primarily on a determination of the quality of the image available to the detector under various conditions and not on the properties of the detector itself except for the resolving power of the detector.

Initially a passive-user system is considered where the navigation satellite detects the infrared energy emitted by the user's engines. Jet aircraft were considered first because of the relatively large amount of infrared energy emitted by their engines. By considering the energy incident on a single resolvable image element it was found that the signal energy available could not be reliably distinguished from changes in the effective background temperature of the earth. It was concluded that a navigation system using passive infrared detection from synchronous altitude is not feasible.

An active-user system is also considered where the navigating users are equipped with high-power, optical-energy sources. A comparison of the various optical sources showed that lasers would yield the highest signal-to-noise ratio because the narrow spectral regions in which their energy is concentrated would allow most of the background noise to be removed by filtering. It was found that the signal energy required for a satisfactory image could only be obtained under very restrictive conditions. Under such conditions, it was also necessary to consider the internal noise of the detector to determine if the signal could be detected. It was found that for a reasonable average source power the signal could not be detected due to the large amount of detector noise present. By using a very high peak power laser it should be possible to detect the user's signal but the present cost of such a laser makes such a system economically impractical considering the limited circumstances under which it could be used.

Although a number of optical systems other than the ones described could be considered it is concluded that optical techniques do not represent a feasible alternative to the use of radio frequency techniques for synchronous navigation satellites.

14. KEY WORDS	LINK A		LINK B		LINK C	
	ROLE	WT	ROLE	WT	ROLE	WT
Aircraft navigation						
Angular resolution						
Geometrical dilution of precision						
Image analysis						
Infrared systems						
Infrared targets						
Navigation satellite						
Navigation system						
Optical image						
Optical navigation system						
Optical systems						
Optical techniques						
Synchronous navigation satellites						
Television systems						